Model Refinement and Reduction for the Nitroxide-Mediated Radical Polymerization of Styrene with Applications on the Model-Based Design of Experiments

by

Mark Daniel Hazlett

A thesis
presented to the University of Waterloo
in fulfillment of the
thesis requirement for the degree of
Master of Applied Science
in
Chemical Engineering

Waterloo, Ontario, Canada, 2012

Author's Declaration

I hereby declare that I am the sole author of this thesis. This is a true copy of the thesis, including any required final revisions, as accepted by my examiners.

I understand that my thesis may be made electronically available to the public.

Mark Daniel Hazlett

Abstract

Polystyrene (PS) is an important commodity polymer. In its most commonly used form, PS is a high molecular weight linear polymer, typically produced through free-radical polymerization, which is a well understood and robust process. This process produces a high molecular weight, clear thermoplastic that is hard, rigid and has good thermal and melt flow properties for use in moldings, extrusions and films. However, polystyrene produced through the free radical process has a very broad molecular weight distribution, which can lead to poor performance in some applications.

To this end, nitroxide-mediated radical polymerization (NMRP) can synthesize materials with a much more consistently defined molecular architecture as well as relatively low polydispersity than other methods. NMRP involves radical polymerization in the presence of a nitroxide mediator. This mediator is usually of the form of a stable radical which can bind to and disable the growing polymer chain. This will "tie up" some of the free radicals forming a dynamic equilibrium between active and dormant species, through a reversible coupling process.

NMRP can be conducted through one of two different processes: (1) The bimolecular process, which can be initiated with a conventional peroxide initiator (i.e. BPO) but in the presence of a stable nitroxide radical (i.e. TEMPO), which is a stable radical that can reversibly bind with the growing polymer radical chain, and (2) The unimolecular process, where nitroxyl ether is introduced to the system, which then degrades to create both the initiator and mediator radicals.

Based on previous research in the group, which included experimental investigations with both unimolecular and bimolecular NMRP under various conditions, it was possible to build on an earlier model and come up with an improved detailed mechanistic model. Additionally, it was seen that certain parameters in the model had little impact on the overall model performance, which suggested that their removal would be appropriate, also serving to reduce the complexity of the model. Comparisons of model predictions with

experimental data both from within the group and the general literature were performed and trends verified.

Further work was done on the development of an additionally reduced model, and on the testing of these different levels of model complexity with data. The aim of this analysis was to develop a model to capture the key process responses in a simple and easy to implement manner with comparable accuracy to the complete models. Due to its lower complexity, this substantially reduced model would me a much likelier candidate for use in on-line applications.

Application of these different model levels to the model-based D-optimal design of experiments was then pursued, with results compared to those generated by a parallel Bayesian design project conducted within the group. Additional work was done using a different optimality criterion, targeted at reducing the amount of parameter correlation that may be seen in D-optimal designs.

Finally, conclusions and recommendations for future work were made, including a detailed explanation of how a model similar to the ones described in this paper could be used in the optimal selection of sensors and design of experiments.

Acknowledgements

First and foremost, thank you God for granting me the strength, perseverance and wherewithal to pursue my education, despite some challenges and setbacks along the way, in order to pursue my chosen calling of becoming an engineer.

Next, I'd like to thank my supervisor, Professor Alexander Penlidis, without whom this thesis would not have been possible. His continual support, encouragement, guidance, and technical assistance have all proven to be of extreme import throughout this at times arduous two-year process.

Additionally, thanks to the Department of Chemical Engineering at the University of Waterloo - and many of its faculty and staff - are in order, as throughout both my undergraduate and graduate careers, many of you have taught me much, both technically and otherwise, while providing me with a positive environment in which to come into my own. In particular; I would like to thank Professor Ali Elkamel - for his supervision of my Fourth-Year Design Project which really sparked my interest in process modeling, and Professor Neil McManus – for introducing me to the fascinating field of polymer science, as well as his assistance in understanding more of the chemistry relevant to this process. Thanks also to my officemates, for their kindness, patience and friendship throughout the last years.

Thanks go out to my friends, whom I've had no shortage of throughout my undergrad, co-op terms and graduate school. They always cheered me up when I was down, were willing to play just as hard (if not harder than) we worked and truly made my time here fly by. So much so that the day my folks dropped me off in residence for the first time, back in September of 2004, seems like just yesterday.

I am extremely grateful for my girlfriend of these past four and a half years, Melanie Snow, who has been a great help in some of the tough times and great company in the good times, has always been a positive influence, and always is willing to lend me that big beautiful brain of hers to help me think through a problem or proofread a paper.

Finally and perhaps most importantly, I would like to thank my wonderful family; my parents, Robert and Janice, for their continued support - financially, spiritually, and emotionally - throughout my lifelong educational process, and of course to the first Melanie to come into my life, awesome little sister that she is, for being the best roommate and friend that a fellow could ask for.

Mark Daniel Hazlett

Table of Contents

List of Figures

List of Tables

Chapter 1: Introduction

Controlled radical polymerization (CRP) is amongst the most active areas of research in polymer science. Nitroxide-mediated radical polymerization (NMRP) is one of the three most popular approaches towards controlled radical polymerization. Polymeric materials synthesized by NMRP can be used as coatings, adhesives, surfactants, dispersants, lubricants, gels, additives and thermoplastic elastomers, as well as materials for biomedical applications. Recently, it has been reported that block copolymers synthesized by NMRP are finding their first industrial use as dispersants in the area of pigments.

The literature on NMRP is extensive and growing. The polymer chemistry aspects of NMRP are relatively well understood. Kinetic models that describe polymerization rate and molecular weight development are available in the literature. Somewhat surprisingly though, very little has been done as far as validation and refinement of these models are concerned.

In this work, the focus has been on modeling of the NMRP of styrene using 2,2,6,6-tetramethyl-1-piperidinyloxy (TEMPO) and later 2,2,5-tri-methyl-4-phenyl-3-azahexane-3-nitroxide (TIPNO). The objectives were to:

- Generate a complete mechanistic model (using the latest, state-of-the-art knowledge and information) for the NMRP process, using both unimolecular and bimolecular initiation systems with both TEMPO and TIPNO controller radicals.

- Investigate the effect on the model of different polymerization conditions such as different temperatures, different controller to initiator molar ratios, and different initiating systems, on conversion, molecular weight averages and polydispersity.

- Utilize a source of reliable experimental data for validation and improvement of the mechanistic mathematical model.

- Develop and assess a simplified model for the key process responses for this process that is significantly less onerous to implement. Compare this simplified model with the higher-level models and experimental data in order to gain an understanding of its utility and limitations.

- Implement the aforementioned models in mechanistic model-based non-linear experimental design schemes, which can further shed light on the most uncertain parts of our process understanding.

- Discuss future applications of these models in the area of sensor selection and further experimental designs.

In Chapter 2, a brief literature review on the topic of controlled radical polymerization (CRP), its characteristics, advantages, disadvantages, utility, and mechanisms of the different CRP variants is conducted. Emphasis is placed on NMRP in this discussion.

Chapter 3 details the reaction mechanism behind, and development of a fully mechanistic model for, the NMRP of styrene using TEMPO. An analysis of this model's performance using the bimolecular process compared with experimental data and across a variety of operating conditions is then performed, followed by further analyses using the unimolecular and TIPNO-initiated processes.

In Chapter 4, a series of refinements are introduced to the fully mechanistic model (FMM), starting again with the bimolecular process, with the aim of improving its performance with respect to the experimental data. Testing of these refinements is conducted, and then these changes are incorporated and tested using the unimolecular and TIPNO processes. The result of these refinements is termed the refined mechanistic model (RMM).

Chapter 5 illustrates the development and testing of a simplified model, aimed at capturing only the key process responses rather than the fully mechanistic view presented by the FMM and RMM.

Chapter 6 details an application of these different model levels in the model-based optimal design of experiments, with comparisons made to a parallel effort using Bayesian experiment designs with linear models. An analysis of the impacts of using the different model levels and changing the optimality criterion on the selection of experiments, is conducted along with the discussion of some case studies.

Concluding remarks are made in Chapter 6 along with a presentation of interesting extensions to this work, including a detailed discussion of a potential application in the optimal selection of sensors using these models. The thesis includes two appendices. Appendix A contains tables of the experimental data used for the figures of Chapter 3, 4, and 5. Appendix B contains code samples and pseudo-code that highlight some of the key steps in the D-optimal design application, as well as information about the availability of the MATLAB Code used in these analyses. The references for each chapter are located at the end of the chapter.

Chapter 2: Literature Background on NMRP

2.1　Brief Outline

This chapter contains a brief description of polystyrene (PS); an outline of the traditional methods for its production and processing, as well as some common uses of PS. This is followed by a more detailed discussion of some of the newer Controlled/Living Radical Polymerization (CRP) methodologies for PS (specifically, Nitroxide-Mediated Radical Polymerization (NMRP), Atom Transfer Radical Polymerization (ATRP) and Reversible Addition-Fragmentation (chain) Transfer polymerization (RAFT)), and also the material properties and potential applications of the polymer produced through these processes (typically having more controlled molecular weight (MW) with a desirable tunable molecular architecture (e.g., more side branching than traditional PS)), including possible commercial applications. From this background discussion, some conclusions will be made regarding what was learned about the future outlook of these relatively recent processes and their implementation.

2.2　Introduction

Polystyrene (PS) is an important commodity polymer, which, in its most commonly used form is a high molecular weight linear polymer, consisting of approximately n = 1000 repeat units [1]. A product of the polymerization of styrene (also known as vinyl benzene), the repeat unit of polystyrene is shown in Figure 2-1.
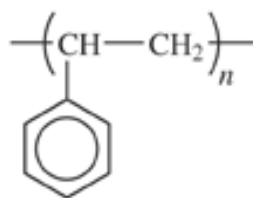
Figure 2-1 - Repeat unit of PS

Styrene can be polymerized via each of four distinct mechanisms (anionic, cationic, free radical and with Ziegler-Natta catalysts), but is typically produced industrially through the free radical process [1]. Reasons include less stringent monomer purity requirements, and milder reaction conditions when compared to other polymerization techniques [2]. Free radical polymerization can be performed over a wide range of temperatures, in solution, in emulsion, or with other trace impurities of reagents, making it an appealing choice [3]. This process produces a high molecular weight, clear thermoplastic that is hard, rigid and has good thermal and melt flow properties for use in moldings, extrusions and films [1]. However, polystyrene produced through the free radical process has a random molecular architecture and generally broad molecular weight distributions, which can lead to poor performance in some applications [3]. Thus, research is being conducted in order to find ways to make these polymers in a more controlled fashion.

Well-defined polymers with precisely controlled structures are accessible by ionic living polymerization (anionic and cationic). However, ionic polymerizations have several practical disadvantages. The polymerization is extremely sensitive to impurities in the reagents; even minute traces of atmospheric gases or water can impact the process [1]. In addition to the level of care that must be taken to prevent impurities, the optimum reaction temperatures are often low, and the process will require excessive cooling.

Newer techniques of controlled radical polymerization can produce materials with a much more consistently defined molecular architecture as well as relatively low polydispersity such as those produced via ionic polymerization, under less stringent reaction conditions more similar to those of free radical polymerization [4].

2.3 Traditional PS Production and Utility

2.3.1 Production

Free radical polymerization (FRP) consists of four main steps; initiation, propagation, termination and chain transfer [2]. In the initiation phase, primary radicals are generated through the decomposition of an initiator molecule such as benzoyl peroxide (BPO) and then the reaction of these primary radicals with monomer to produce radicals with chain length 1. The next step is propagation, where the repeated addition of monomer molecules to the radicals formed during initiation takes place. Each propagation reaction increases the length of the polymer chain by 1, and continued repetition of this step results in long polymer chains. Eventually, the propagating polymer radical will stop growing and the radical will be destroyed either through coupling (combination) or disproportionation. Additionally, chain transfer to a smaller molecule can occur. This causes polymer chains to stop growing, but does not decrease the overall radical concentration of the system, as a new smaller radical will be formed. Figure 2-2 details the reactions that take place in these steps.

$$I \xrightarrow{\textbf{k}_d} 2\ R\bullet_{in}$$

$$R\bullet_{in} + M \xrightarrow{\textbf{k}'_p} R\bullet_1$$

Initiation

$$R\bullet_1 + M \xrightarrow{\textbf{k}_p} R\bullet_2$$

$$\vdots$$

$$R\bullet_r + M \xrightarrow{\textbf{k}_p} R\bullet_{r+1}$$

Propagation

$$R\bullet_r + R\bullet_s \quad\begin{array}{l} \nearrow^{\textbf{k}_{tc}} P_{r+s} \\ \searrow_{\textbf{k}_{td}} P_r + P_s \end{array}$$

Termination

$$R\bullet_r + H{-}T \xrightarrow{\textbf{k}_{tr}} P_r + T\bullet$$

Chain transfer
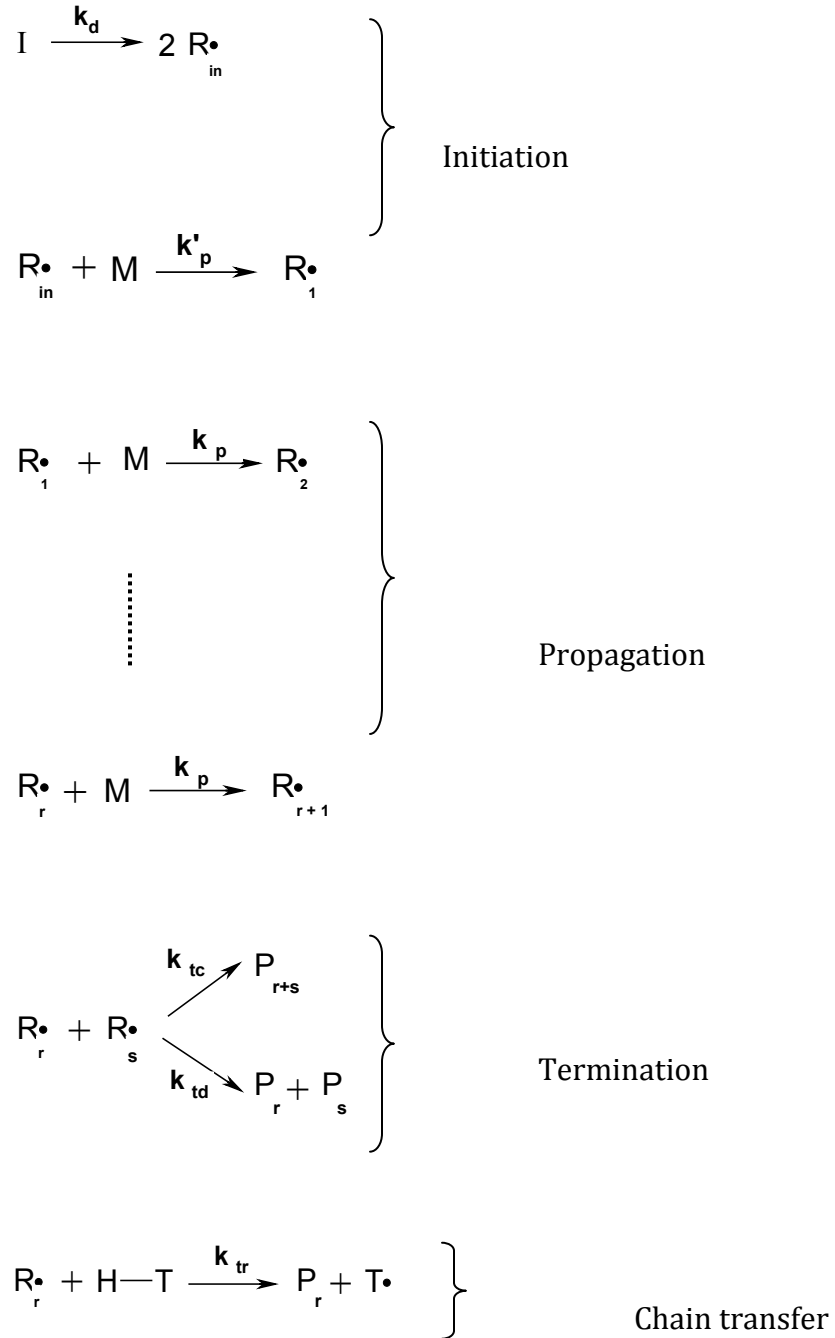
Figure 2-2: General reaction scheme for FRP

It is important to note that all these reaction steps occur concurrently in free radical polymerization, and that all of these steps occur within seconds [2]. This means that in order to proceed, a constant supply of radicals must be available. This is typically provided

through a choice of an initiator with a sufficiently long half-life such that decomposition will continue throughout the reaction.

A repercussion of these simultaneous reactions is that the instantaneous degree of polymerization over the course of the reaction will vary considerably, resulting in a relatively high polydispersity (PDI) [2]. Additionally, since all steps take place concurrently, it is very difficult to control chain end groups, composition or structure. Table 2-1 lists some of the advantages and disadvantages of traditional free radical polymerization, although the borderline between advantages and disadvantages can be somewhat grey.

Table 2-1: Advantages and disadvantages of FRP

Free Radical Polymerization (FRP)	
Advantages:	Disadvantages:
Robust process, can be used over wide range of operating conditions	High PDI
Low sensitivity to monomer impurities	Diffusional effects significant at high conversion
Fast propagation, so high MW's can be reached in a timely manner	Poor control of polymer structure/tacticity
Well understood and used widely in industry	Cannot be used for formation of block polymers

2.3.2   Utility

Typical polystyrene is produced and used in a wide variety of films, extrusions, foams and moldings, as it is a very inexpensive, light, strong and thermally stable plastic [1]. The uses of polystyrene can vary widely, as polystyrene can take a variety of forms. Polystyrene can be injection molded to make a variety of objects, from toys to CD cases to plastic dining utensils to food packaging to petri dishes and other laboratory containers as an alternative to glass. Further, PS foams can be used as thermal insulation in buildings or food packages, where it is appealing also due to its odorless and tasteless nature. PS is also often used as a

shock dampener in the packaging of fragile objects, whether it is as solid foam blocks or pellets of expanded polystyrene.

2.4   Newer Synthesis Methodologies

There are several approaches to controlled radical polymerization (CRP) possible. Current research has mainly concentrated around three of them, NMRP, ATRP and RAFT [4]. In general, these methodologies rely on a dynamic equilibrium between growing free radicals and dormant species [5].

2.4.1   Atom Transfer Radical Polymerization
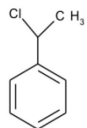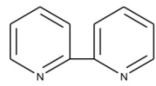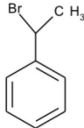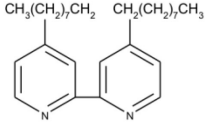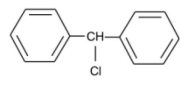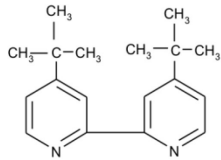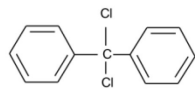
Since the discovery of ATRP in 1995, the technical literature on ATRP has been growing very rapidly [6]. Radical generation in ATRP involves an organic halide undergoing a reversible redox process catalyzed by a transition metal compound such as cuprous halide. The equation below shows the general mechanism of ATRP system catalyzed with copper bromide (CuBr (L)). The system consists of an initiator that has an easily transferable halide atom (R–Br) and a catalyst. The catalyst (or activator) is a lower oxidation state metal halide (CuBr (L)) with a suitable ligand (L). Polymerization begins when the halide atom transfers from the initiator to the catalyst and forms a free radical (R•) and metal halide of the higher oxidation state (CuBr$_2$ (L)). This step is called activation or forward reaction. The deactivation step or backward reaction pushes the reaction back to form the dormant species (R–Br).

$$R\!-\!\!-\!Br \ + \ CuBr\,(L) \ \underset{k_d}{\overset{k_a}{\rightleftharpoons}} \ R\bullet \ + \ CuBr_2(L)$$
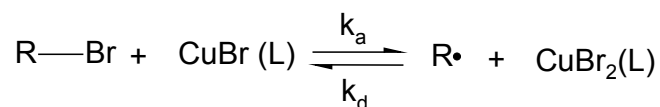
Initiator choice is fairly important in ATRP. The carbon-halide bond must be relatively weak in order for the halogen atom to be reversibly moved from the dormant species to the catalyst. Common halides used are chlorides and bromides. Also of great importance is the selection of which catalyst to use. Suitable ligands should complex with a metal halide to

form the ATRP catalyst. The metal halide should have at least two oxidation states and should have good affinity toward halogen atoms. Systems using Cu, Ru, Ni, Pd, and Fe transition metals in conjunction with suitable ligands have been used as catalysts. Table 2-2 shows some ATRP initiators, metal halides and ligands [6].

Table 2-2: Some ATRP initiators, metal halides and ligands.

Initiators	Metal halide	Ligand
	CuCl	
	CuBr	

2.4.2   Reversible Addition-Fragmentation Chain Transfer Polymerization

Conventional free radical polymerization with the addition of thiocarbonylthio compounds that serve as RAFT agents for control has been of research interest since its discovery in the mid to late 80s [7]. Instead of the reversible termination of chains seen in the other CRP methods, RAFT controls chain growth through reversible chain transfer as per the reaction below, involving the reaction of polymeric radical species ($R_m^{\bullet}$, $R_n^{\bullet}$) and the reversible transfer of the chain transfer agent (Z) back and forth to each other.

The structures of R_mZ and R_nZ are identical, except that the numbers of monomer repeat units present may be different. A RAFT polymerization involves a conventional radical

initiator (i.e. BPO), and a chain transfer agent (Z), which is a compound containing a dithioester, dithiocarbamate, trithiocarbonate or xanthate moiety (See Figure 2-3) [8]. The key to the success of RAFT polymerizations lies in the high reactivity of the thiocarbonyl group towards the propagating radicals.

$$R_m\text{---}Z + R_n^\bullet \xrightleftharpoons{K_{exch}} R_m^\bullet + R_n\text{---}Z$$
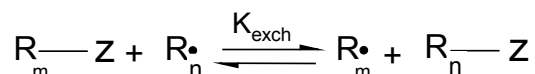
The active species concentration must be kept low compared to that of the dormant species in order to provide good control of MW and therefore PDI [8]. To do this, one can limit the amounts of initiator and capping agent.

| dithioester | xanthate | dithiocarbamate | trithiocarbonate |
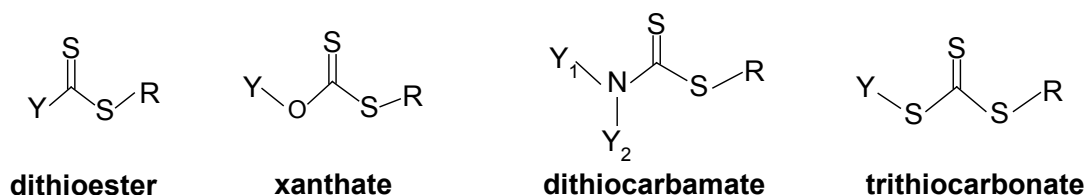
Figure 2-3: General structures of RAFT chain transfer agents

2.4.3 Nitroxide-Mediated Radical Polymerization

NMRP involves radical polymerization in the presence of a nitroxide mediator. This mediator is usually of the form of a stable radical which can bind to and disable the growing polymer chain [9]. This will "tie up" some of the free radicals forming a dynamic equilibrium between the active and dormant species, through a reversible coupling process, as shown in Figure 2-4. This reaction must be carried out at elevated temperatures (100 – 140 °C) or else the reverse reaction will dominate and the dormant species will be stable, causing the nitroxide to act as an inhibitor [10].

This type of CRP can be performed through either a unimolecular or bimolecular process. The bimolecular process can be initiated with a conventional initiator (i.e., BPO) but in the presence of a stable nitroxide radical (i.e., TEMPO), which is a stable radical that can reversibly bind with the growing polymer radical chain [9], as illustrated in Figure 2-4.
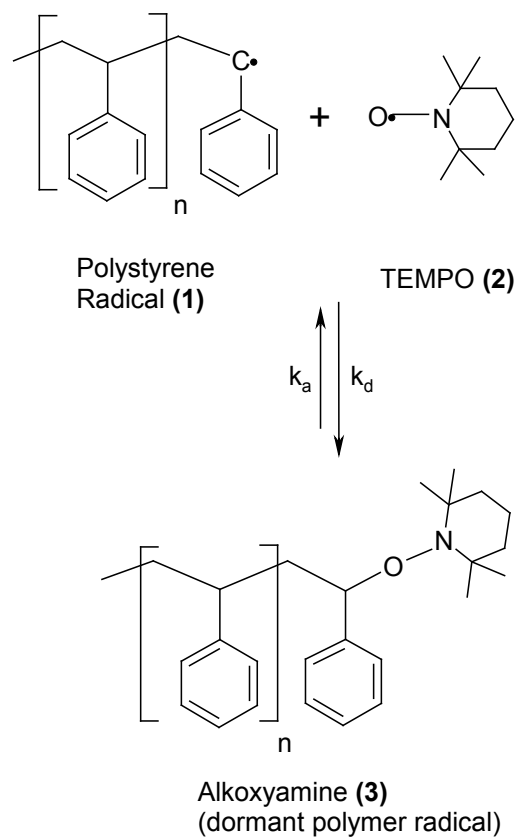
Figure 2-4: Chemistry of key reaction in NMRP

The key equilibrium reaction is the same for both the unimolecular and bimolecular processes, however they differ in the source of the initiator and controller. In the unimolecular case, rather than adding both controller and initiator directly, nitroxyl ether is introduced to the system, which then degrades to create in-situ both initiator and mediator radicals, in a 1:1 ratio. The reaction involved with this process is outlined in Figure 2-5.
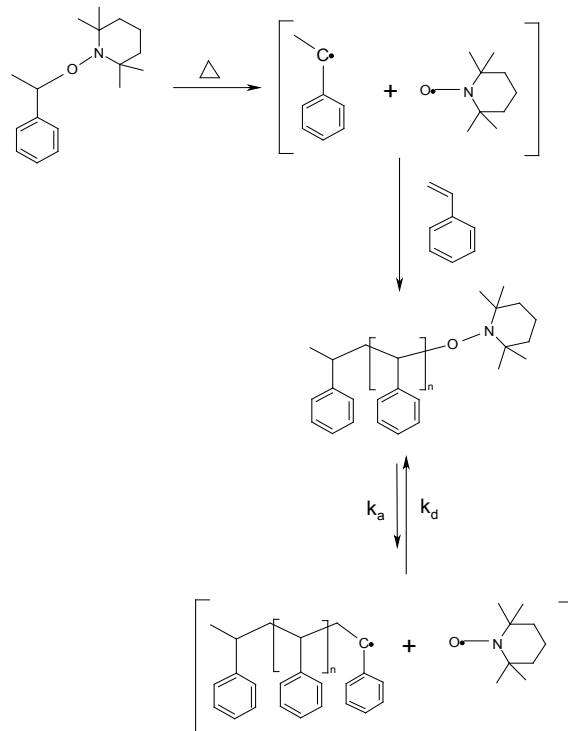
Figure 2-5: Chemistry of unimolecular initiation

The primary advantage of the unimolecular process over the bimolecular process is that the structure of the polymers prepared can be controlled to a much greater extent. Since the unimolecular initiator contains the initiating radical and nitroxide radical in precisely the correct (1:1) stoichiometry, the number of initiating sites per polymerization is precisely known. As a result, the molecular weight can be more accurately controlled, since there is never an excess of either radical in the system (i.e., there is no opportunity for a slightly incorrect ratio when using a unimolecular process, as the initiator and controller come from the same reagent).

2.5 Material Properties and Applications of CRP

2.5.1 Properties

CRP can allow for a variety of structures to be produced that would be impossible under FRP, due to the more stringent control of molecular structure, composition and tacticity [5]. Figure 2-6 shows some of the structures that are possible with CRP techniques.
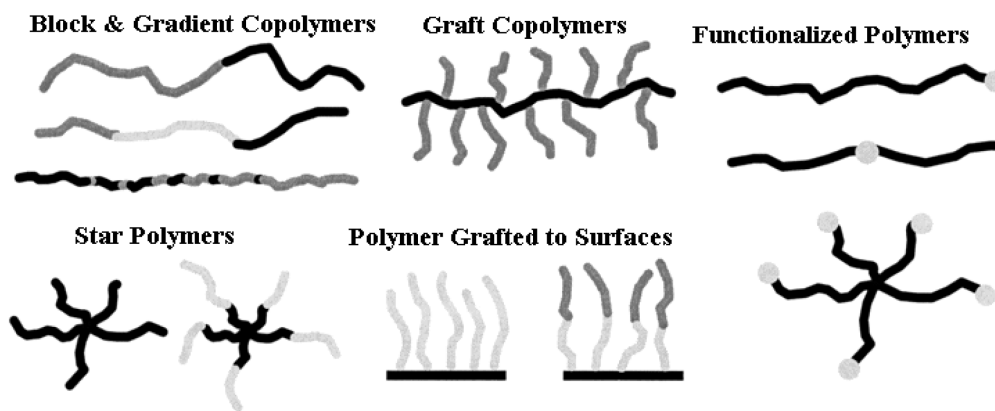
Figure 2-6 - Examples of structures made by CRP techniques

Not all of these structures have been shown to be possible with polystyrene, however, though the potential ability to create these types of structures is one of the main driving forces behind research into CRP techniques. One very promising utility of polystyrene produced through CRP is that of use in block copolymers which serve as an additional way to fine-tune the material properties of a polymer [11]. An important copolymer of polystyrene is styrene-butadiene rubber, used in many applications, including car tires and latex paints.

Another very interesting use for CRP polystyrene is in the development of functionalized polymers, where blocks of polymer can be built with functional groups interspersed throughout. In this way one can further modify the material properties of the polymer, as well as creating the ability for a specialized membrane (either through catalysis or facilitated transfer of an agent through the membrane).

2.5.2   Applications

Among the first CRP-based products in production are acrylic block copolymers, brought to market in 2005 by Ciba Specialty Chemicals (now part of BASF), aimed to offer superior rheological performance and improved stabilization of pigment dispersions in coating applications [12]. These block copolymers were synthesized through NMRP using n-butylacrylate, dimethylaminoethyl acrylate and styrene as monomers.

Well-defined polymers such as those made using CRP, potentially including polystyrene, could be well suited for biomedical applications, controlled drug release/targeting, antimicrobial surfaces, or steering enzyme activity. In the case of controlled drug release, the use of functionalized polymer immunonanoparticles containing drugs that need to be targeted to specific regions is being investigated by many groups [13].

There are many other exciting potential applications for CRP polystyrene including potential use in microelectronics, soft lithography, optoelectronics, specialty membranes, sensors, and components for microfluidics [11].

2.6   The Future of CRP PS

As described previously, there are several exciting potential applications for synthesizing polymer of a well-defined nature, and although there is much research being undertaken in the field of CRP, the amount of industrial production of CRP polymers is only on the scale of about 10% of that of more traditional methods [11]. There are still some issues to be dealt with before CRP can be made more competitive as a practical polymerization technique.

Some of the issues associated with CRP (and NMRP in particular) are [3, 4, 5, 10, 11] :

- Slower polymerization than FRP

- NMRP largely limited to styrenic monomers (TEMPO functions better with styrene)

- Low molecular weights only

- Narrow polydispersity can be undesirable in certain uses

- Mediating agents can be inefficient or expensive to synthesize

- Pressure vessels and/or heat exchange may be needed, so costs can be high (NMRP needs to operate at temperatures greater than the boiling point of water)

Once some of these engineering challenges can be overcome, more widespread use of some of these techniques may be seen. Until then, it is suspected that use of CRP PS will be limited to more specialized cases where the value added due to the application needs is of greatest impact.

Chapter 3: Development of a Fully Mechanistic Model

3.1   Reaction Scheme

This chapter is focused on detailing the mechanistic model used as the starting point for this research, as presented in the work of Nabifar [1] and Nabifar et al. [2]. The model described in [1] was a preliminary attempt, so several additions had to be made in order to render the model more complete. The first such action was to add the material balance for the dimer species – which is among the material balances presented by Bonilla et al. when discussing a more detailed mechanism and model [3]. With this addition, the model can work for either unimolecular or bimolecular nitroxide-mediated radical polymerization, with reasonably good performance, especially at low to medium conversions.

The reaction mechanism used as the basis for the derivation of the model is the one proposed by Bonilla et al. [3] and is summarized in Table 3-1 below. The mechanism includes the following reactions: chemical initiation, reversible nitroxyl ether decomposition (for the monomolecular process), monomer (Mayo) dimerization, thermal self-initiation, propagation, reversible monomeric and polymeric alkoxyamine formation (production of dormant species), alkoxyamine decomposition, rate enhancement, transfer to monomer and dimer, as well as conventional termination. All rate constants are assumed to be independent of chain length.

Table 3-1 - Steps in the Reaction Mechanism

Description of Step	Reaction
Chemical initiation	$I \xrightarrow{k_d} 2R_{in}^{\bullet}$
Nitroxyl ether decomposition	$NO_E \underset{k_{d2}}{\overset{k_{a2}}{\rightleftarrows}} R_{in}^{\bullet} + NO_x^{\bullet}$
Mayo dimerization	$M + M \xrightarrow{k_{dim}} D$
Thermal initiation	$M + D \xrightarrow{k_{ia}} D^{\bullet} + M^{\bullet}$
First propagation (primary radicals)	$R_{in}^{\bullet} + M \xrightarrow{k_p} R_1^{\bullet}$
First propagation (monomeric radicals)	$M^{\bullet} + M \xrightarrow{k_p} R_1^{\bullet}$
First propagation (dimeric radicals)	$D^{\bullet} + M \xrightarrow{k_p} R_1^{\bullet}$
Propagation	$R_r^{\bullet} + M \xrightarrow{k_p} R_{r+1}^{\bullet}$
Dormant living exchange (monomeric alkoxyamine)	$M^{\bullet} + NO_x^{\bullet} \underset{k_{da}}{\overset{k_a}{\rightleftarrows}} MNO_x$
Dormant living exchange (polymeric alkoxyamine)	$R_r^{\bullet} + NO_x^{\bullet} \underset{k_{da}}{\overset{k_a}{\rightleftarrows}} R_r NO_x$
Alkoxyamine decomposition	$MNO_x \xrightarrow{k_{decomp}} M + HNO_x$
Rate enhancement reaction	$D + NO_x^{\bullet} \xrightarrow{k_{h3}} D^{\bullet} + HNO_x$
Termination by combination	$R_r^{\bullet} + R_s^{\bullet} \xrightarrow{k_{tc}} P_{r+s}$
Termination by disproportionation	$R_r^{\bullet} + R_s^{\bullet} \xrightarrow{k_{td}} P_r + P_s$
Transfer to monomer	$R_r^{\bullet} + M \xrightarrow{k_{fM}} P_r + M^{\bullet}$
Transfer to dimer	$R_r^{\bullet} + D \xrightarrow{k_{fD}} P_r + D^{\bullet}$

Table 3-2 cites the kinetic rate constants used, most of which are presented as Arrhenius functions of activation energies and temperature [4]. The physical properties of the monomer, polymer and initiator as used in the calculations are listed in Table 3-3.

Table 3-2 - Rate Constant Values (T [K], R [cal mol^{-1} K^{-1}]) [4]

Rate Constant	Units	Bimolecular	Unimolecular
k_d(BPO)	s^{-1}	$1.7 \times 10^{15} \exp\left(-\dfrac{30000}{RT}\right)$	-
f		0.54-0.55	-
k_{dim}	L mol^{-1} s^{-1}	$188.97 \exp\left(-\dfrac{16185.1}{RT}\right)$	$188.97 \exp\left(-\dfrac{16185.1}{RT}\right)$
k_{ia}	L mol^{-1} s^{-1}	$6.359 \times 10^{12} \exp\left(-\dfrac{36598.55}{RT}\right)$	$6.359 \times 10^{12} \exp\left(-\dfrac{36598.55}{RT}\right)$
k_p	L mol^{-1} s^{-1}	$4.266 \times 10^{7} \exp\left(-\dfrac{7769.17}{RT}\right)$	$4.266 \times 10^{7} \exp\left(-\dfrac{7769.17}{RT}\right)$
k_{t0}	L mol^{-1} s^{-1}	$2.002 \times 10^{10} \exp\left(-\dfrac{3081.84}{RT}\right)$	$2.002 \times 10^{10} \exp\left(-\dfrac{3081.84}{RT}\right)$
k_{td}/k_{t0}		0.0	0.0
k_{fM}	L mol^{-1} s^{-1}	$9.376 \times 10^{6} \exp\left(-\dfrac{13372}{RT}\right)$	$9.376 \times 10^{6} \exp\left(-\dfrac{13372}{RT}\right)$
k_{fD}	L mol^{-1} s^{-1}	50	50
k_{a2}	s^{-1}	0.0	$2.0 \times 10^{13} \exp\left(-\dfrac{29683}{RT}\right)$
k_{d2}	L mol^{-1} s^{-1}	0.0	$5.03 \times 10^{9} \exp\left(-\dfrac{3722}{RT}\right)$
k_{da}	L mol^{-1} s^{-1}	$5.03 \times 10^{9} \exp\left(-\dfrac{3722}{RT}\right)$	$5.03 \times 10^{9} \exp\left(-\dfrac{3722}{RT}\right)$
k_a	s^{-1}	$2.0 \times 10^{13} \exp\left(-\dfrac{29683}{RT}\right)$	$2.0 \times 10^{13} \exp\left(-\dfrac{29683}{RT}\right)$
k_{decomp}	s^{-1}	$5.7 \times 10^{14} \exp\left(-\dfrac{36639.6}{RT}\right)$	$5.7 \times 10^{14} \exp\left(-\dfrac{36639.6}{RT}\right)$
k_{h3}	L mol^{-1} s^{-1}	0.001	0.001

In the previous tables, k_d is the initiator decomposition rate constant, f the initiator efficiency (i.e., the fraction that participates in the reaction), k_{dim} the Mayo dimerization rate constant, k_{ia} the rate constant of thermal initiation between monomer and dimer, kp is the propagation rate, k_{t0} the termination rate constant, k_{fM} the rate constant for chain transfer to monomer, k_{fD} the rate constant for chain transfer to dimer, ka2 the rate constant for nitroxyl ether decomposition, kd2 the rate of nitroxyl ether reforming from the active radical species, k_{da} the rate constant for the nitroxide mediator radicals coupling with the living polymer radicals, k_a the rate constant for the dormant species' separation into the polymer and controller radicals, k_{decomp} the rate constant of alkoxyamine decomposition, and finally, k_{h3} is the rate constant for the dimer's reaction with the controller radical to produce a living dimer radical and a decomposed alkoxyamine (referred to as the rate enhancement reaction).

Table 3-3 - Relevant Physical Properties (T [K]) [4]

Property	Units	Value
ρ_M	kg L $^{-1}$	$0.9193 - 0.000665(T - 273.15)$
ρ_P	kg L $^{-1}$	$0.9926 - 0.000265(T - 273.15)$
MW_M	g mol^{-1}	104.12
MW_{init}	g mol^{-1}	242.23
T_{gM}	K	185.0
T_{gP}	K	378.0

In Table 3-3, ρ represents density and T_g the glass transition temperature for monomer (M) or polymer (P). MW is molecular weight and subscript init denotes initiator.

The reaction mechanism described in this section describes both the unimolecular and bimolecular initiating options. The key differences are in the rate constants that differ between these processes (see Table 3-2) and either activate or deactivate reaction pathways (as depicted in Table 3-1). For instance, the unimolecular case uses the decomposition of the nitroxyl ether as its source of both initiator and controller, rendering

those reactions/rate constants important, while making the ones used for BPO decomposition and controller efficiency less relevant. The core parts of the process (i.e., the equilibrium between initiator and controller, and the polymerization itself) are the same for both of these pathways.

3.2   Overall Mass Balances for the Different Species

In order to be modeled, the system needed to be rearranged into a system of material balance differential equations. Based on the reaction mechanism outlined in Table 3-1, the following are the thirteen material balances for the different species present during the batch NMRP polymerization of styrene. Equation 3-3, describing the mass balance of the dimer species was a new addition to the model presented in Nabifar [1].

$$\frac{d[I]}{dt} = -k_d[I] \hspace{4cm} \text{Eq. 3-1}$$

$$\frac{d[M]}{dt} = -2k_{dim}[M]^2 - k_{ia}[M][D] - k_p[M]([D^\cdot] + [M^\cdot] + [R_{in}^\cdot]) - k_p[M][R^\cdot]$$
$$- k_{fM}[M][R^\cdot] + k_{decomp}[MNO_x] \hspace{2.5cm} \text{Eq. 3-2}$$

$$\frac{d[D]}{dt} = k_{dim}[M]^2 - k_{ia}[M][D] - k_{h3}[NO_x^\cdot][D] - k_{fD}[D][R^\cdot] \hspace{1.5cm} \text{Eq. 3-3}$$

$$\frac{d[NO_E]}{dt} = -k_{a2}[NO_E] + k_{d2}[NO_x^\cdot][R_{in}^\cdot] \hspace{3cm} \text{Eq. 3-4}$$

$$\frac{d[M^\cdot]}{dt} = k_{ia}[M][D] - k_p[M][M^\cdot] - k_{da}[NO_x^\cdot][M^\cdot] + k_a[MNO_x] + k_{fM}[M][R^\cdot] \hspace{1cm} \text{Eq. 3-5}$$

$$\frac{d[R_{in}^{\cdot}]}{dt} = 2fk_d[I] - k_p[M][R_{in}^{\cdot}] + k_{a2}[NO_E] - k_{d2}[NO_x^{\cdot}][R_{in}^{\cdot}] \qquad \text{Eq. 3-6}$$

$$\frac{d[D^{\cdot}]}{dt} = k_{ia}[M][D] - k_p[M][D^{\cdot}] + k_{h3}[NO_x^{\cdot}][D] + k_{fD}[D][R^{\cdot}] \qquad \text{Eq. 3-7}$$

$$\frac{d[NO_x^{\cdot}]}{dt} = -k_{h3}[NO_x^{\cdot}][D] - k_{da}[NO_x^{\cdot}][R^{\cdot}] + k_a[R_rNO_x] - k_{da}[NO_x^{\cdot}][M^{\cdot}]$$
$$+ k_a[MNO_x] - k_{d2}[NO_x^{\cdot}][R_{in}^{\cdot}] + k_{a2}[NO_E] \qquad \text{Eq. 3-8}$$

$$\frac{d[HNO_x]}{dt} = k_{h3}[NO_x^{\cdot}][D] + k_{decomp}[MNO_x] \qquad \text{Eq. 3-9}$$

$$\frac{d[MNO_x]}{dt} = k_{da}[NO_x^{\cdot}][M^{\cdot}] - k_a[MNO_x] - k_{decomp}[MNO_x] \qquad \text{Eq. 3-10}$$

$$\frac{d[RNO_x]}{dt} = k_{da}[NO_x^{\cdot}][R^{\cdot}] - k_a[RNO_x] \qquad \text{Eq. 3-11}$$

$$\frac{d[R^{\cdot}]}{dt} = k_p[M]([D^{\cdot}] + [M^{\cdot}] + [R_{in}^{\cdot}]) - (k_{tc} + k_{td})[R^{\cdot}]^2 - k_{da}[NO_x^{\cdot}][R^{\cdot}]$$
$$+ k_a[R_rNO_x] - k_{fM}[M][R^{\cdot}] - k_{fD}[D][R^{\cdot}] \qquad \text{Eq. 3-12}$$

$$\frac{d[P]}{dt} = k_{fM}[M][R^{\cdot}] + k_{fD}[D][R^{\cdot}] + k_t[R^{\cdot}]^2 \qquad \text{Eq. 3-13}$$

The rates of initiator decomposition, monomer, dimer, and nitroxyl ether consumption are given in Equations 3-1 through 3-4. Next, Equations 3-5 through 3-8 are the corresponding rate equations for monomeric, primary, dimeric, and stable nitroxyl radicals, respectively. The material balances for hydroxylamine species, monomeric and polymeric alkoxyamines (dormant species) are given next. Finally, Equations 3-12 and 3-13 represent the material balances for polymeric radicals and dead polymer species, respectively.

3.3 Moment Equations for Molecular Weight Prediction

In order to follow the molecular weight development, in terms of number and weight average molecular weights, the method of moments is used. There are three polymer populations in this system: "living" polymer radicals, dead polymer molecules, and dormant species. The moments for "living" radical, dormant and dead species are defined in Equations 3-14, 3-15 and 3-16, as follows.

$$\lambda_i = \sum_r r^i R_r \qquad \text{Eq. 3-14}$$

$$\delta_i = \sum_r r^i R_r ON_x \qquad \text{Eq. 3-15}$$

$$\mu_i = \sum_r r^i P_r \qquad \text{Eq. 3.16}$$

Once the mass balance equations for polymer molecules of the three types and for all lengths are derived, based on the reaction mechanism outlined above, the application of the method of moments produces the following equations for moments zero, one and two, respectively, of living polymer radicals (Equations 3-17 through 3-19), dormant polymer (Equations 3-20 through 3-22), and dead polymer (Equations 3-23 through 3-25).

$$\frac{d(\lambda_0)}{dt} = k_p[M]([D^{\cdot}] + [M^{\cdot}] + [R_{in}^{\cdot}]) - k_t[\lambda_0]^2 - k_{da}[NO_x^{\cdot}][\lambda_0] + k_a[R_r NO_x]$$
$$- k_{fM}[M][\lambda_0] - k_{fD}[D][\lambda_0] + k_a[\delta_0] \qquad \text{Eq. 3-17}$$

$$\frac{d(\lambda_1)}{dt} = k_p[M]([D^{\cdot}] + [M^{\cdot}] + [R_{in}^{\cdot}] + [\lambda_0]) - k_t[\lambda_0][\lambda_1] - k_{da}[NO_x^{\cdot}][\lambda_1]$$
$$- k_{fM}[M][\lambda_1] - k_{fD}[D][\lambda_1] + k_a[\delta_1] \qquad \text{Eq. 3-18}$$

$$\frac{d(\lambda_2)}{dt} = k_p[M]([D^{\cdot}] + [M^{\cdot}] + [R_{in}^{\cdot}] + [\lambda_0] + 2[\lambda_1]) - k_t[\lambda_0][\lambda_2]$$

$$- k_{da}[NO_x^{\cdot}][\lambda_2] - k_{fM}[M][\lambda_2] - k_{fD}[D][\lambda_2] + k_a[\delta_2]$$

<div align="right">Eq. 3-19</div>

$$\frac{d(\delta_0)}{dt} = k_{da}[NO_x^{\cdot}][\lambda_0] - k_a[\delta_0]$$

<div align="right">Eq. 3-20</div>

$$\frac{d(\delta_1)}{dt} = k_{da}[NO_x^{\cdot}][\lambda_1] - k_a[\delta_1]$$

<div align="right">Eq. 3-21</div>

$$\frac{d(\delta_2)}{dt} = k_{da}[NO_x^{\cdot}][\lambda_2] + k_a[\delta_2]$$

<div align="right">Eq. 3-22</div>

$$\frac{d(\mu_0)}{dt} = \frac{1}{2}k_{tc}[\lambda_0]^2 + k_{td}[\lambda_0]^2 + k_{fM}[M][\lambda_0] + k_{fD}[D][\lambda_0]$$

<div align="right">Eq. 3-23</div>

$$\frac{d(\mu_1)}{dt} = k_{tc}[\lambda_0][\lambda_1] + k_{td}[\lambda_0][\lambda_1] + k_{fM}[M][\lambda_1] + k_{fD}[D][\lambda_1]$$

<div align="right">Eq. 3-24</div>

$$\frac{d(\mu_2)}{dt} = k_{tc}([\lambda_0][\lambda_2] + [\lambda_1]^2) + k_{td}[\lambda_0][\lambda_2] + k_{fM}[M][\lambda_2] + k_{fD}[D][\lambda_2]$$

<div align="right">Eq. 3-25</div>

Finally, calculation of the number average (given by Equation 3-26) and weight average (given by Equation 3-27) molecular weights can be done based on the moments of the polymer populations, using the expressions shown below. The definition of the polydispersity index (PDI) as discussed in this thesis is given by Equation 3-28.

$$\overline{M}_n = MW_m\left(\frac{\mu_1 + \lambda_1 + \delta_1}{\mu_0 + \lambda_0 + \delta_0}\right)$$

<div align="right">Eq. 3-26</div>

$$\overline{M}_w = MW_m\left(\frac{\mu_2 + \lambda_2 + \delta_2}{\mu_1 + \lambda_1 + \delta_1}\right)$$

<div align="right">Eq. 3-27</div>

$$PDI = \left(\frac{\overline{M}_w}{\overline{M}_n}\right)$$

<div align="right">Eq. 3-28</div>

3.4   Solution of System of Equations in MATLAB

Mathworks' MATLAB® was the software used in the computational solution of this system of equations. Gear's method was implemented for the solution, as the system is stiff. The model (prediction) profiles for the batch nitroxide-mediated radical polymerization of styrene were generated for a variety of different operating conditions, and compared against empirical data in the group as well as from elsewhere in the literature.

3.4.1   Comparison to Data – Bimolecular Case

The model profiles produced from the solution of the equations of the fully mechanistic model (FMM) of sections 3.2 and 3.3 were then compared to experimental data from Nabifar ([1], [5]) in our group. The data used for the generation of this plots is available in Appendix A. Figure 3-1 shows the modeled bimolecular conversion profile compared with data at reaction conditions T = 130 °C, and R = [TEMPO]/[BPO] = 1.1, which will be considered the base case for this discussion.
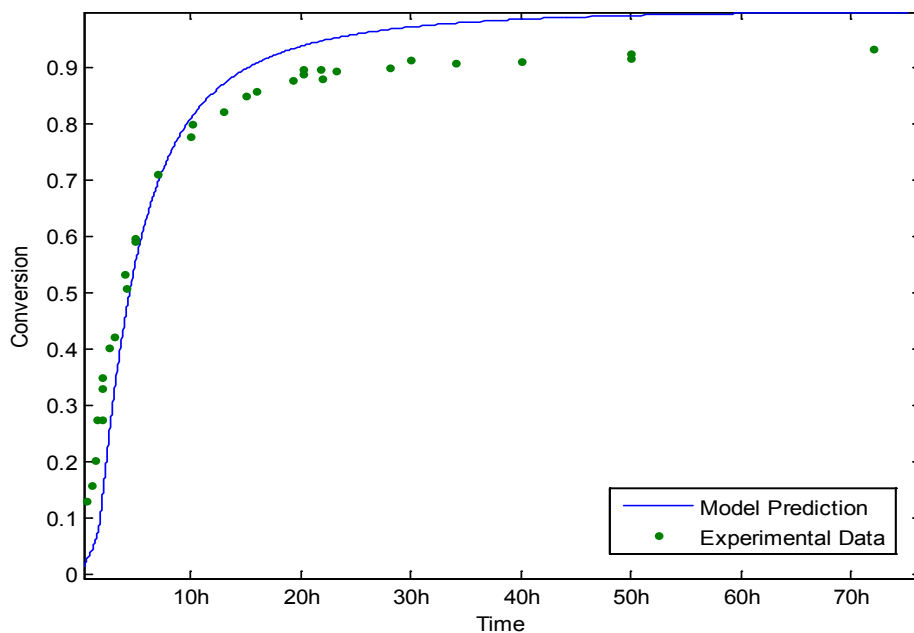
Figure 3-1 – Comparison of model conversion profile with experimental data (T= 130 °C; R = 1.1)

It is seen from Figure 3-1 that the FMM model slightly underestimates conversion in the earlier stages, but then crosses and overestimates the data after about 9h or 70% conversion. This is in agreement with prior work utilizing a similar model, including that of Roa-Luna et al. [5]. Looking now at Figure 3-2, which shows the predicted $\ln([M_0]/[M])$ versus what was obtained experimentally, again, under-prediction (even if slight) is seen in the early reaction stages, followed by larger overpredictions later. However, the simulated profile emulates better the expected theoretical shape that the graph should take (a straight line) in the event of instantaneous initiation and no termination. This may suggest that the model inaccurately provides for the initiation and termination steps of the process as actually occurred in the experimental cases, overestimating the impact of initiation to a small degree, and underestimating that of termination by a much larger one, when compared to the data.
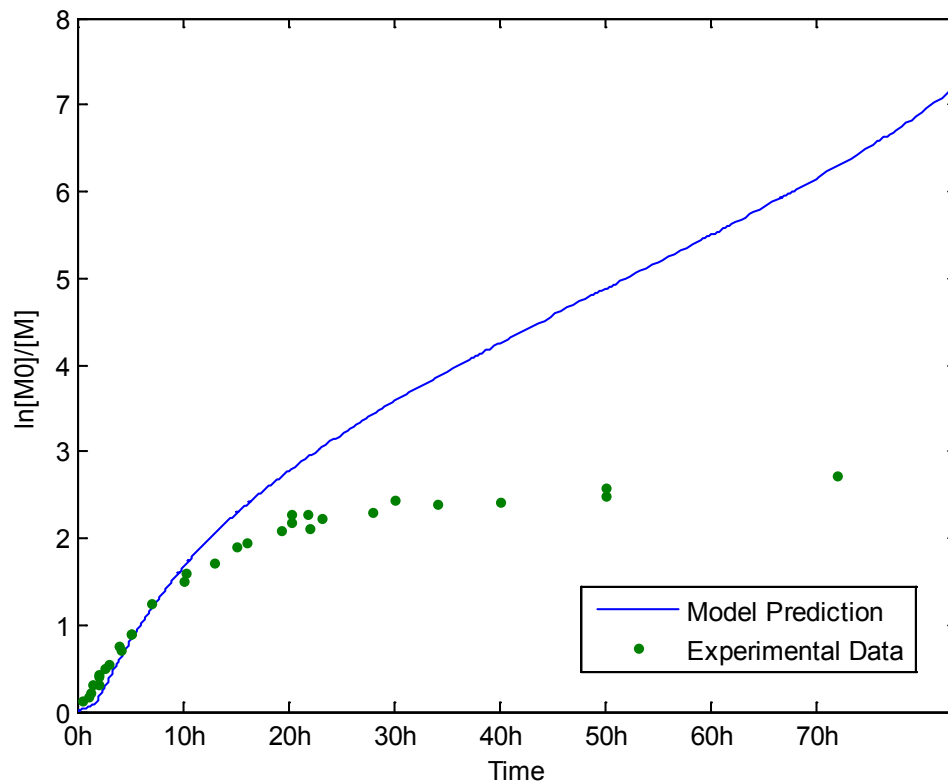
Figure 3-2 – $\ln([M_0]/[M])$ versus time profile compared to experimental data (T= 130 °C; R = 1.1)

28
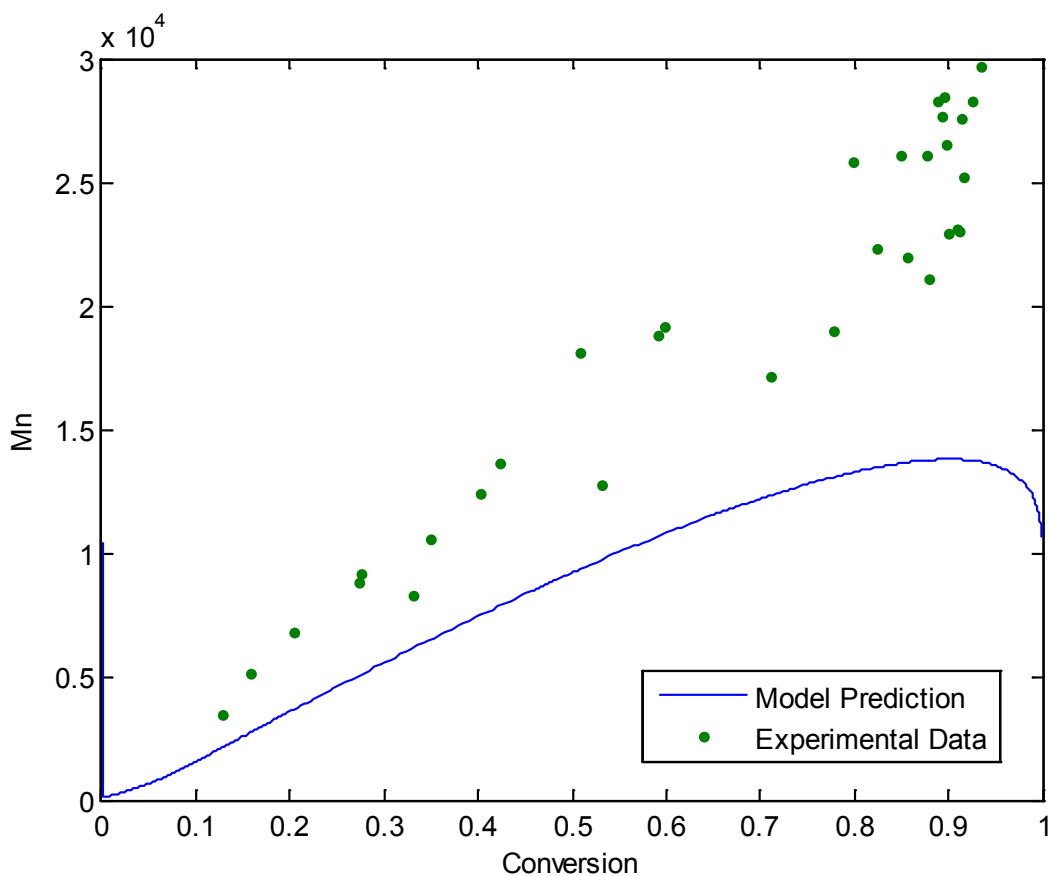
Figure 3-3 Number average molecular weight vs. conversion profile compared to experimental data (T= 130 °C; R = 1.1)

Figure 3-3 shows the predicted versus actual number average molecular weight (M_n) at the same reaction conditions. From this it is seen that the FMM prediction that is made for M_n is substantially lower, and grows less quickly, than the data. The simulated Mn actually begins to decrease at very high conversions, according to the profile, which should not be the case. From here on, the symbols M_n and M_w, used to represent number average and weight average molecular weights, respectively, refer to cumulative (accumulated) molecular weight averages (and not instantaneous ones).
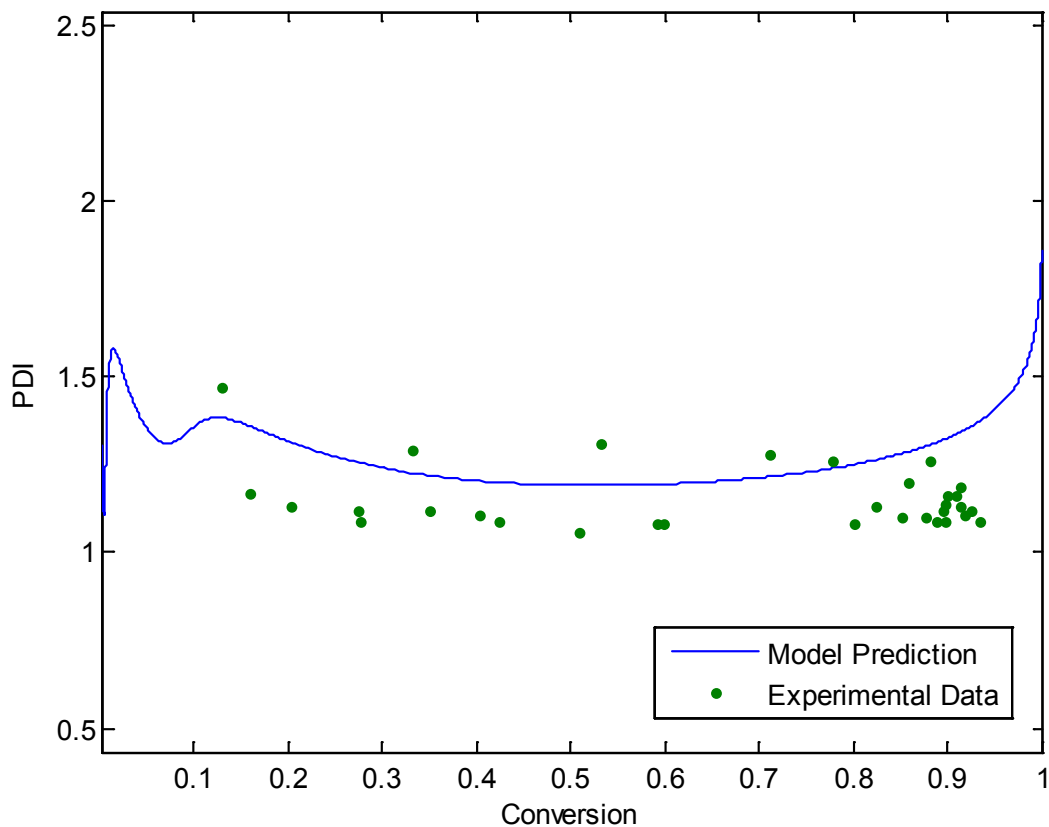
Figure 3-4 PDI vs. conversion profile compared to experimental data (T= 130 °C; R = 1.1)

The PDI prediction (Figure 3-4) is somewhat more acceptable when compared to the data, though it appears to be near the top of the data range, with the majority of points below. This suggests that the prediction may be slightly higher than it optimally should be. Also, the anomalous decrease in number average molecular weight, seen at high conversion, is also echoed here in the PDI profile.

3.4.2 Change in Temperature –Bimolecular Case

As mentioned in Nabifar [1], the equilibrium between active and dormant species is the defining reaction in NMRP. Since all of the rate constants are described as functions of temperature, temperature has a very important role in influencing this equilibrium. To this end, the simulation was run with different temperatures – and the effects on the generated

profiles were then examined to ensure that the model behaved as expected. Figure 3-5 shows the simulated versus experimental conversion for T = 120 °C, and [TEMPO]/[BPO] = 1.1, compared with experimental data. From this it is seen that the model still provides a similar fit, as in the case with T= 130 °C; R = 1.1, with an underestimation at lower conversion, shifting to an overestimation at higher conversion.
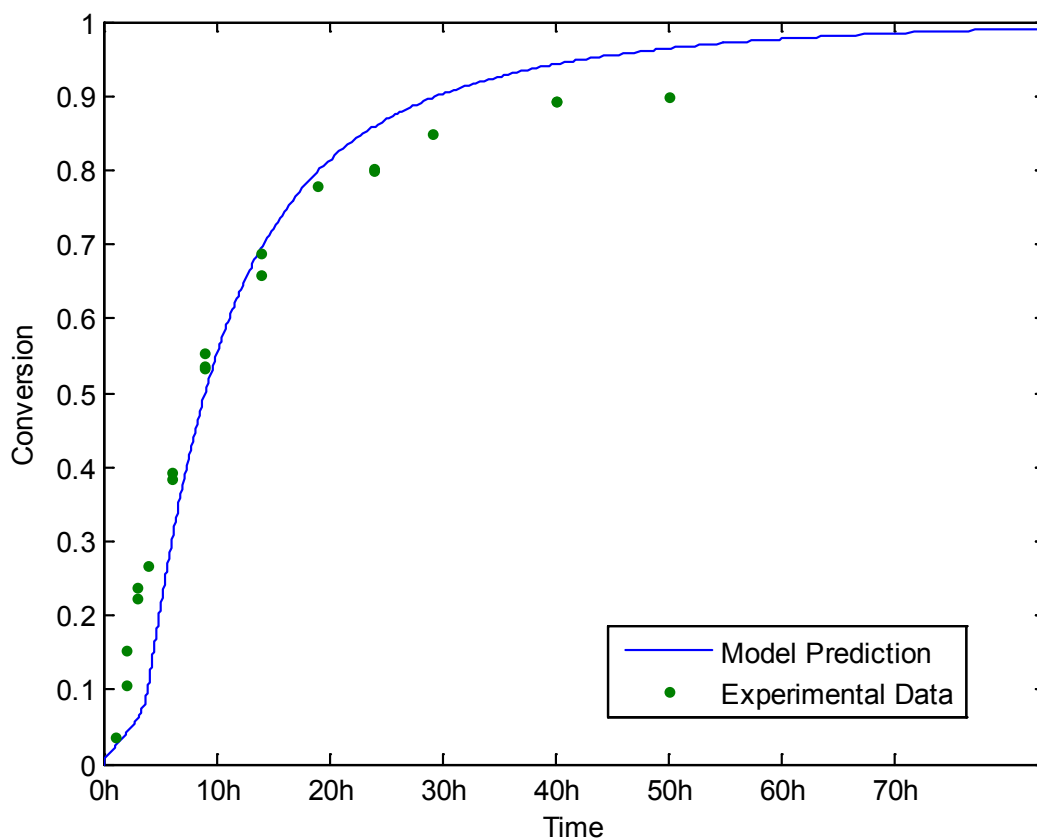
Figure 3-5 - Conversion vs. Time for T =120 °C, R = 1.1

The generated polydispersity index (PDI) profile, illustrated in Figure 3-6, again shows relatively good agreement with the experimental data, though there are a couple of anomalous regions at the two extremes of high and low conversion. However unlike with the higher temperature setting, the predicted PDI is never seen to be as low as that obtained through experimentation (some of the data points were above the predicted PDI at the higher temperature setting (see Figure 3-4)).
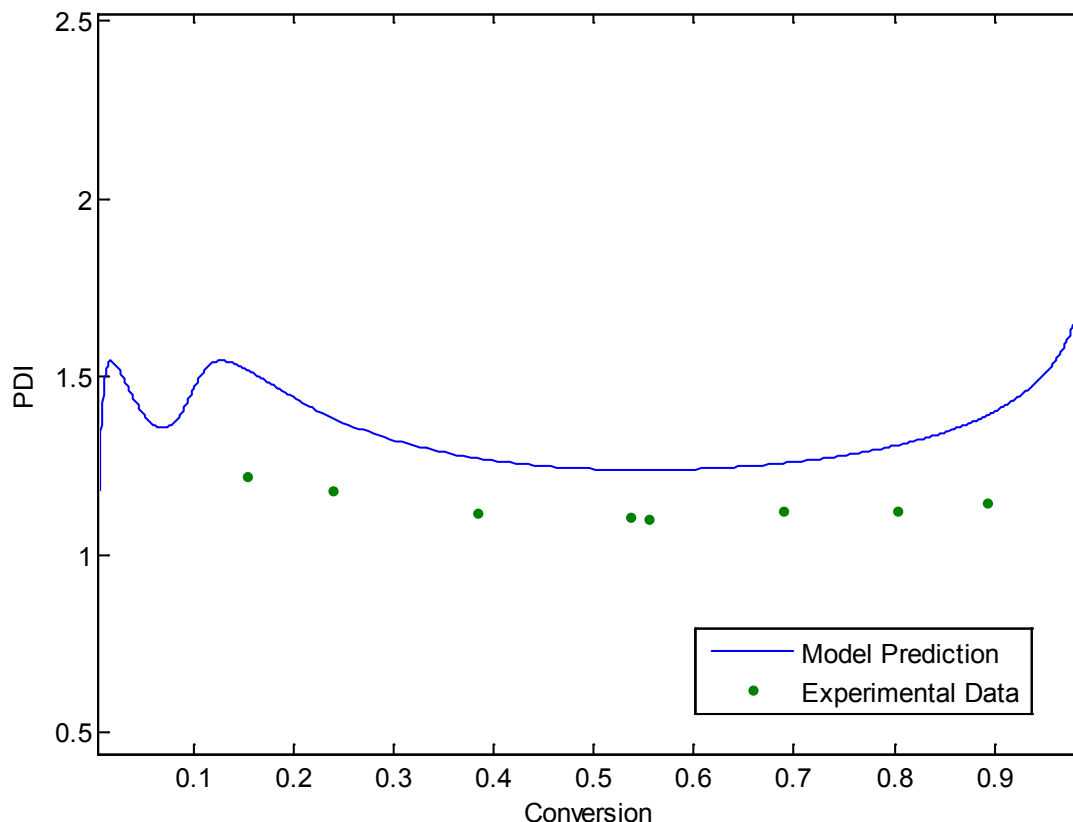
Figure 3-6 - PDI vs Conversion for T = 120 °C, R = 1.1

The conversion profiles generated showed faster conversion with higher temperature, as well as decreasing lag in the initiation phase, as shown in Figure 3-7. When looking at the M_n profile (Figure 3-8), the nonlinearity seen earlier was observed to be more severe at lower temperature, and less severe as temperature increased. Additionally, the rate at which the M_n increased was seen to be faster with higher temperature, as expected – this is depicted in Figure 3-8. This contrasts with typical free radical polymerization, where this decrease of MW would be the opposite of what was expected, as the temperature increase has a strong impact on the rates of the key reaction of NMRP, where the nitroxide radical binds and unbinds with the developing radicals during the propagation phase of this process. Equation 5-13, as discussed later in this thesis, describes this relationship.

32
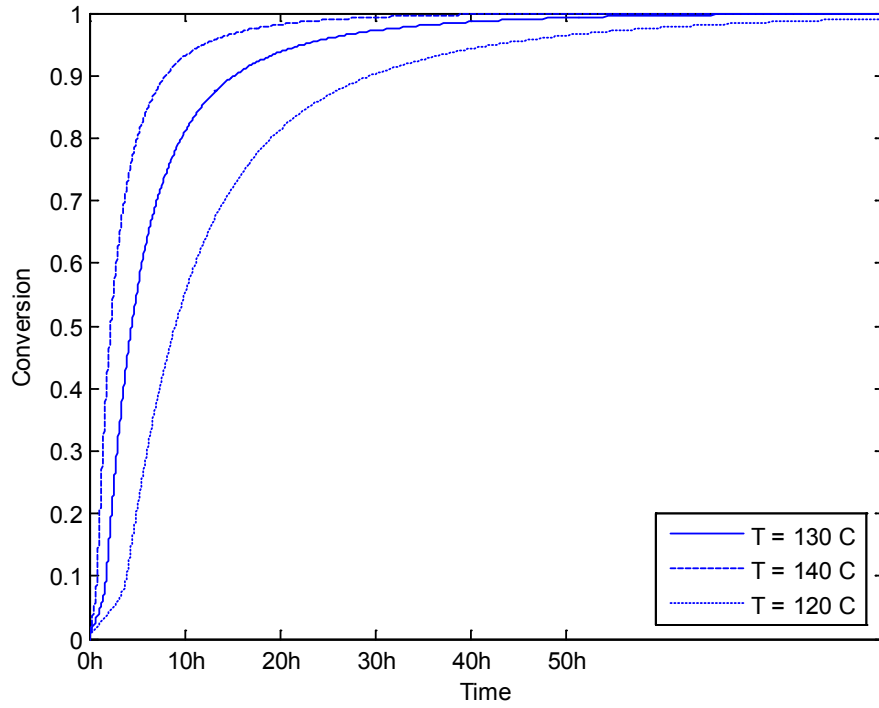
Figure 3-7 - Impact of change in temperature on simulated profiles, R = 1.1
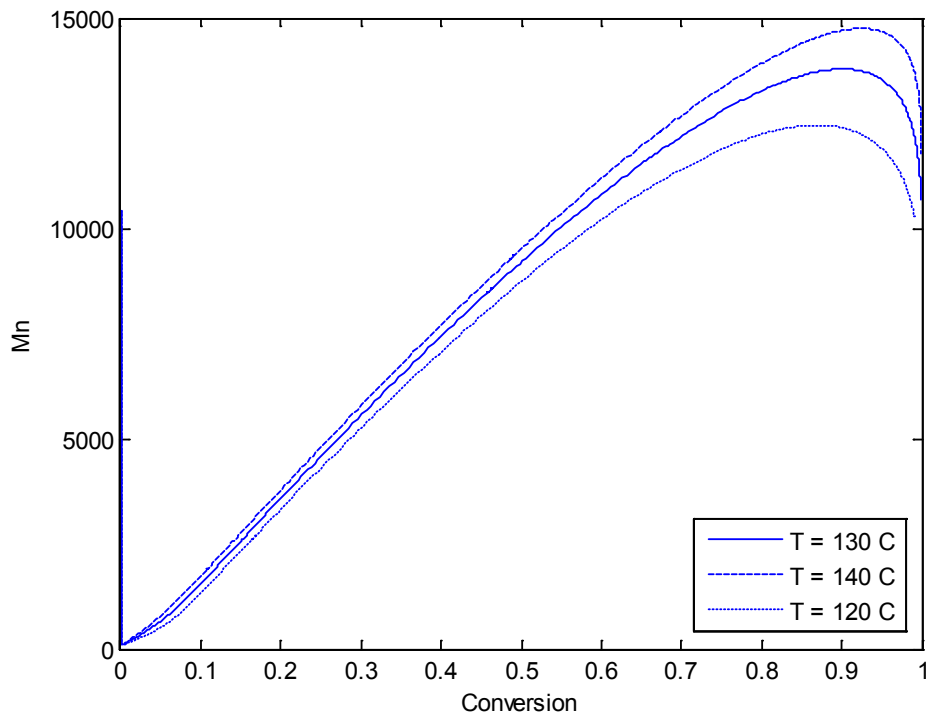
Figure 3-8 - Impact of change in temperature on $\underline{M}_n$ profiles, R = 1.1

33
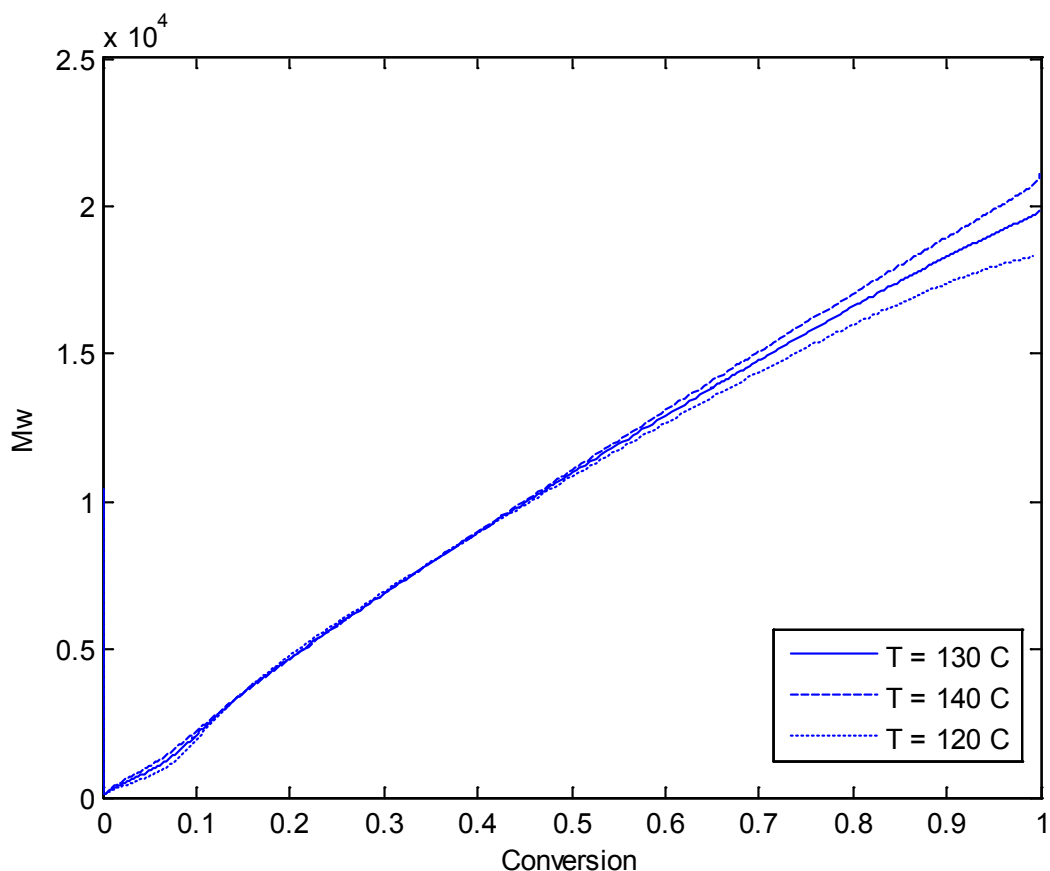
Figure 3-9 - Impact of change in temperature on $\underline{M}_w$ profiles, R = 1.1

Similar trends were seen in the plot of M_w versus conversion, as depicted in Figure 3-9 – though nonlinearities, especially at high conversion levels, appear to a lesser extent than in the M_n. This leads to somewhat lower PDI predictions with lower temperature – as shown in Figure 3-10, which depicts the impact of temperature change on PDI profiles. The simulation indicates that lower PDI values are obtained when the reaction takes place under higher temperatures.
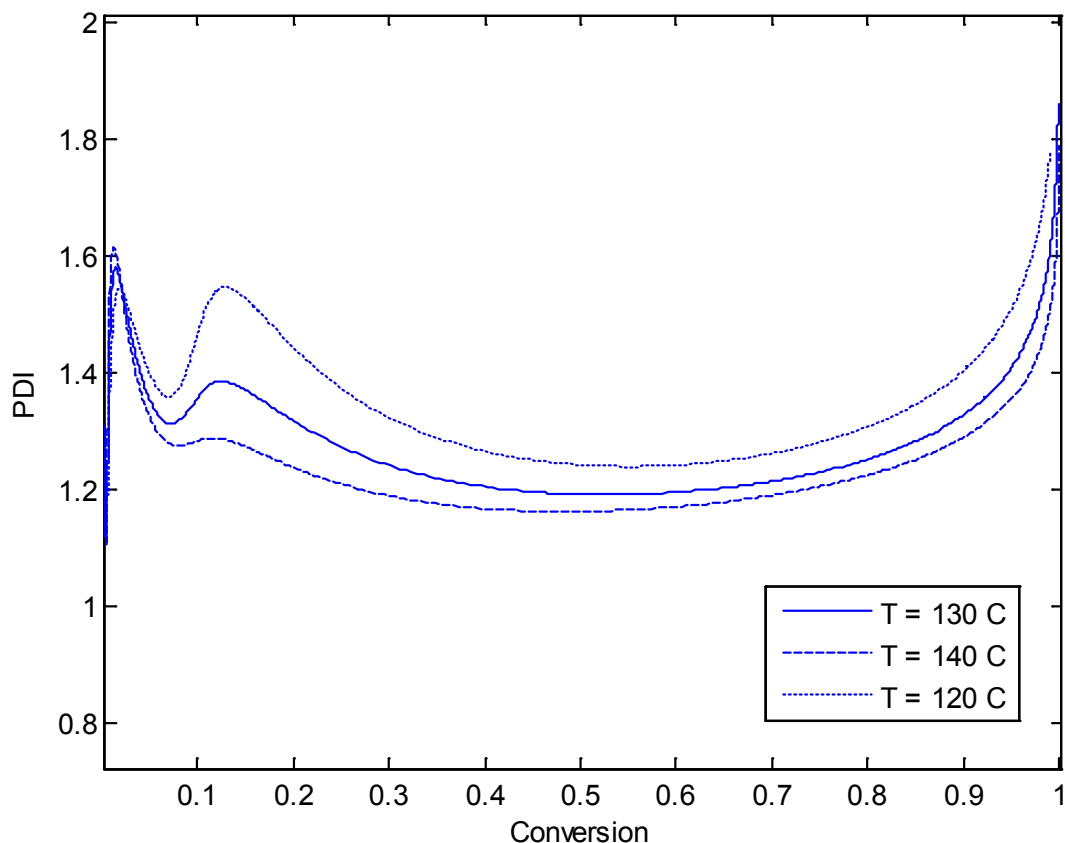
Figure 3-10 – Effects of changing T on PDI profiles, R = 1.1

3.4.3   Effect of [TEMPO]/[BPO] Ratio – Bimolecular Case

The other major factor that influences this reaction is the [TEMPO] to [BPO] ratio (referred to as R), as the concentrations of these species directly influence the concentrations of dormant and active species, respectively.   For this reason it is important to note the effects of varying this ratio, and that the model responds appropriately in this regard. Deviating from our previously discussed R = 1.1, Figure 3.11 shows the simulated conversion profile of T = 130 °C and R = 0.9 compared with data from Nabifar [1].
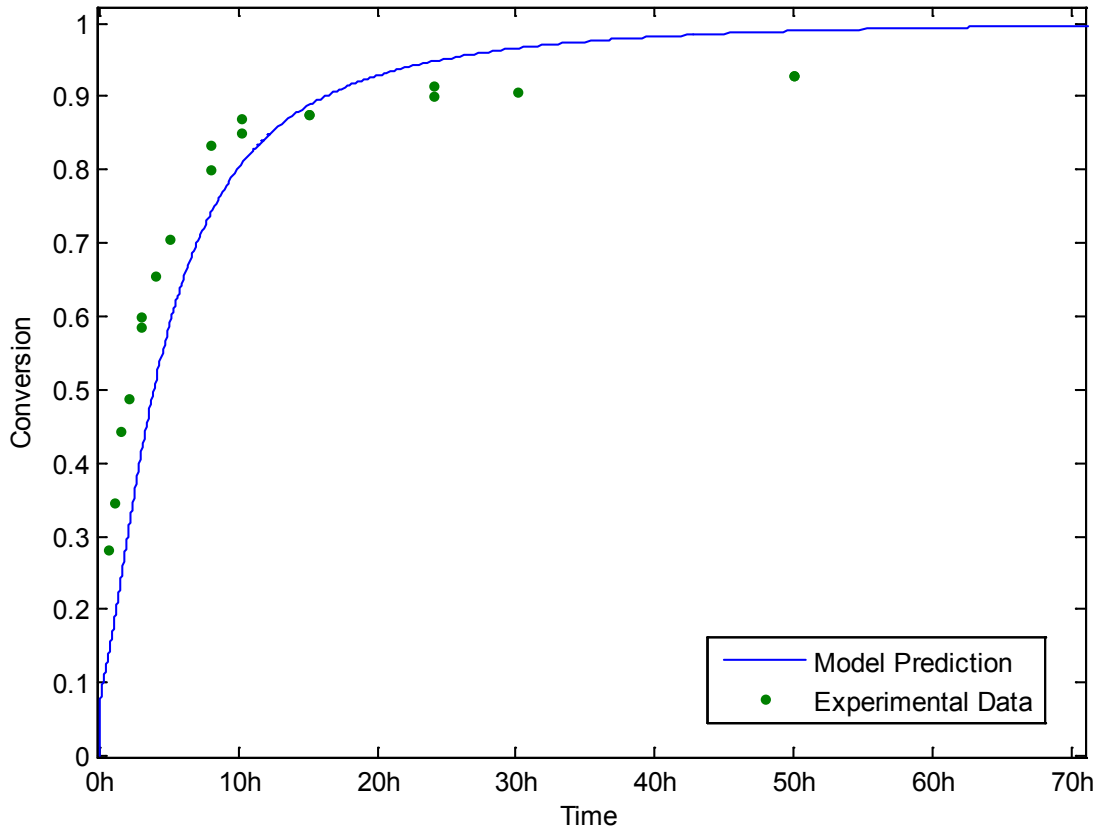
Figure 3-11 - Conversion vs. Time profile for T = 130 °C and R = 0.9

As can be seen, the same under- followed by over-estimation of the data is found, though the conversion at which the profile crosses the data points is seen to be somewhat higher. Figure 3.12 depicts the PDI profile in this case, which also can be seen to deviate from the experimental data at high conversion, as it did in the case with a higher R (see Figure 3-4).
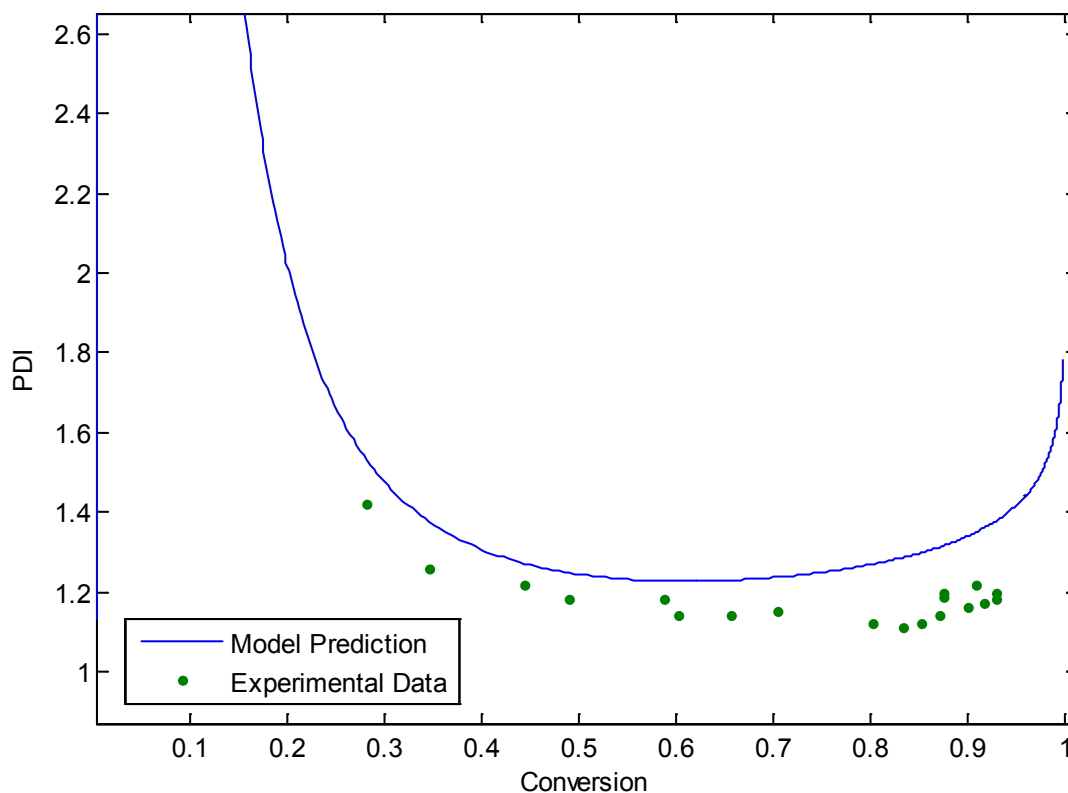
Figure 3-12 - PDI vs. Conversion for T = 130 °C and R = 0.9

Next, the effects of varying the ratio on the model predictions were investigated. Figure 3-13 shows the conversion profiles with both higher and lower R values than our base case (R = 1.1). As expected, increasing the amount of controller present slows down the overall conversion. The lag seen at the beginning with higher controller values is due to that more of the initiator is 'tied up' by the controller, so less of it is free to react with the monomer, which is the primary reason for the slower rate of change of conversion overall. This results in slower MW development as shown in Figures 3-14 and 3-15 for M_n and M_w, respectively. The impact on the PDI profile is seen to be larger at low conversion, with all the profiles ending up in quite close agreement at high conversion, as seen in Figure 3-16.
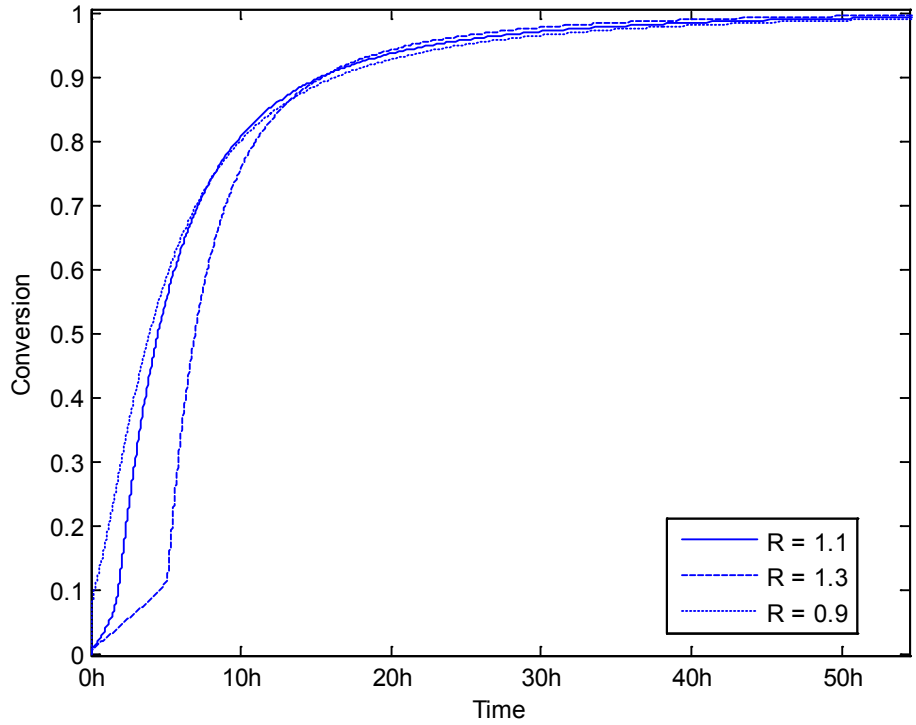
Figure 3-13 – Effect of varying R on conversion-time profile, T = 130 °C
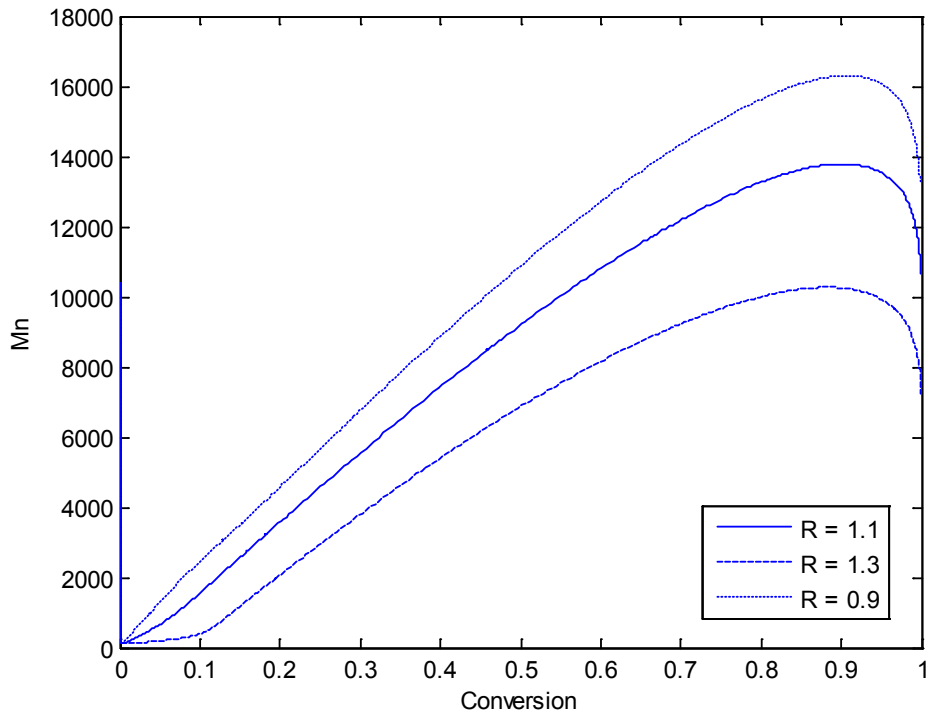
Figure 3-14 - Effect of varying R on $\underline{M}_n$-conversion profile, T = 130 °C
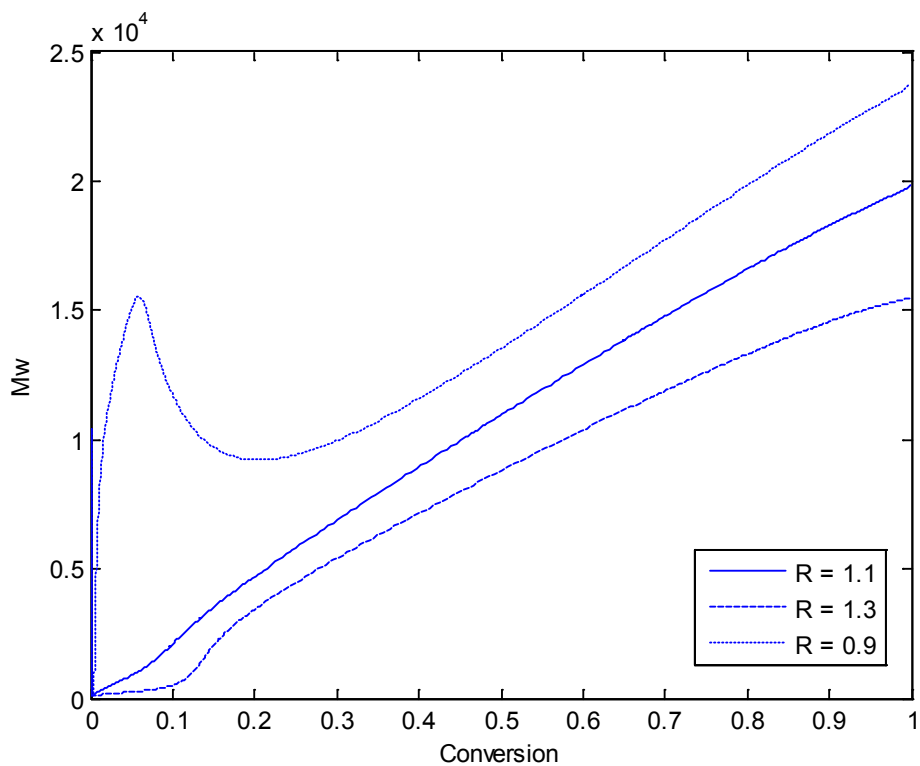
Figure 3-15 - Effect of varying R on Mw-conversion profile, T = 130 °C
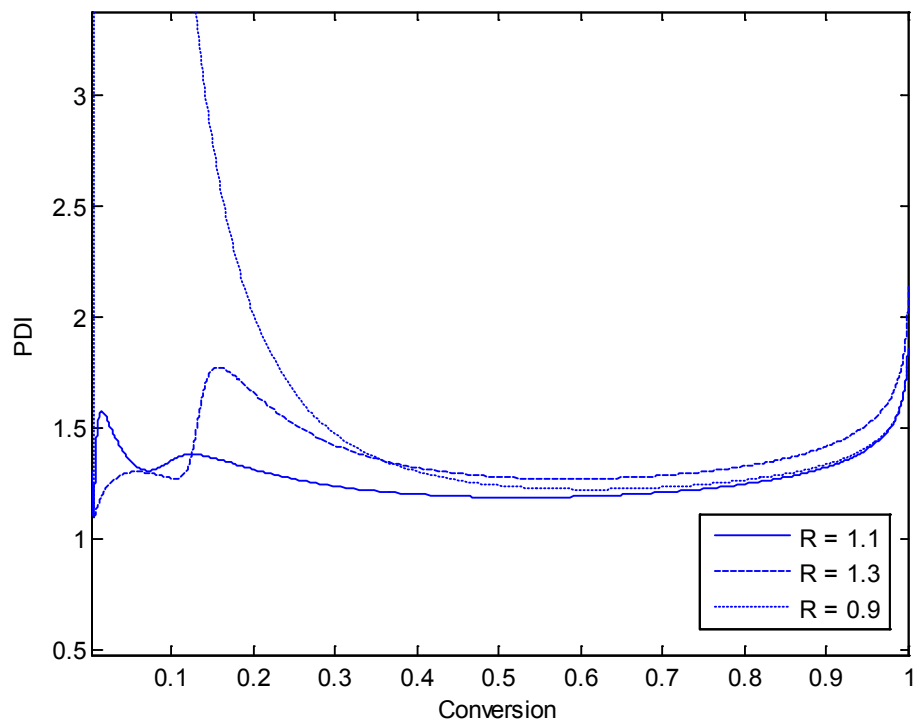
Figure 3-16 Effect of varying R on PDI-conversion profile, T = 130 °C

39

3.5   Unimolecular Case

The simulation for the unimolecular case was then compared with data from another researcher in our group, Michelle Zhou [6].   Figure 3-17 illustrates the simulated conversion versus time profile against experimentally obtained data using a unimolecular initiator (an alkoxyamine made by combining BPO and TEMPO) at 120 °C with initial initiator concentration of 0.050 mol/l. As in the bimolecular case, good prediction at low to medium conversion gives way to overestimation at later stages. In this particular profile, the divergence appears to occur around 60% conversion or after about 10 hours of reaction, which is similar to the crossover point in the bimolecular case (See, for example Figure 3-1).
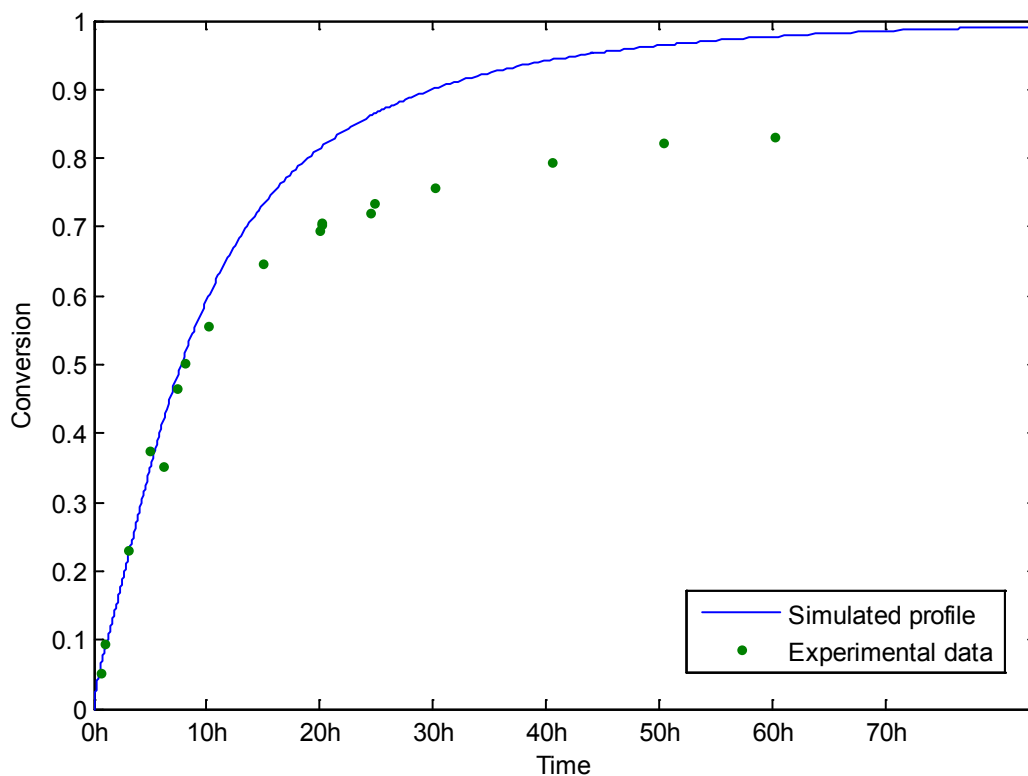
Figure 3-17 - Conversion vs. time profile compared with experimental data; Unimolecular case, T = 120 °C
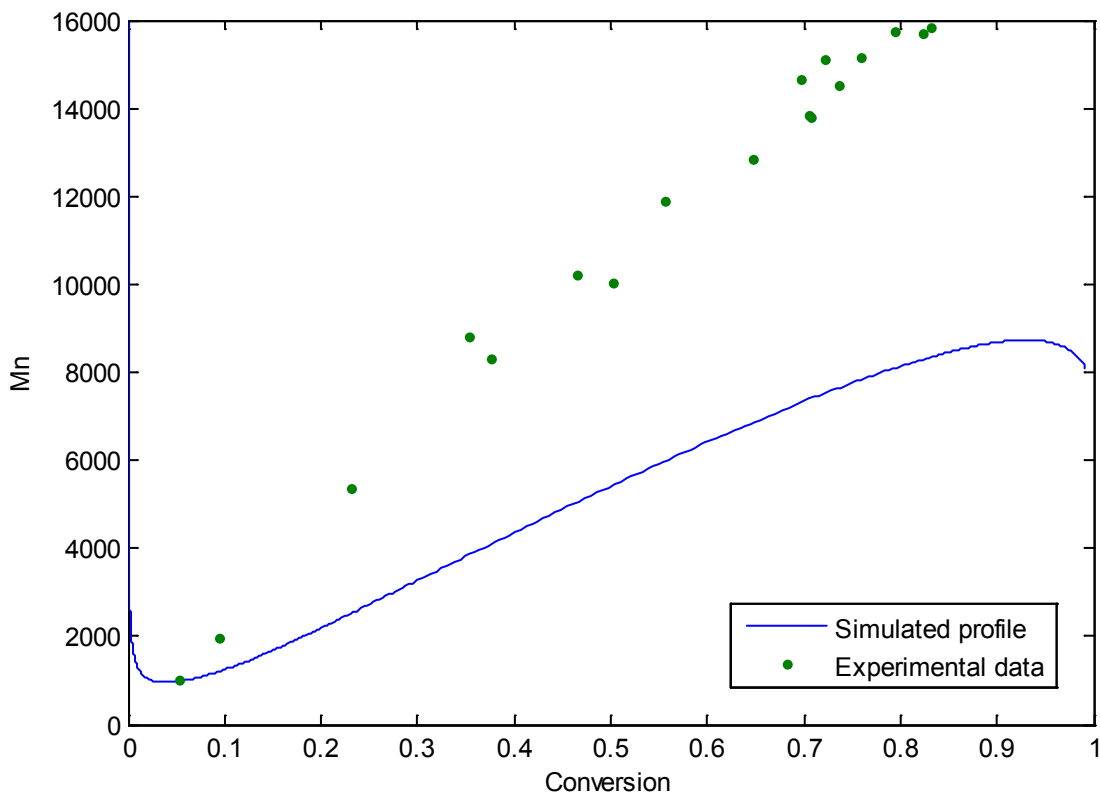
Figure 3-18 - Unimolecular M_n vs. conversion profile compared with experimental data; Unimolecular case, T = 120 °C

The unimolecular cumulative number average molecular weight versus conversion profile generated, as seen in Figure 3-18, starts off high at very low conversion, then falls rapidly before growing nearly linearly. However, the rate of growth shown by the simulation is much lower than that of the data, so the modeled profile tends to again diverge from the data points as conversion increases above 10%. The same decrease in number average molecular weight is again noted at high conversion levels (~95%) as in the bimolecular case (see, for example, Figure 3-3).
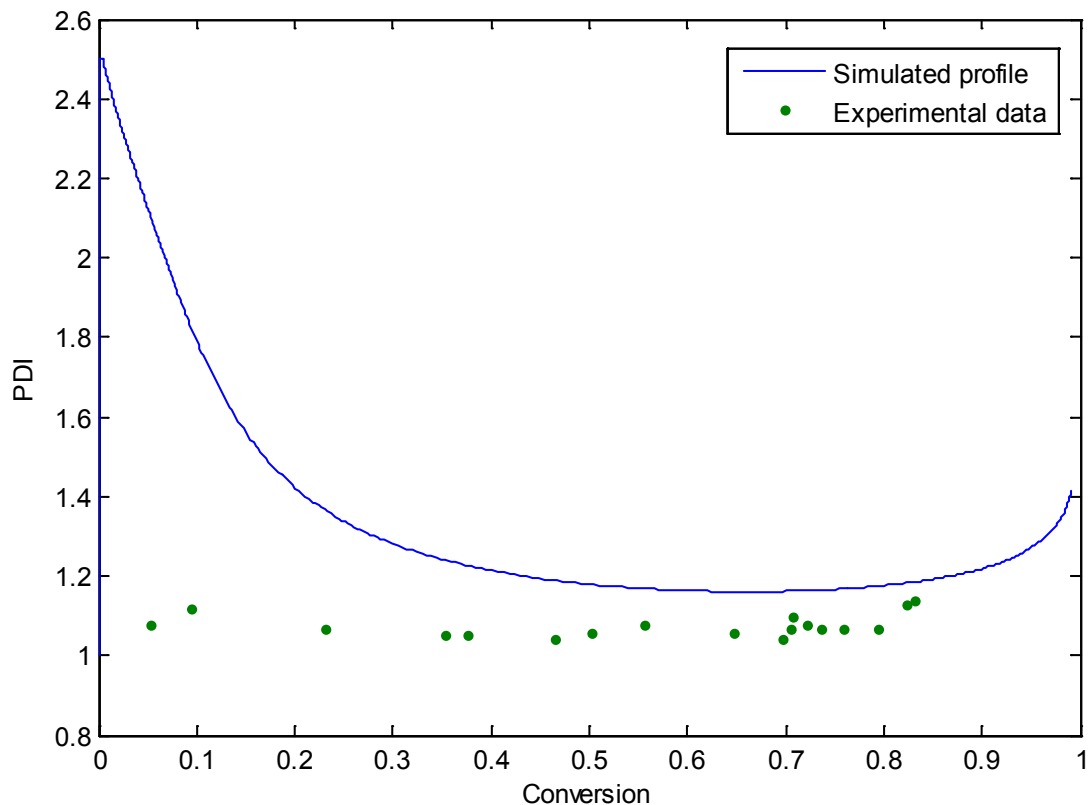
Figure 3-19 - Unimolecular PDI vs. conversion profile compared with experimental data, T = 120 °C

Figure 3.19 depicts the PDI versus conversion profile generated by this model. Starting very high at low conversion, the simulation gets reasonably close to the data as the conversion gets higher, but then again deviates at ultra-high conversion due to the upswing in the estimation of number average molecular weight. This matches the overall trends seen in the bimolecular case, as discussed previously.

3.6 Use of a Different Nitroxide Radical (TIPNO)

There has been interest in recent literature as far as comparing the use of additional controller types for styrene NMRP ([7], [8]). One such initiator, 2,2,5-tri-methyl-4-phenyl-3-azahexane-3-nitroxide, or TIPNO, was selected for such a comparison. TIPNO is important, because it allows for the NMRP of a wider range of monomers than TEMPO, as well as leading to faster polymerizations [7].

To this end, an investigation was conducted into the efficacy of the fully mechanistic model for this different controller radical. Some comparisons between the results and literature values (as well those obtained experimentally by other members of our group) are presented.

3.6.1 Changes Required

In order to use the FMM to model NMRP with TIPNO, some parameters needed to be established. The rate constants pertaining to BPO and styrene would not be impacted, however those for the very important steps involving the nitroxide controller would be. A literature search was conducted, and these values were obtained. The case involving the use of a TIPNO nitroxide radical is a unimolecular case, and so the results are most comparable to the unimolecular case as discussed in Section 3.5. The impacted rate constants are presented in Table 3-4, as calculated from the obtained equilibrium constant, K (defined as k_{a2}/k_{d2}), and activation rate constant, k_{a2}, values provided by Drache et al. [7].

Table 3-4 – Parameter changes required for use of FMM with TIPNO as controller, T = 120 °C [7]

Parameter	TEMPO Value	TIPNO Value
k_a , k_{a2}	6.165×10^{-4}	3.2×10^{-3}
k_{da} , k_{d2}	4.278×10^{7}	4.3×10^{5}

The differences in these values would suggest that the polymerization rate using the TIPNO mediator would be higher, as the ratio between the activation and deactivation rates (k_a and k_d) is greater.

3.6.2   Preliminary Assessment

Once these values were obtained, it was simply a matter of substitution into the FMM and solving. Preliminary results of this model are seen in Figure 3-20, which uses conversion data from the same paper where these parameter estimates were obtained from [7].
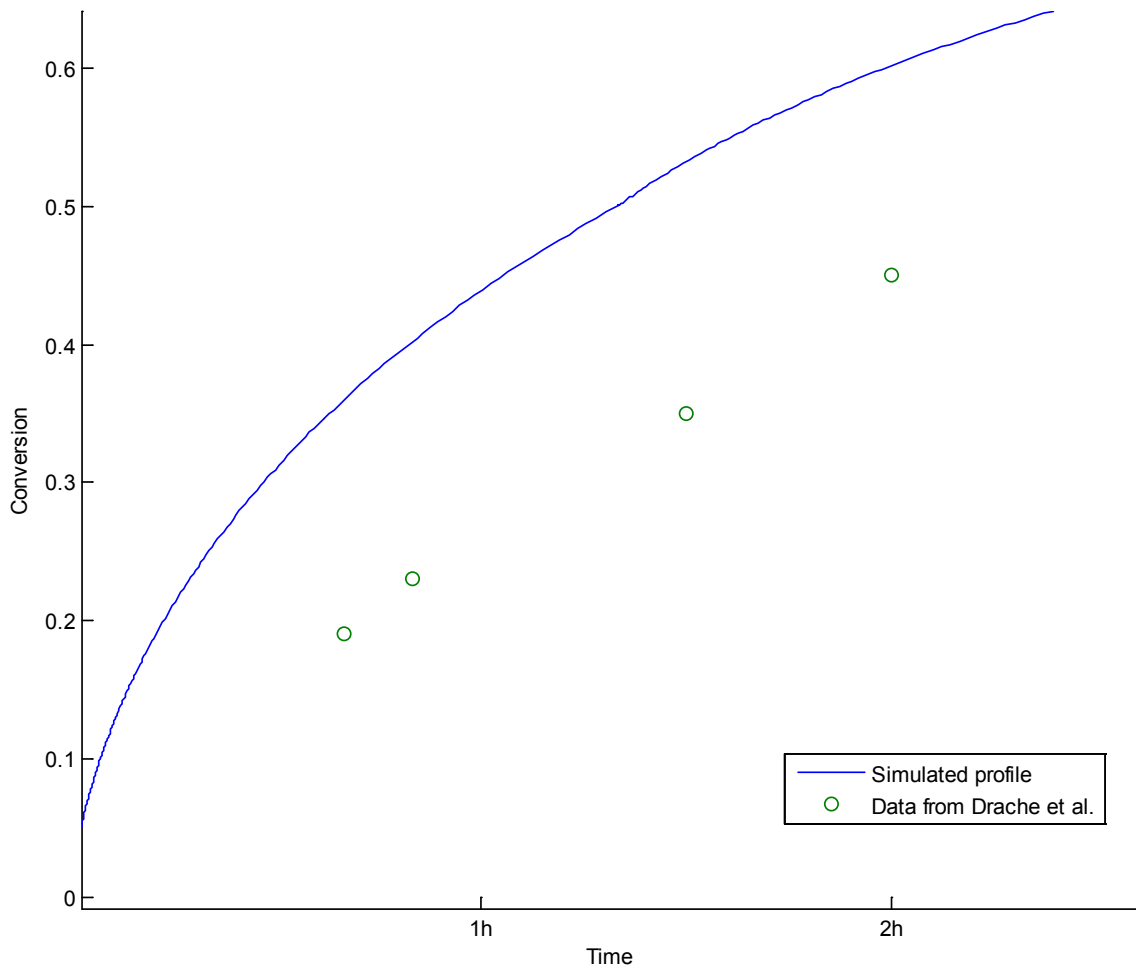
Figure 3-20 - Conversion vs. time profile compared with data from Drache et al. [7].

44

This figure shows relatively close agreement in trends between this model and the data upon which these parameter estimates were based, with somewhat higher conversion values being predicted than were obtained experimentally.
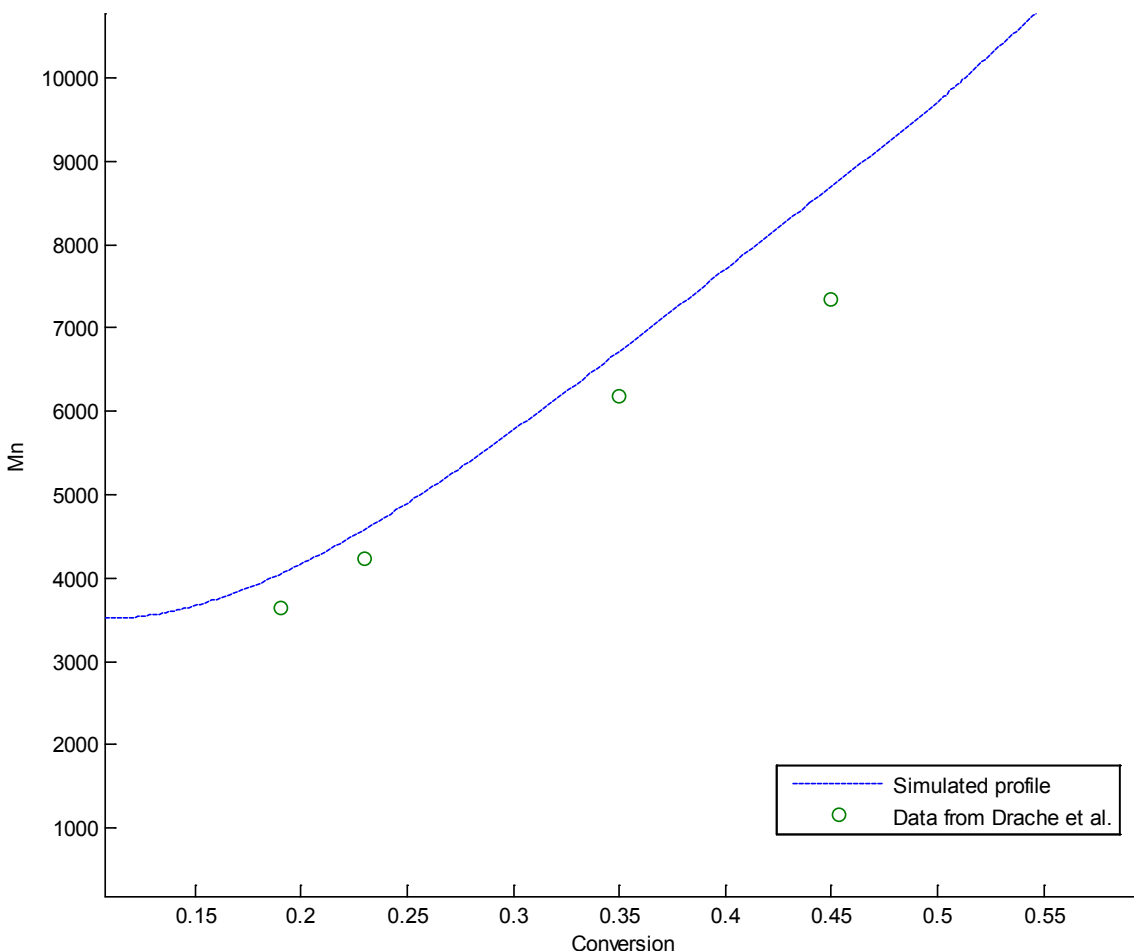
Figure 3-21 - Number average MW vs. Conversion profile compared with data from Drache et al. [7]

Figure 3-21 shows relatively good agreement between the $\underline{M}_n$ estimates obtained with this model and those provided by Drache et al. [7]. These results, however, are only for a quite narrow conversion range, so data over a wider range of values should be sought out for use in further analyses.

3.6.3   Comparison to More Experimental Data

Fortunately, more extensive data sets were available within our group, and therefore comparisons between model predictions and experimental data over a wider data range were possible. The results obtained from the solution of the FMM with these parameter changes were compared to experimental data using the TIPNO controller radical from Nabifar [9].   The profiles generated by the model show relatively good agreement with the experimental data, under relatively typical conditions for NMRP. The conversion profile generated by the FMM is shown compared to the experimental data in Figure 3-22.
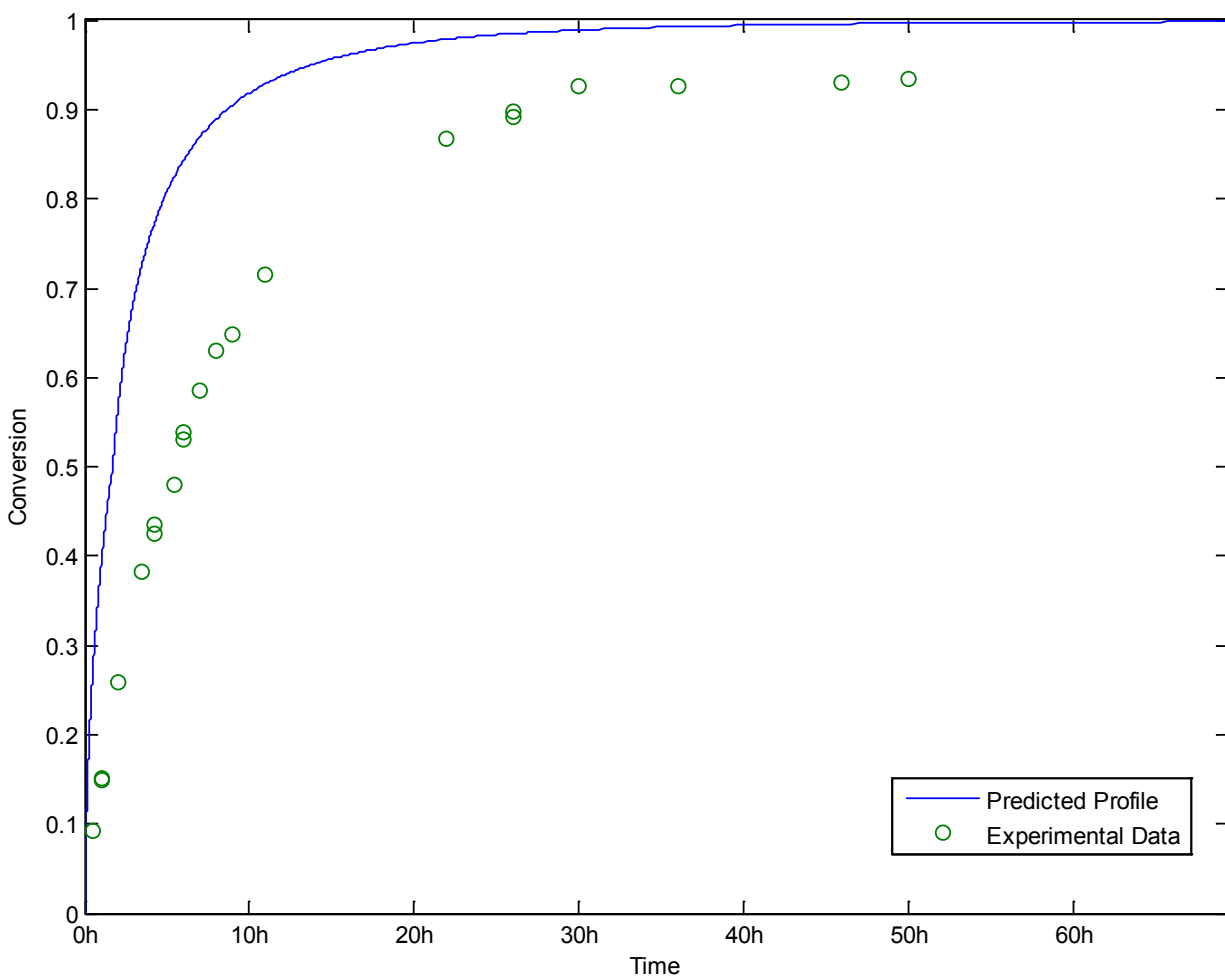
Figure 3-22 – Conversion profile versus experimental data for TIPNO, T = 120 °C

From this figure, it can be seen that the FMM's predictions are in reasonably good agreement with the experimental data when it comes to the conversion versus time profile for this case, however the conversion is estimated somewhat higher than the data supports throughout the time range.
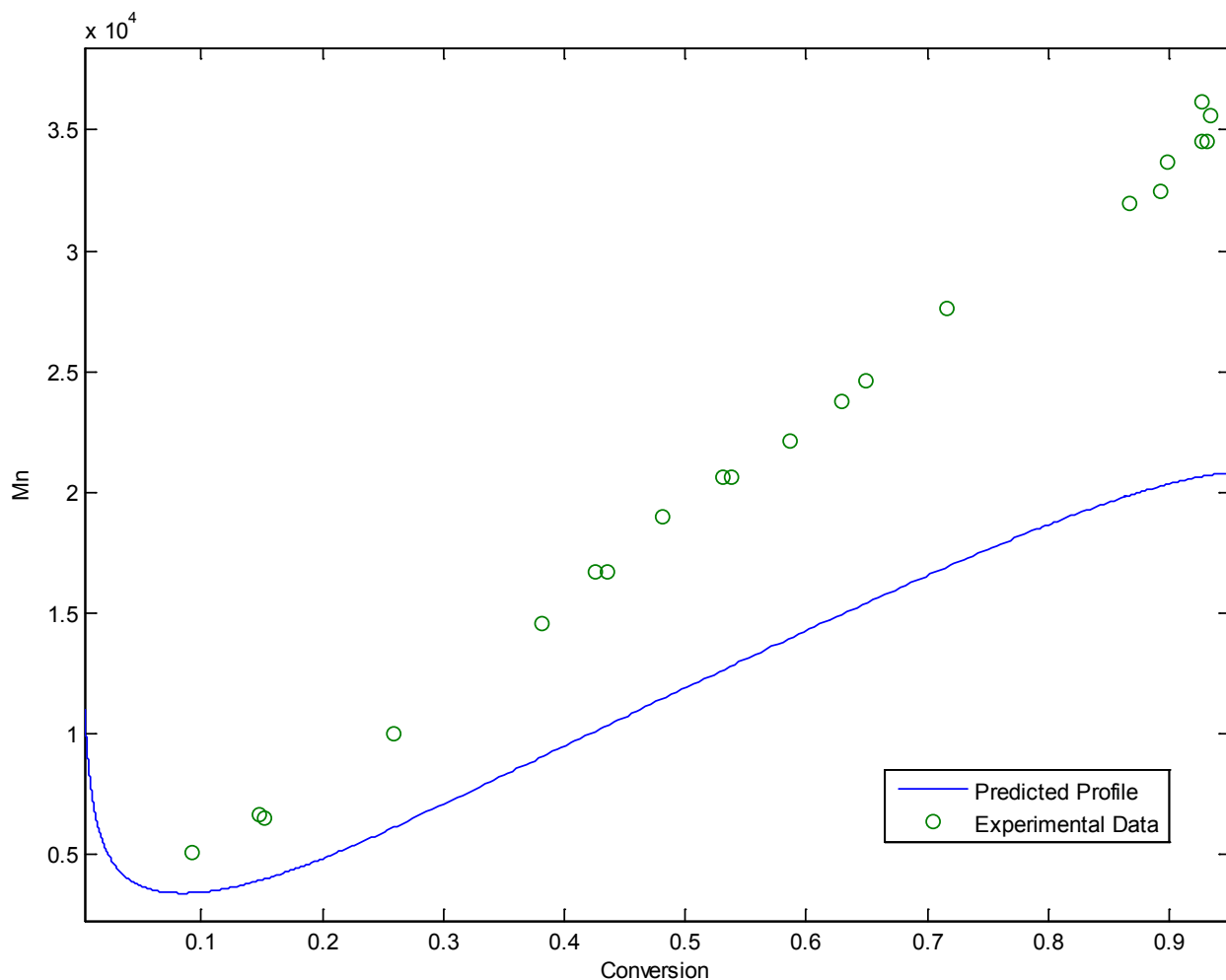
Figure 3-23 - Number Average MW profile versus experimental data for TIPNO, T = 120 °C

The cumulative number average molecular weight versus conversion profile generated for the TIPNO case, as seen in Figure 3-23, starts off high at very low conversion, then falls rapidly before growing nearly linearly. However, the rate of growth shown by the simulation is again much lower than that of the data, so the modeled profile tends to again diverge from the data points as conversion increases.

3.6.4   TIPNO vs. TEMPO

Certain differences were noted between the results from the TIPNO and TEMPO processes, and these will be discussed below. In general, and as was expected (due to the higher activation and deactivation rates), the rate of polymerization was seen to be higher than that when using TEMPO.
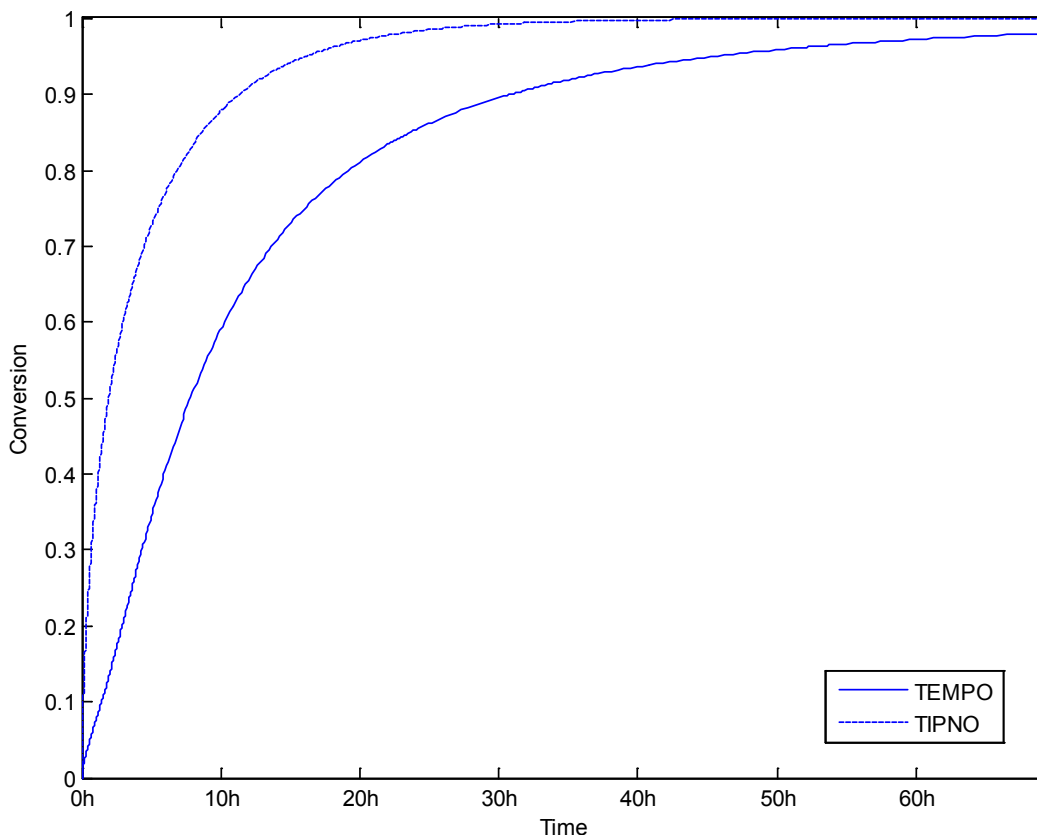
Figure 3-24 - Conversion profiles for unimolecular TIPNO and TEMPO cases, 120 °C

Figure 3-24 illustrates the conversion profiles predicted for both unimolecular TEMPO and TIPNO at 120 °C. From this, it can be seen that TIPNO is predicted to result in a faster rate of conversion (i.e., the monomer is consumed faster). The results predict that the TIPNO process will consume the entirety of the monomer significantly more quickly than the TEMPO process (after approximately 30 hours versus a significantly greater time of 70 or more hours). The overall trends of the profiles are seen to be in general agreement.

48
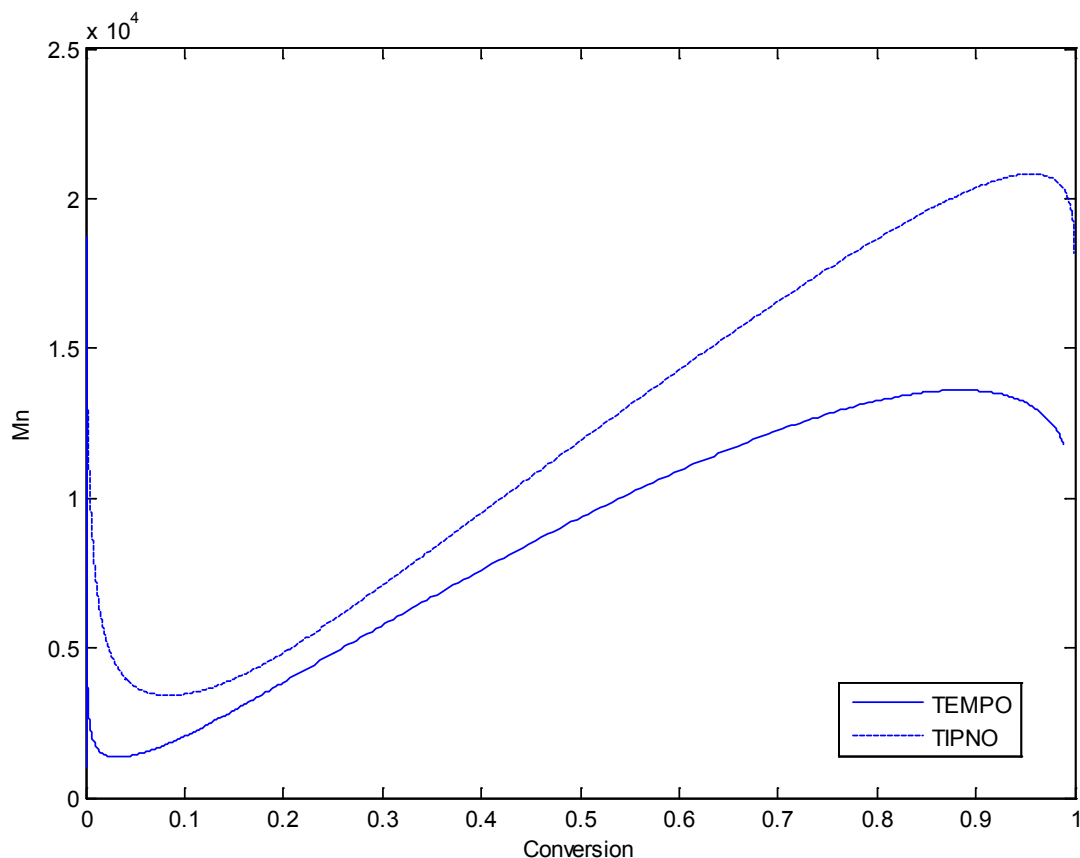
Figure 3-25 – Number average MW profiles for unimolecular TIPNO and TEMPO cases, 120 °C

Figure 3-25 illustrates the generated number average molecular weight profile for TIPNO versus that for TEMPO. As can be seen, the molecular weight develops more quickly for the modeled TIPNO process, which is to be expected as the monomer is being consumed much more rapidly. The same decrease in MW at very low and high conversions is seen in both cases, and the general trends are in agreement. In general, these differences were to be expected, as the equilibrium constant (K) when TIPNO is used is larger than when TEMPO is employed (see again Table 3-4).

3.7 Concluding Remarks

At this point, we have a functioning fully mechanistic model that captures the overall trends of styrene NMRP, with unimolecular and bimolecular TEMPO as well as unimolecular TIPNO controllers.

There is evident room for improvement as far as the model's ability to fit the obtained data. This is a very complex and difficult to solve model, involving a large, stiff system of differential equations that must be solved together with numerous Arrhenius equations for the various rate constants. What makes matters worse is the fact that many of these rate constant values are highly uncertain, as they are arrived at usually by guessing rather than formal parameter estimates based on experimental data. Overall, however, the model trends upon first use seem quite satisfactory.

Therefore, from this point, two main priorities are clear: model refinement and model reduction – that is improving the predictive power and reducing the amount of computation required to generate model profiles. Chapter 4 will deal with the first goal, of model refinement – seeking to improve the agreement between these models and the experimental data. The goal of a more simplified model will be addressed in Chapter 5.

Chapter 4: Mechanistic Model Refinements and Updates

This chapter will focus on the details of the various efforts that were taken in an attempt to improve the mechanistic model outlined in Chapter 3. As was noted in section 3.4, the trends seen were overall satisfactory, and the model made generally reasonable predictions in many cases, but there was definite room for improvement.

4.1 Efficiency Factors

An investigation into the impact of radical efficiency was conducted. The previous modeling effort incorporated the typical efficiency factor (f) for the initiator, but it was felt that the implementation of an analogous factor for the controller would likely make sense, and that the tuning of these factors could improve model fit.

4.1.1 Investigation of Controller Efficiency (f_c)

Experimentalists in the literature have alluded to the controller participating in side reactions other than coupling with the initiator radical and forming the dormant species. Through the introduction of a controller efficiency factor, f_c – analogous to the well-accepted initiator efficiency, f – which can be defined as the controller fraction able to produce dormant species, improvements to model fit can be made. Murari et al. [1] analyzed different combinations of these f and f_c values, concluding that the optimal combination is f = 0.37 and fc = 0.70 (giving better model fits). This combination as well as others were investigated. Figure 4.1 illustrates the impact of these optimal settings from Murari et al. on the conversion profile against our bimolecular base case from section 3.4 – T = 130 °C and R = 1.1. As in Chapter 3, the experimental data from Nabifar [2] are used for the bimolecular process. For the purposes of this effort, the data is assumed to be accurate, as the experimentation was well-designed with many replicates.

As can be seen from this Figure, there is little impact on the conversion profile from the implementation of this parameter. The conversion profile still follows the same shape, just slightly lagging the curve of the profile without the f_c term.
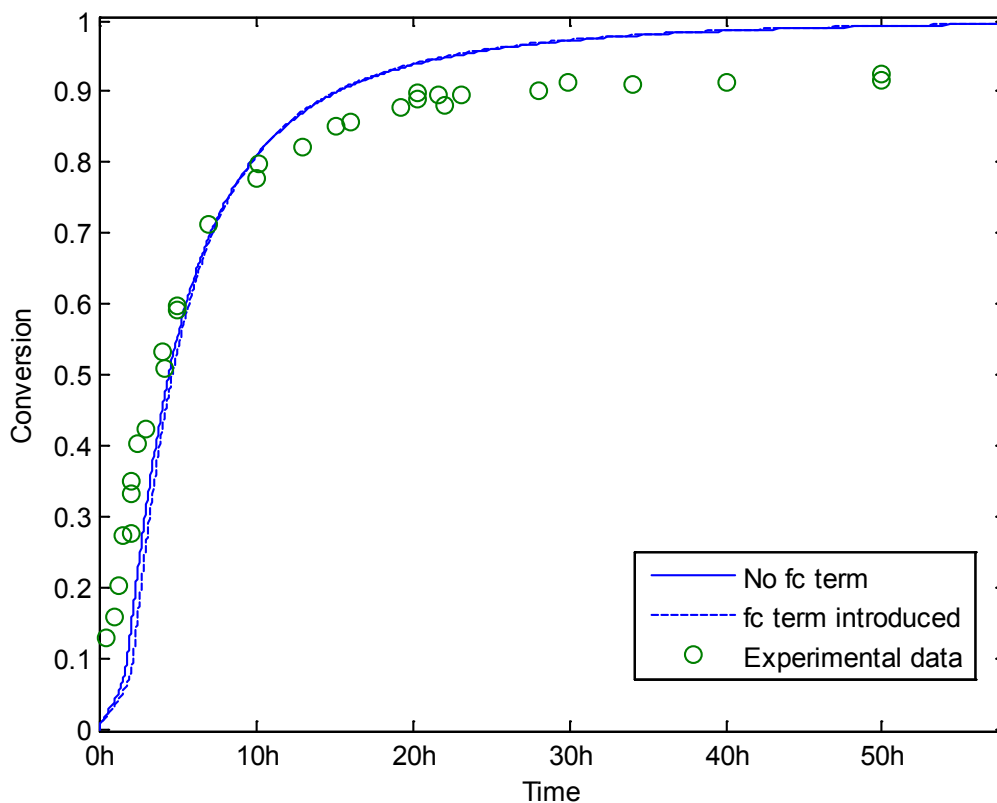
Figure 4-1 - Effect of f_c on conversion profile (T = 130 °C and R = 1.1)

However, much more important gains are seen in the average molecular weights, M_n and M_w, as shown in Figures 4-2 and 4-3, respectively. The generated number average molecular weight, M_n, profile is seen to be substantially closer to the experimental data with the introduction and optimization of this factor, though still retains the decrease at high conversions, deviating from the data points. The weight average molecular weight, M_w, sees a similar gain in fit to the data, though some more nonlinearity is now seen to be present in the profile.
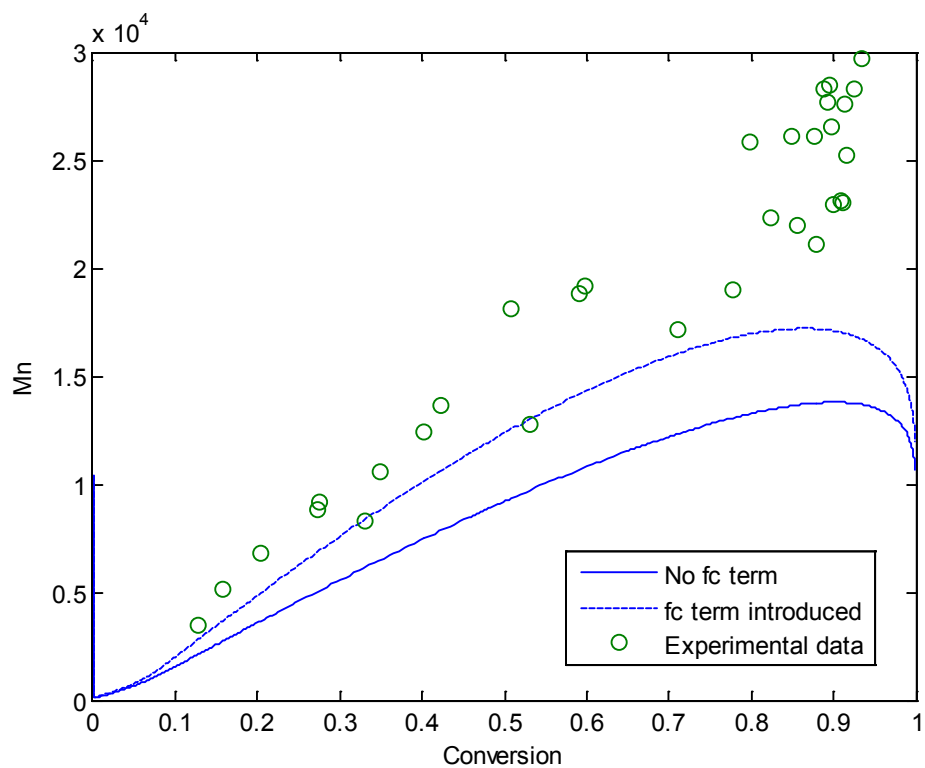
Figure 4-2 - Effect of f_c on number average molecular weight profile (T = 130 °C and R = 1.1)
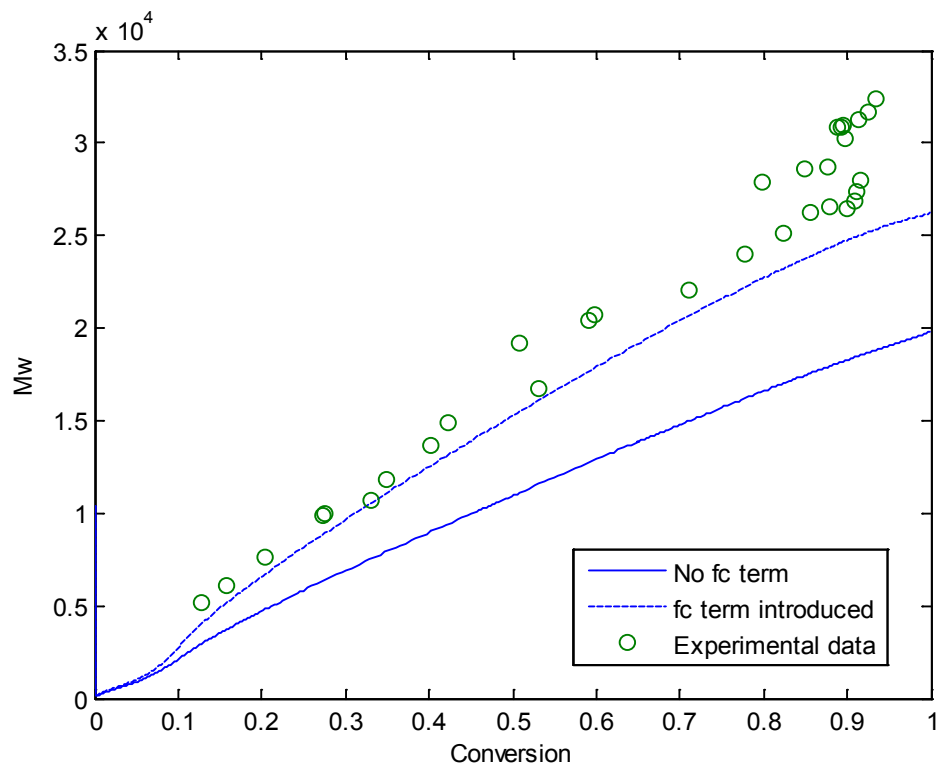
Figure 4-3 - Effect of f_c on weight average molecular weight profile (T = 130 °C and R = 1.1)

53

There is a small increase of the PDI prediction with the implementation of this parameter, as shown in Figure 4-4. However, this is just due to the fact that the relative gain in the M_w is greater than that in the M_n. Overall, based on the new picture revealed in Figures 4-1 to 4-4 , there is a net gain for the model's predictive capabilities.
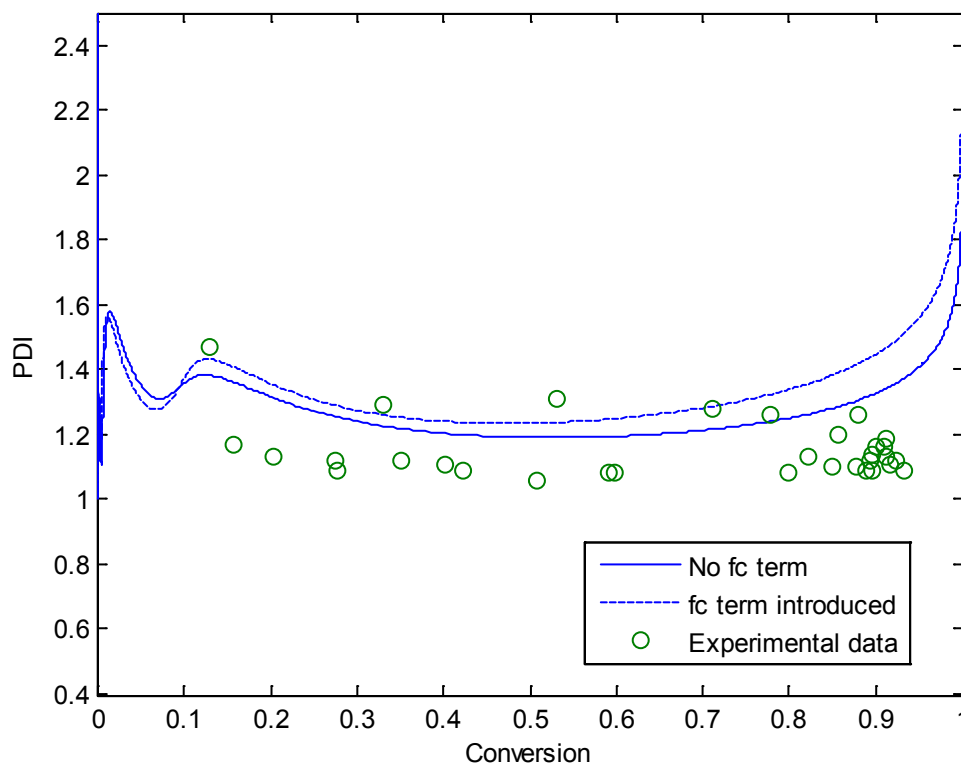
Figure 4-4 – Effect of f$_c$ on weight polydispersity index profile (T = 130 °C and R = 1.1)

These trends can be verified in the unimolecular case, as well. The plots for this case and others not discussed in this section can be found in Section 4.3.1 of this thesis.

4.1.2   Investigation of Changing Initiator and Controller Efficiencies

At this point, it was proposed that the efficiencies might change with conversion, as the relative amounts of the species might impact their amount of association with one another. After some investigation, it was determined that higher efficiencies at lower conversion followed by lower efficiencies as conversion progressed allowed for an improvement in the predicted profiles' agreement with experimental data. Figure 4-5 illustrates the impact on

the conversion profile of increased initial values of these efficiencies coupled with decreasing them at higher conversion values. From this profile, it is seen that improved agreement is seen at low conversion values, whereas the higher conversion range deviates little from the previous case. Table 4-1 provides the changes to the f and f_c values that were made with respect to conversion.

Table 4-1 – Changing f and f_c values with conversion

Parameter	Initial Value	Value for Conversion > 0.5
f	0.4	0.37
f_c	0.7	0.35
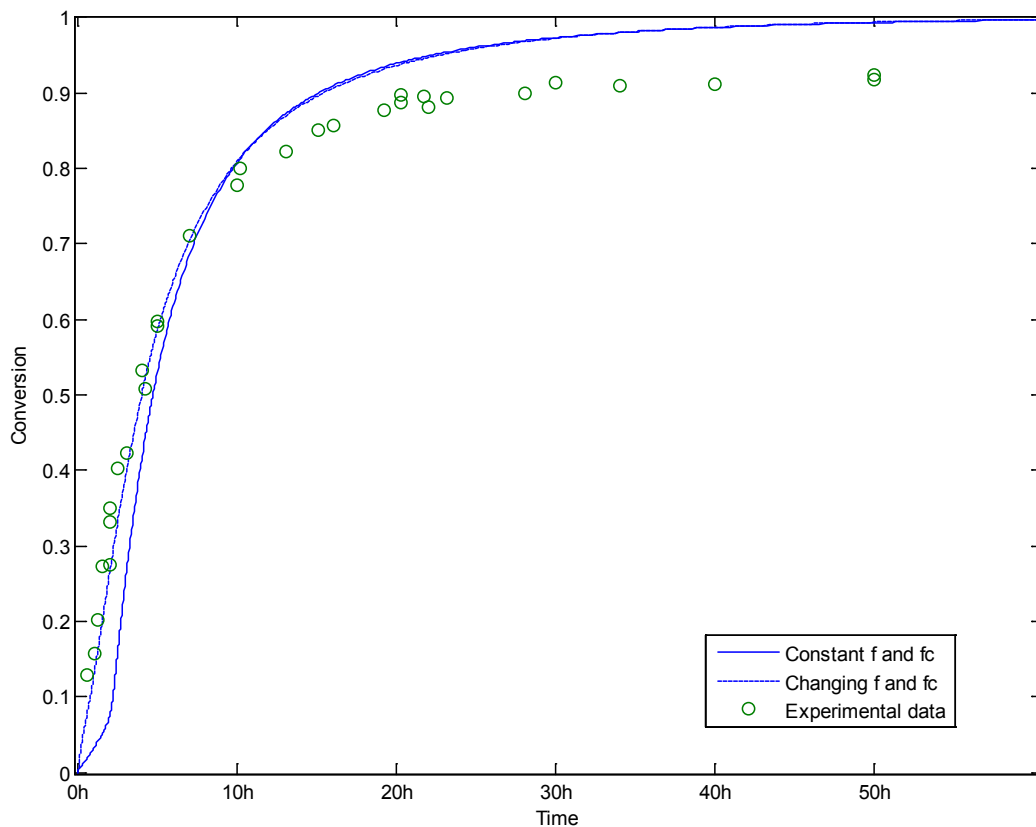
Figure 4-5 - Impact of varying f and fc profiles on conversion profile (T = 130 °C and R = 1.1)

Figure 4-6 illustrates the impact of these changes on the number average molecular weight profile, where the values predicted are seen to increase. This had the result of an overall improvement and better agreement with experimental data – though the decrease of the predicted values as was seen earlier at high conversion values is still present. Figure 4-7 shows the impact on the weight average molecular weight profile, where an increase in the model's predicted values is also seen – bringing the profile into better agreement with the experimental data.
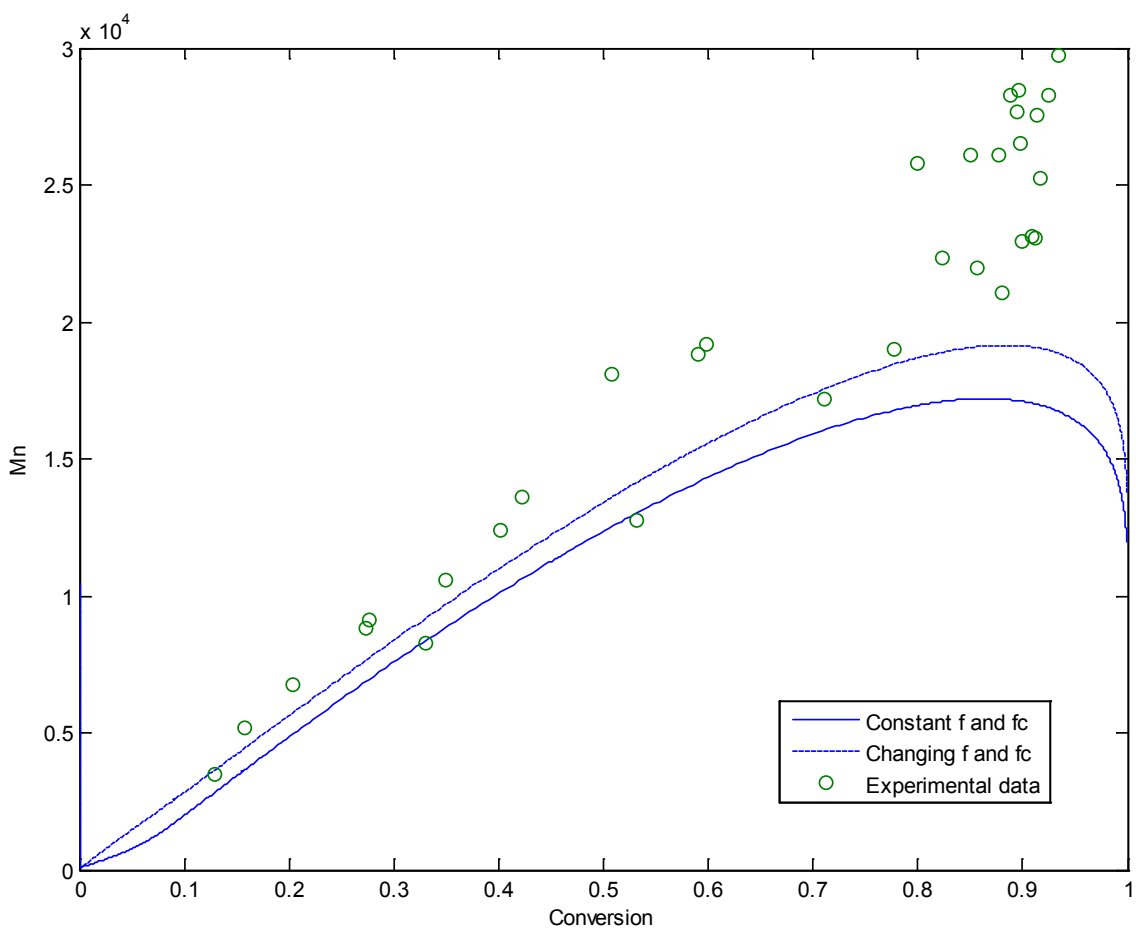
Figure 4-6 - Impact of varying f and fc profiles on M_n profile (T = 130 °C and R = 1.1)
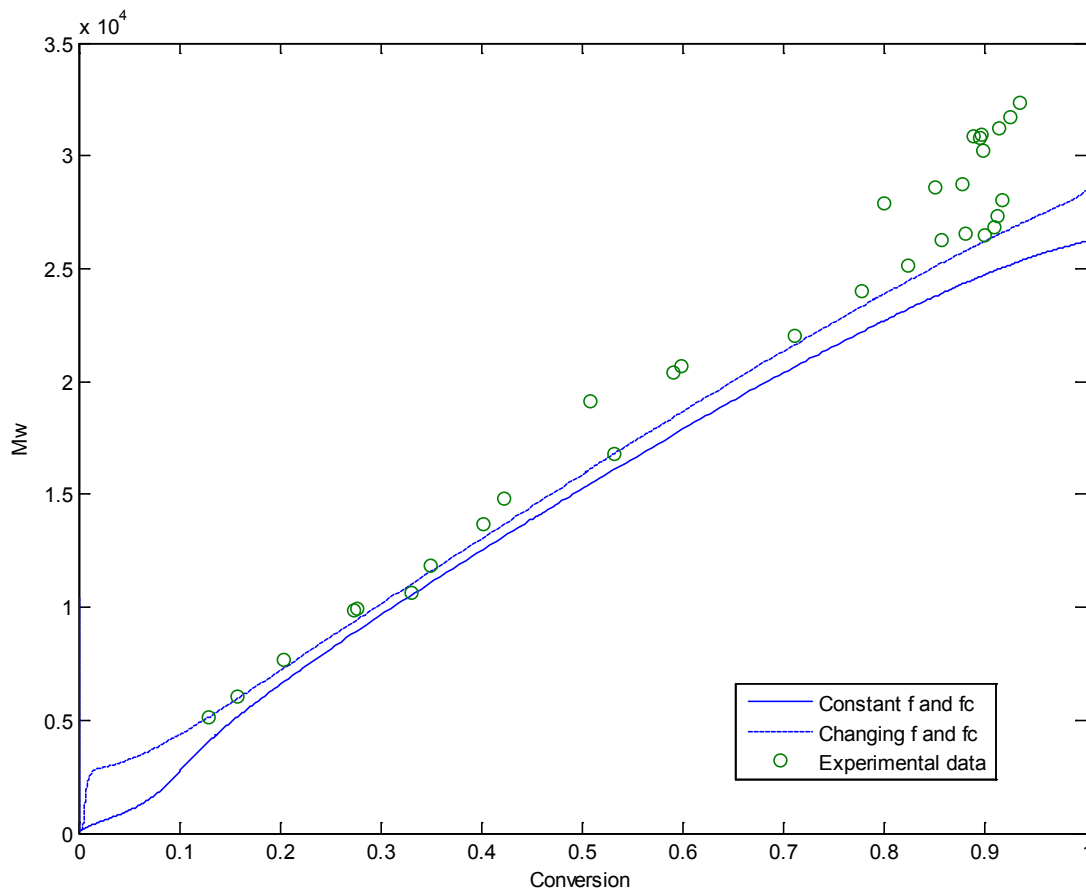
Figure 4-7 – Impact of varying f and fc profiles on M_w profile (T = 130 °C and R = 1.1)

Figure 4-8 shows the resultant PDI profile, where, due to the relatively greater increases seen in the M_n compared to the M_w profile, the generated PDI profile is seen to decrease initially, bringing it into better agreement with the experimental data. Due to the decrease of the M_n profile at high conversion, the PDI profile is still seen to increase at high conversion values – causing deviation from the experimental data.
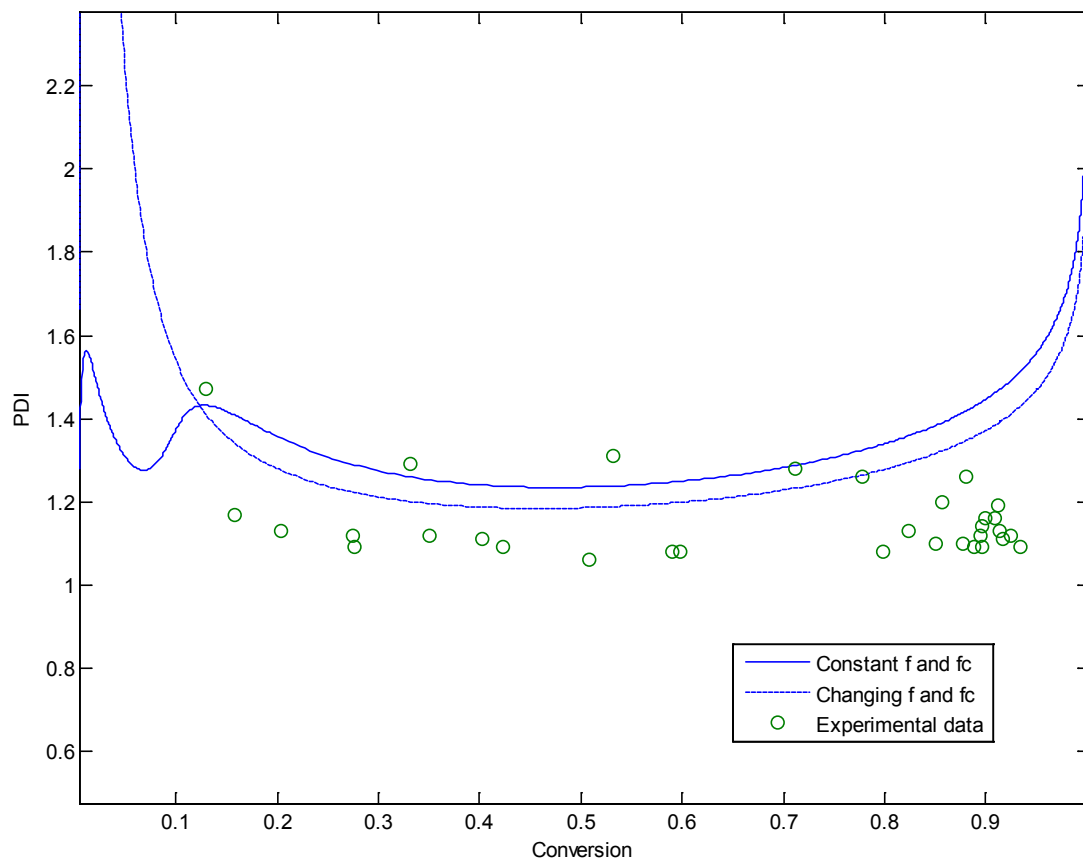
Figure 4-8 - Impact of varying f and f$_c$ profiles on PDI profile (T = 130 °C and R = 1.1)

In general, the adoption of these changes to the f and f$_c$ parameters were seen to greatly improve model fit for these important profiles, and will be carried forward in the future steps for model refinement.

4.2 Parametric Sensitivity

At this point, a more detailed investigation into the impact of perturbations of some of the parameters deemed more important in the mechanism on the modelling trends/predictions was conducted. The specific investigations of this (parametric) sensitivity analysis and their resultant effects on the modelled process will be discussed in this section of the thesis.

4.2.1 Investigation of Rate of Dimerization (k_{dim})

Bonilla et al. [3] and Belincanta-Ximenes et al. [4] performed sensitivity analyses suggesting that both conversion and molecular weight estimates from a mechanistic model of this process were highly sensitive to changes in k_{dim}, the rate constant governing the rate of dimerization. This makes sense, as the dimerization not only consumes monomer, but also the dimer produced takes part in some of the reactions as described in the full mechanistic model. Therefore, it seemed prudent to investigate the impact of changes to the rate of dimerization on our model. Table 4-2 shows the impact of the reduction of k_{dim} on some of the more important process responses.

Table 4-2 - Impact of changes to dimerization rate to key estimates (T = 130 °C and R = 1.1)

Parameter	Value at 130 °C	Time for Conversion = 0.75	$\underline{M}_n$ at conversion = 0.75	$\underline{M}_w$ at conversion = 0.75
$k_{dim} = k_{dim,0}$	3.14×10^{-7}	8.10 hours	1.814×10^4	2.269×10^4
$k_{dim} = \dfrac{k_{dim,0}}{2}$	1.57×10^{-7}	10.32 hours	1.971×10^4	2.362×10^4
$k_{dim} = \dfrac{k_{dim,0}}{4}$	7.85×10^{-8}	12.95 hours	2.088×10^4	2.417×10^4

Reduction of the rate of dimerization resulted in an improvement in model fit in several interesting ways. First, in the bimolecular case, an improvement was seen in fit of the conversion vs. time profile generated by the model, as well as in the number and weight average molecular weight estimates (and therefore PDI estimation). These trends are shown in Figures 4-9 to 4-12, and a discussion of the impacts on each particular trend follows.
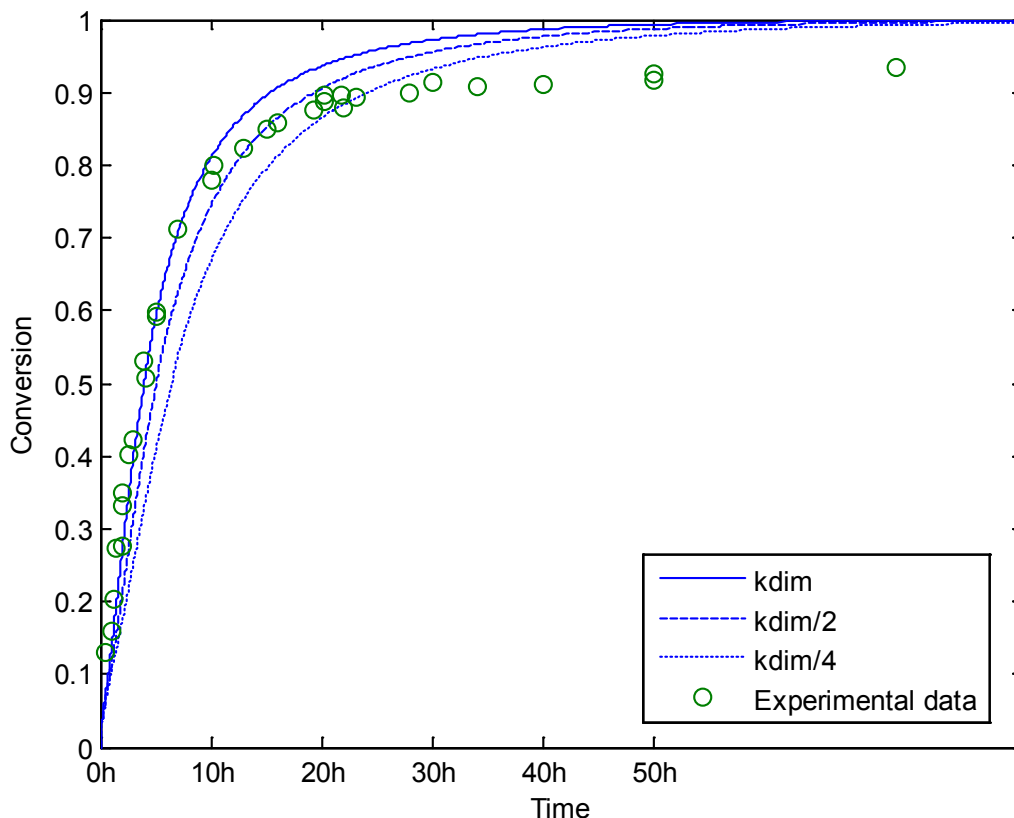
Figure 4-9 – Impact of reduction of dimerization rate on conversion profile (T = 130 °C and R = 1.1)

Figure 4-9 illustrates the impact of reducing the amount of dimerization that occurs on conversion. Decreasing k_{dim} slows the rate of increase seen in the conversion profile, such that it underestimates the conversion at earlier reaction times, but still eventually the predictions exceed the conversions obtained experimentally. It could be argued that the overall fit of the conversion profile is improved with a modest decrease in k_{dim}, but worsens with larger reductions to this value.

Figure 4-10 shows the impact of the change in dimerization rate on the number average molecular weight profile. Decreasing the amount of dimerization is seen to have a positive impact on the fit of this profile, moving the prediction from the extreme low end of the experimental data range up to somewhere in the middle. Figure 4-11 shows similar gains in accuracy for the generated weight average molecular weight profile, though the magnitude of this shift is seen to be somewhat smaller.
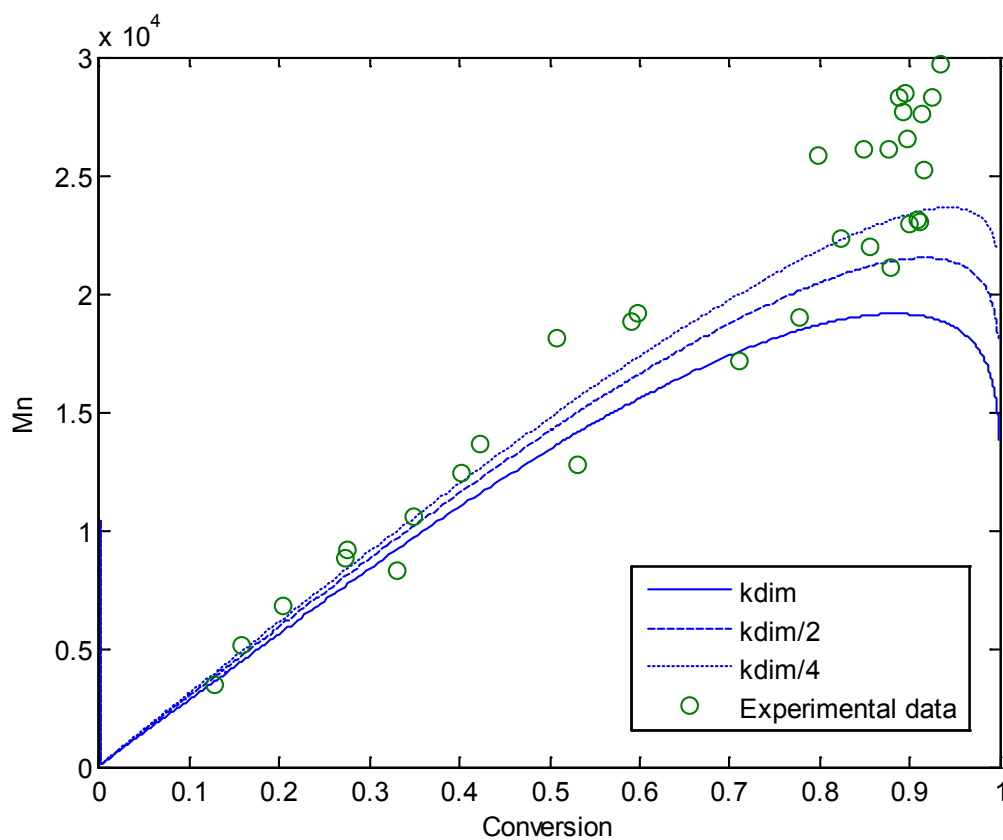
Figure 4-10 Impact of reduction of dimerization rate on M_n profile (T = 130 °C and R = 1.1)
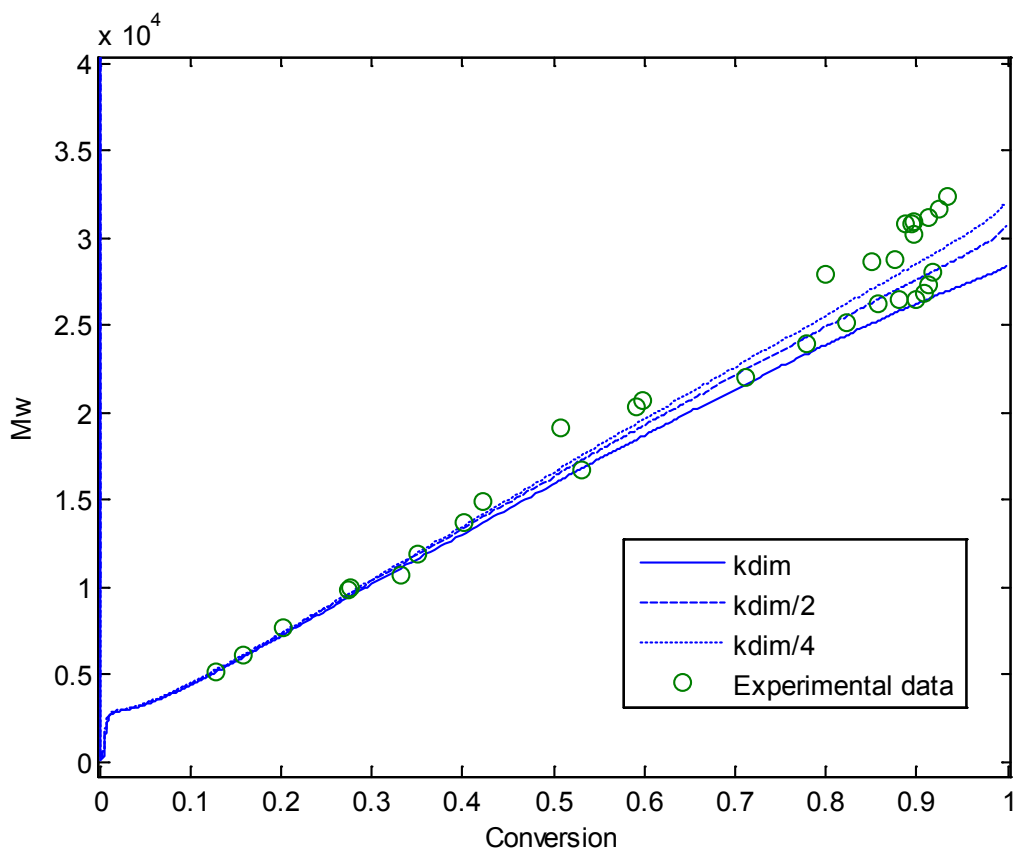
Figure 4-11 Impact of reduction of dimerization rate on M_w profile (T = 130 °C and R = 1.1)

Figure 4-12 shows the impact of the reduction of k_{dim} on the PDI profile. It lowers the predicted profile, and therefore the overall picture becomes more accurate with respect to the data points. This makes sense as the predicted number average molecular weight was seen to have increased by a greater amount than the weight average molecular weight, as mentioned previously.
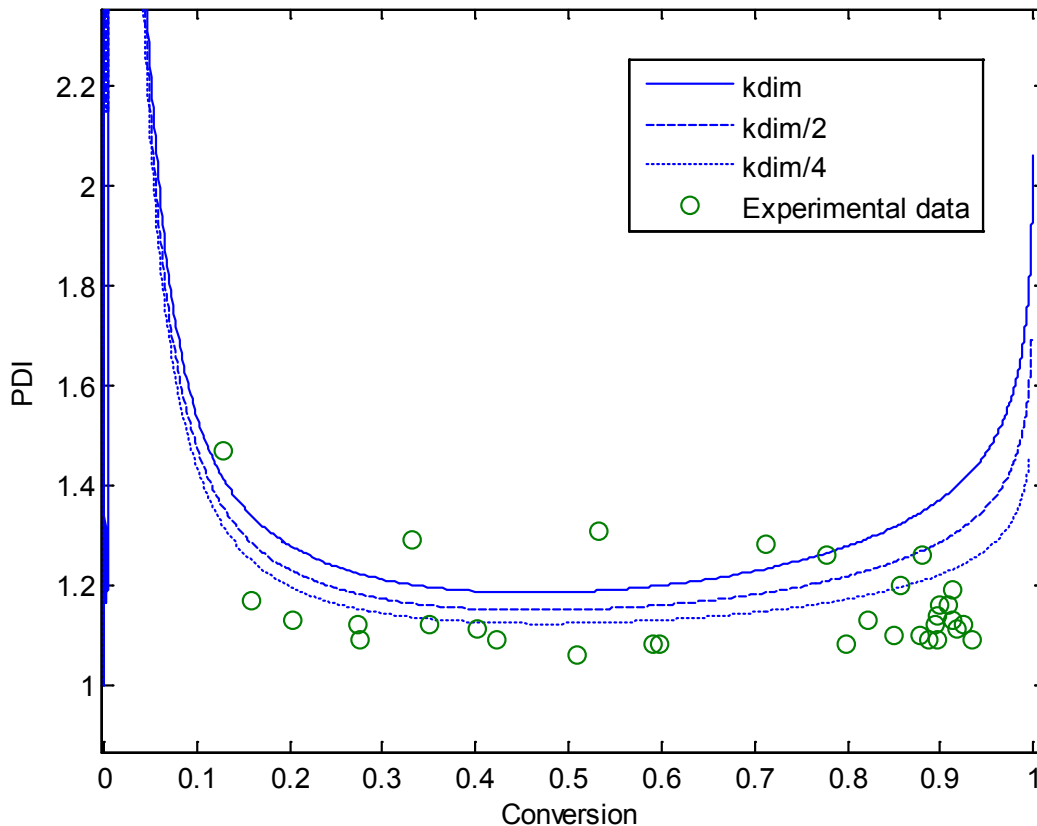
Figure 4-12 Impact of reduction of dimerization rate on PDI profile (T = 130 °C and R = 1.1)

These trends were also verified in the case of the unimolecular process. Figure 4-13 shows the impact of the reduction of k_{dim} on the conversion profile, which, as in the bimolecular case, substantially decreases conversion rate. In Figure 4-14, the impact of this change on the number average MW is improving the profile's agreement with the experimental data. The downward curvature of this profile at high conversion was seen to lessen with decreasing k_{dim}, leading to better predictions at these high conversion values. The improvements seen in these MW profiles as well as the PDI profile (Figure 4-15) due to the reduction of k_{dim} are significant, suggesting that reactions involving the dimer may be contributing to some of the poor fit that has been observed in earlier modelling efforts.
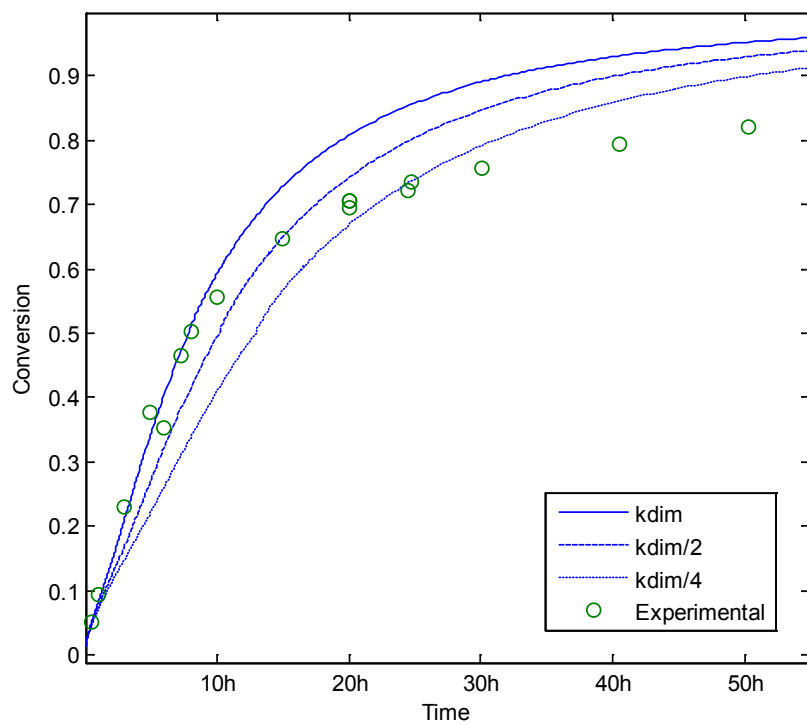
Figure 4-13 – Impact of reducing k_{dim} on conversion for unimolecular process (T = 120 °C)
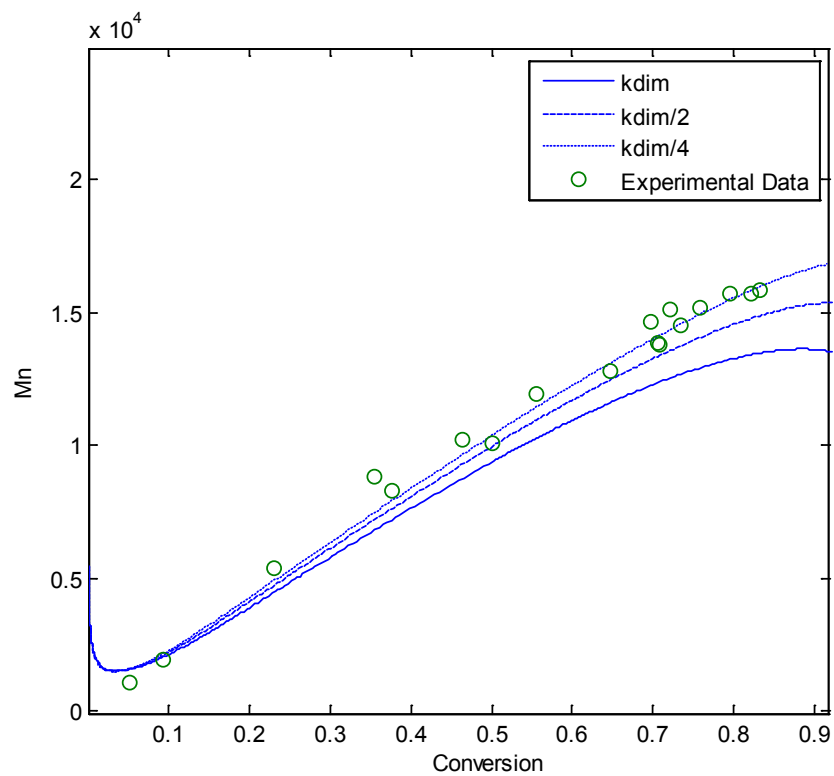
Figure 4-14– Impact of reducing k_{dim} on M_n for unimolecular process (T = 120 °C)

Figure 4-15 illustrates the impact of decreasing k_{dim} on the generated PDI profile. In this figure, the generated profile is seen to get closer to the bulk of the data points, with the upward curvature at high conversion values diminishing as well.
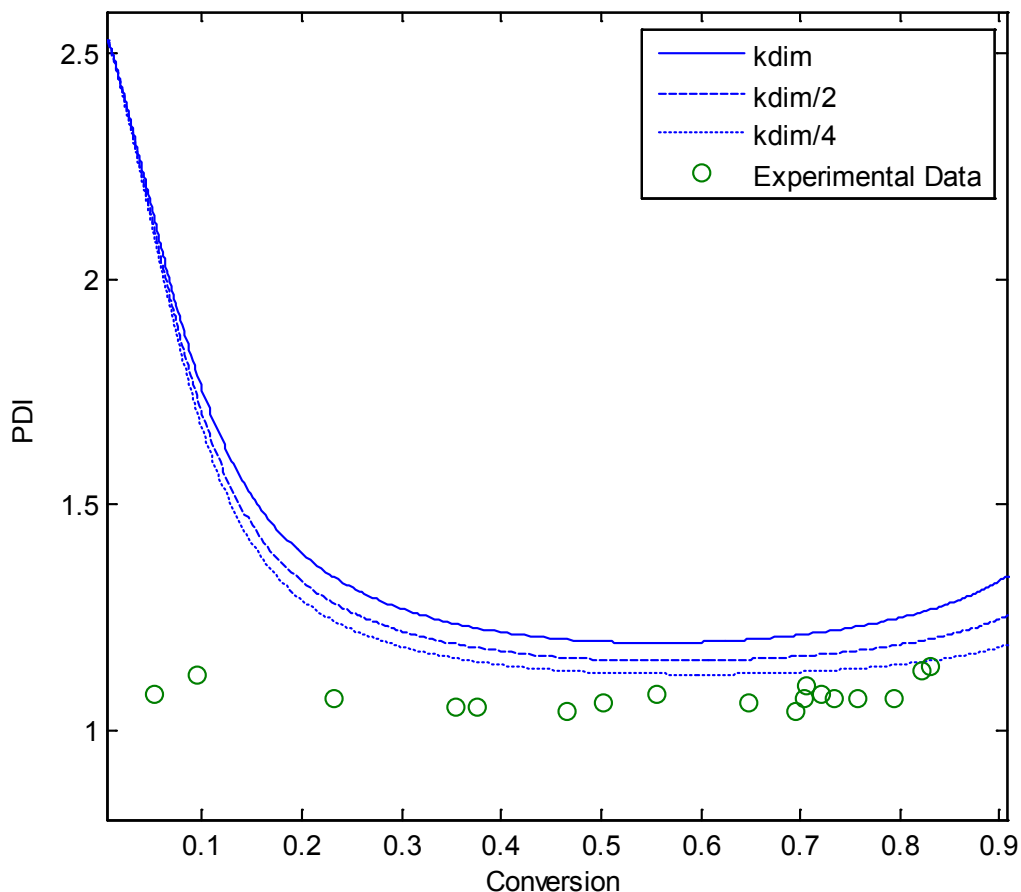
Figure 4-15– Impact of reducing k_{dim} on PDI for unimolecular process (T = 120 °C)

Based on the impact that the decrease of the rate constant k_{dim}, and therefore the resultant concentration of the dimer species is seen to have on the performance of the model predictions, it is evidently worthwhile to investigate the impact of some of the key reactions involving the dimer, such as that of chain transfer to dimer.

4.2.2   Contribution of Transfer to Dimer (kfD)

The impact of changes to the dimerization rate led to questions regarding the specific contributions of some of the reactions that the dimer is involved in, such as the chain transfer to dimer. Some investigation has already been discussed in the literature, and there is some disagreement as to how significant this chain transfer is in the overall reaction scheme. Grezta and Matyjaszewski [5] reported that high amounts of transfer to dimer are necessary in this process; however, Belincanta et al. [4] disagreed – even suggesting that it may be altogether unnecessary. Removal of the transfer to dimer reaction from the model (i.e., rate constant k_{fD}=0) led to some interesting results as will be discussed in this section.

Figure 4-16 shows the effects on the conversion profile of first halving the dimerization rate, followed by eliminating the transfer to dimer term. In the case of the conversion profile, almost no effect is seen from this removal versus the reduced dimerization case, which makes sense, theoretically.
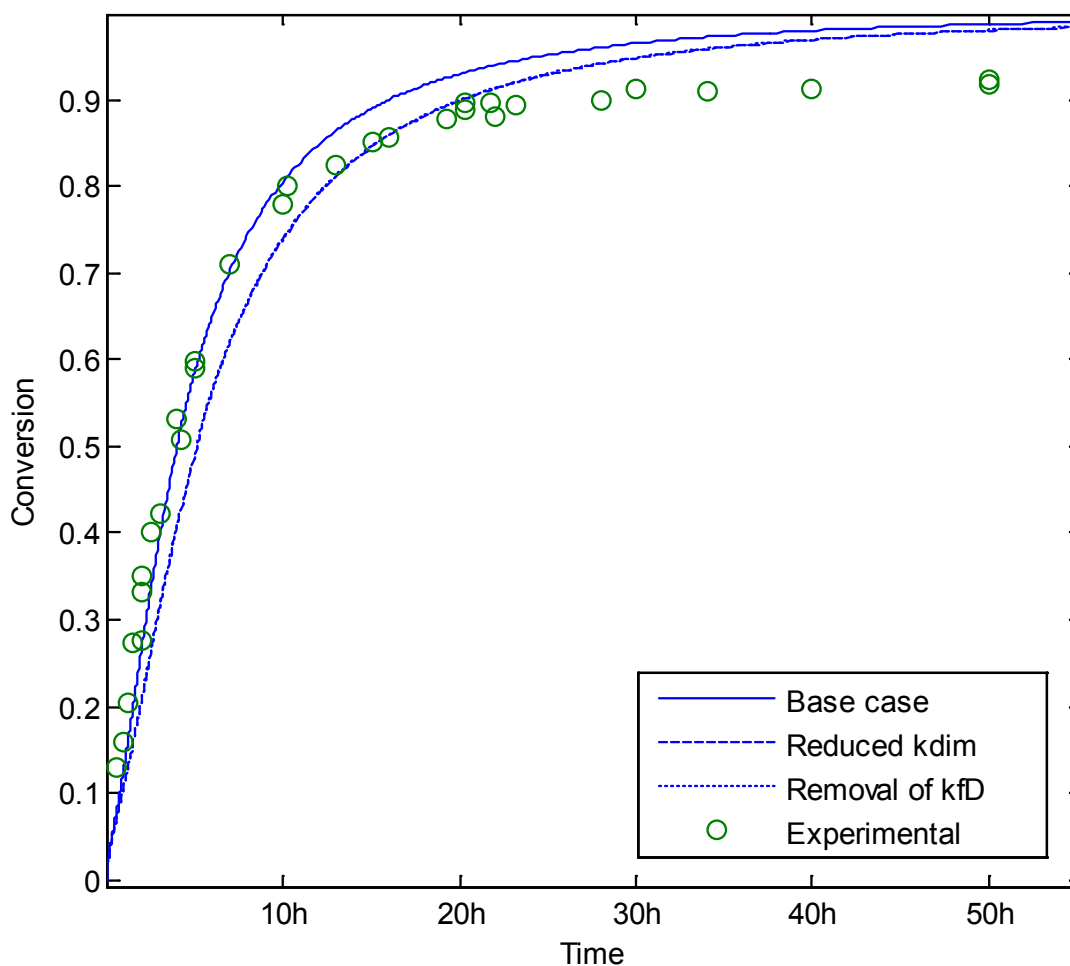
Figure 4-16 - Impacts of removal of k_{fD} on conversion profile (T = 130 °C and R = 1.1)

Where the impact of the removal of this chain transfer reaction is even more evident is in the generated number average molecular weight profile. Figure 4-17 shows the impact of this change on the M_n profile, including both improved fit through the centre of the data, as well as the elimination of the large inaccuracies that were previously seen as the model reaches high conversion. The generated M_n profile is seen to finally produce a profile that is in good agreement with our data across the whole conversion range.
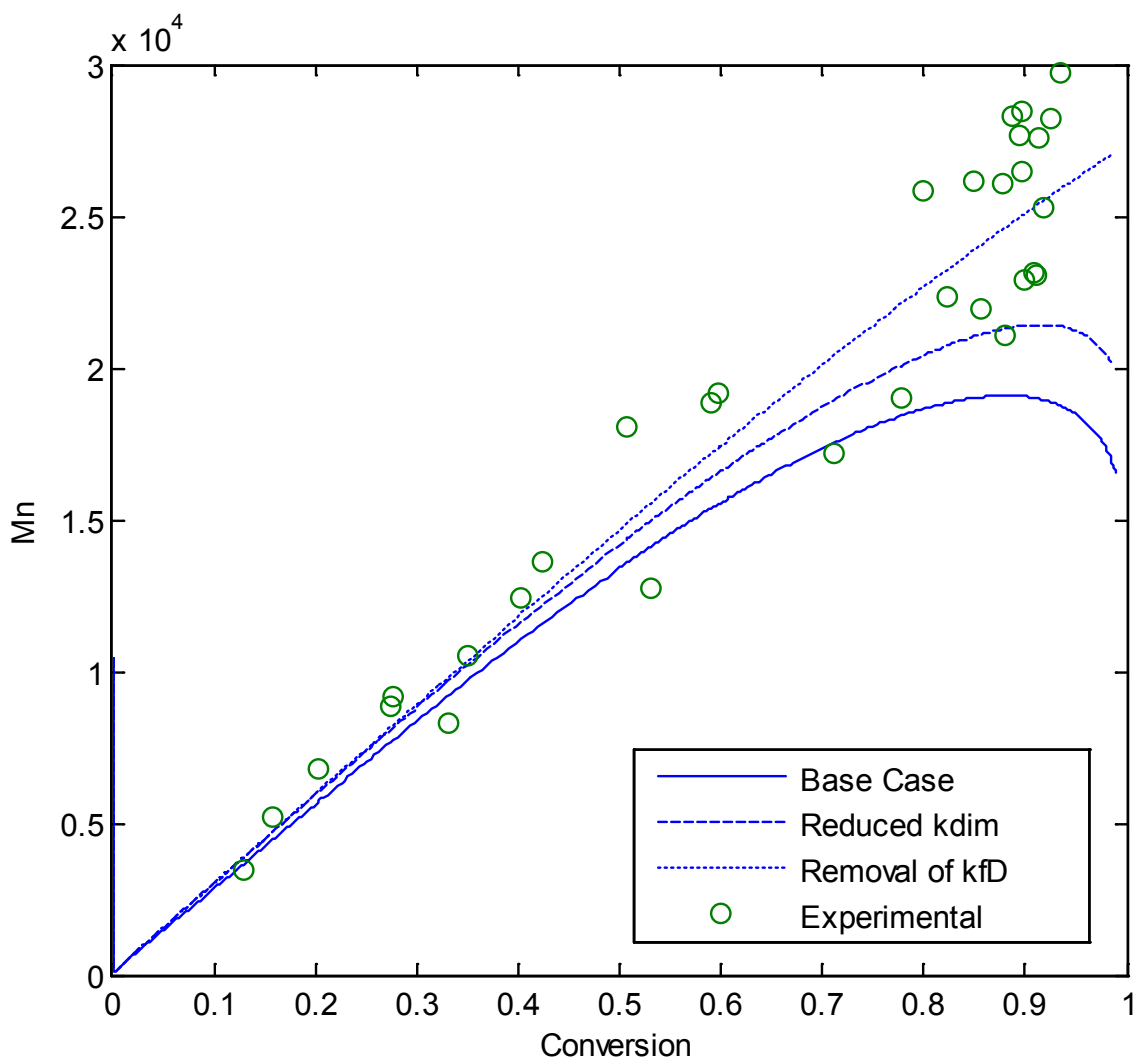
Figure 4-17 - Impact of removal of k_{fD} on M_n profile (T = 130 ℃ and R = 1.1)

This change is also seen to improve the weight average MW estimate, as depicted in Figure 4-18, though changes in this profile are to a smaller extent than those to the number average MW. The changes in both these MW estimates are echoed in the PDI profile, shown in Figure 4-19, where the generated profile is now in excellent agreement with the experimental data. Therefore the omission of this term from the model is considered to be a success and will be adopted in future simulation steps.
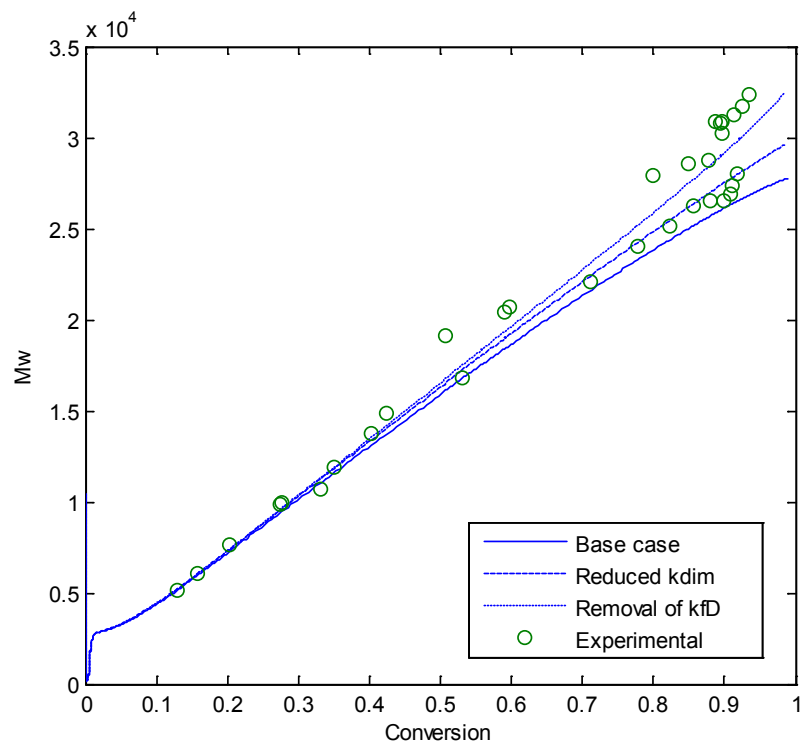
Figure 4-18 - Impact of removal of k_{fD} on M_w profile (T = 130 °C and R = 1.1)
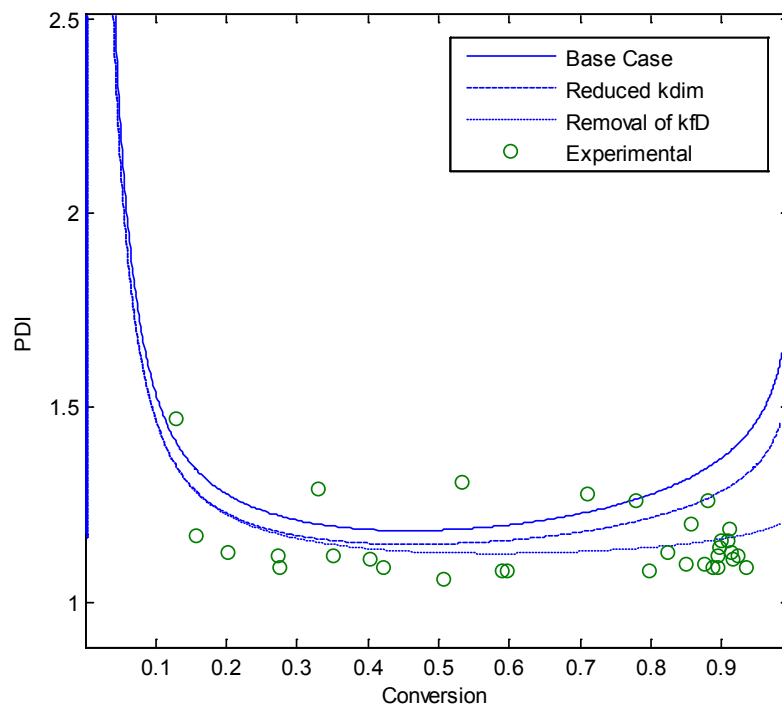
Figure 4-19 – Impact of removal of k_{fD} on PDI profile (T = 130 °C and R = 1.1)

69

4.2.3   Contribution of Transfer to Monomer (k_{fM})

As we were able to achieve good performance results via the removal of the contribution of the transfer to dimer reaction ($k_{fD}=0$) which was seen to improve model performance, especially of the molecular weight estimates, it made sense that the transfer to monomer term ($k_{fM}=0$) might also be a good candidate for sensitivity studies. Figure 4-20 shows the impact of the removal of this term on the generated conversion profile. As can be seen, this term has negligible impact on conversion, as no visible difference is seen between the conversion profiles generated.
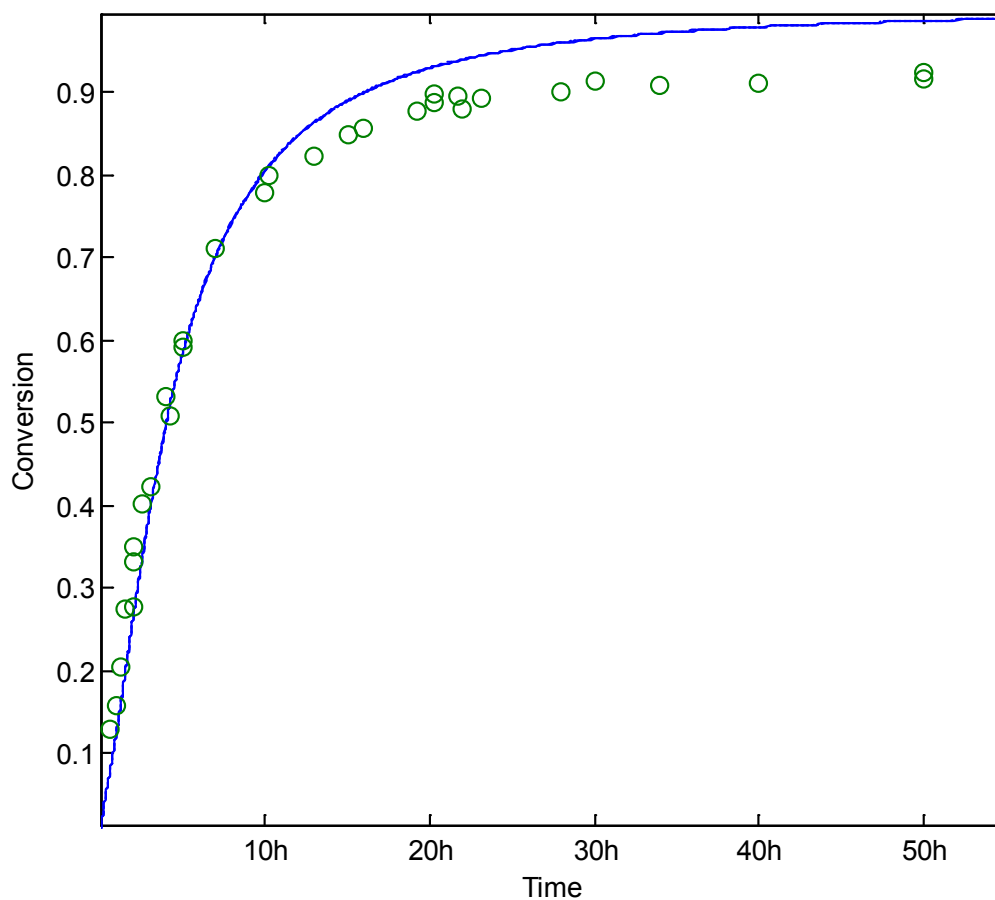
Figure 4-20 - Impact of removal of k_{fM} on conversion profile (T = 130 °C and R = 1.1)

The effects of this term's removal on the molecular weight average profiles are seen to be more substantial. Figure 4-21 shows the generated M_n profiles, where it is seen that the removal of this term further improves the predicted profile. Figure 4-22 shows a similar trend with the M_w profile. Figure 4-23 indicates an improvement in the PDI profile's accuracy, which makes sense as the increase seen in the values predicted for M_n is larger than that for M_w.
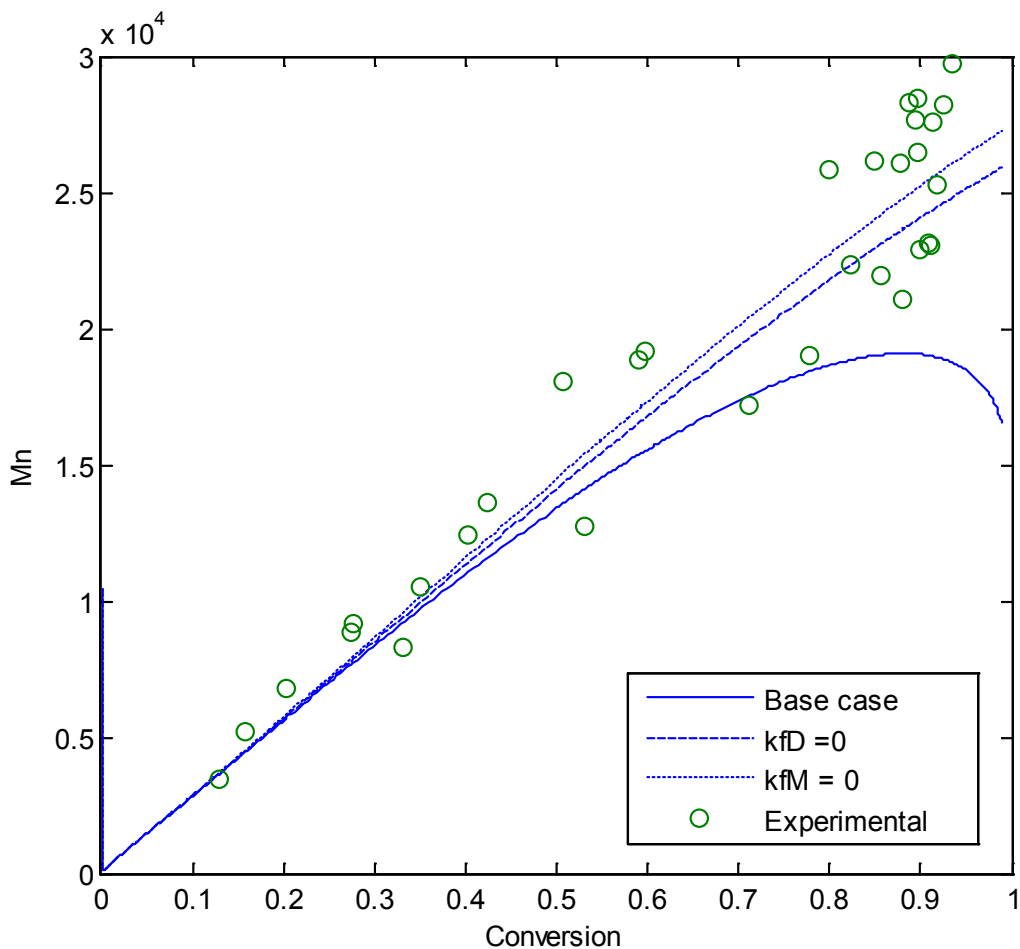
Figure 4-21 - Impact of removal of k_{fM} on M_n profile (T = 130 °C and R = 1.1)

From this it appears that not only can one remove these chain transfer reactions from the model without significant losses in predictive power, but in fact, the model's performance improves with the removal of the terms for chain transfer.
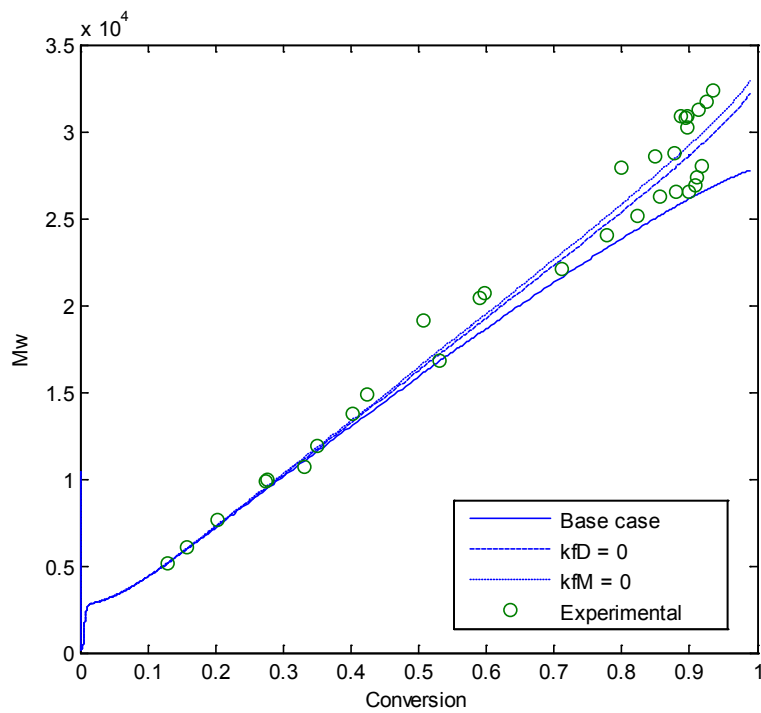
Figure 4-22 - Impact of removal of k_{fM} on M_w profile (T = 130 °C and R = 1.1)
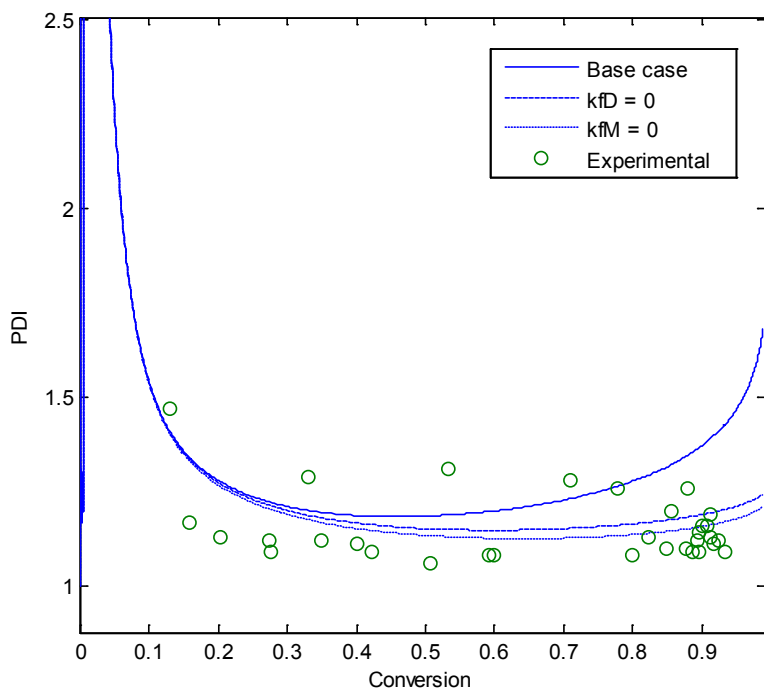
Figure 4-23 - Impact of removal of k_{fM} on PDI profile (T = 130 °C and R = 1.1)

72

4.3 Impact on the Unimolecular Case

At this point, we have a very well-fitting model for the experimental data available for the bimolecular process. It seems prudent that the impact of some of these changes on the model should be evaluated for the unimolecular case in order to decide if they should be adopted in that case as well. Again, experimental data from within our group is utilized for comparisons ([2], [6]).

4.3.1 Efficiency Factors

Application of the efficiency factors f and f_c as discussed in Section 4.1 to the unimolecular case yielded several interesting results. Figure 4-24 illustrates the impact that the introduction of the f_c term has on the conversion profile for the unimolecular case.
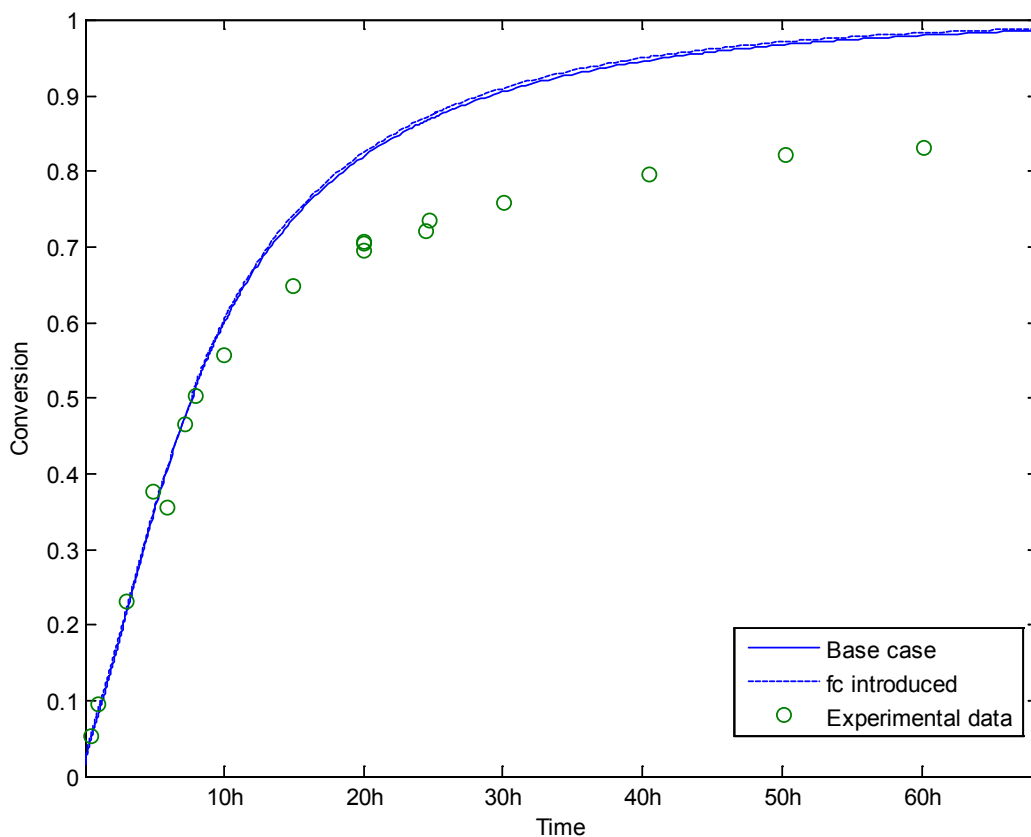
Figure 4-24 - Impact of introducing f_c on the unimolecular conversion profile (T = 120 °C)

As can be seen from this figure, unlike in the bimolecular case, the effect of this change is negligible. For comparison, the impact of the same change to the model for the bimolecular case was shown in Figure 4-1. Figure 4-25 illustrates the effect on the cumulative number-average molecular weight profile ($\underline{M}_n$).
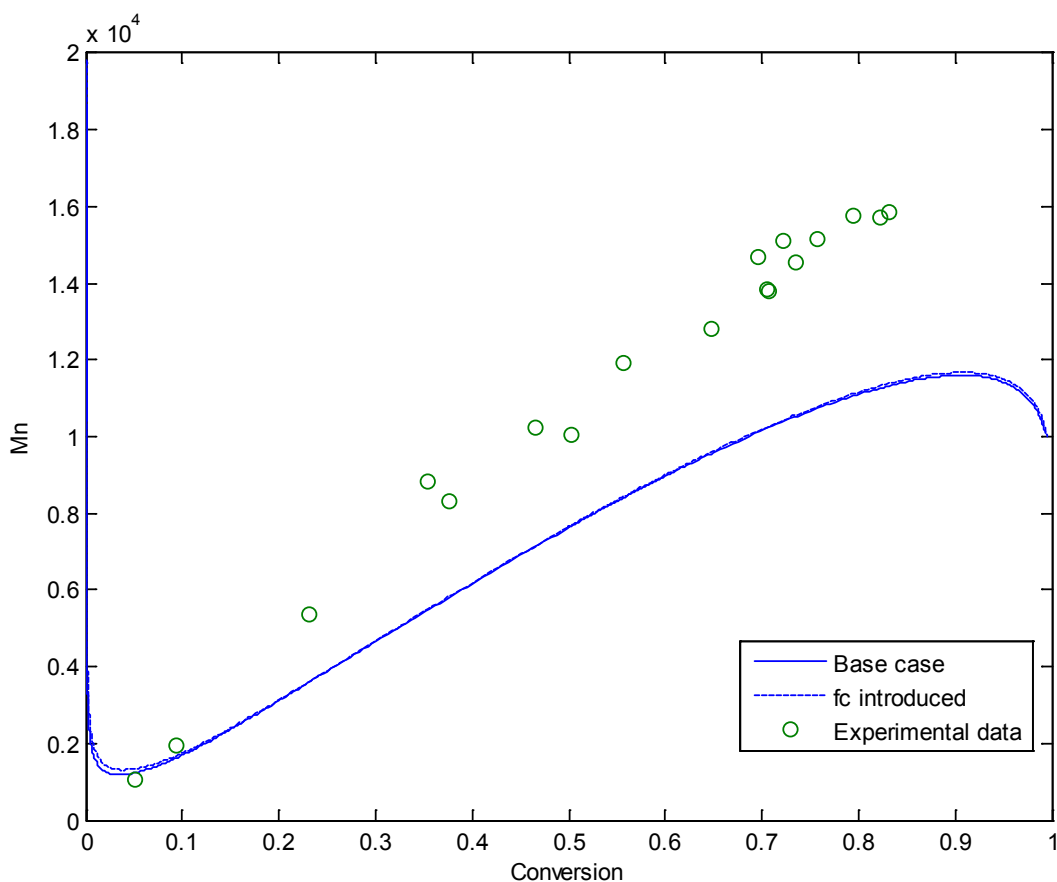
Figure 4-25 - Impact of introducing f_c on the unimolecular $\underline{M}_n$ profile (T = 120 °C)

Again, this change is seen to be negligible compared to the impacts seen in the bimolecular case, illustrated by Figure 4-2, previously. As would be expected given the negligible impacts on conversion and molecular weights, the PDI similarly sees little impact from the addition of the f_c term. This is shown in Figure 4-26, whereas the equivalent bimolecular case can be seen in Figure 4-4.
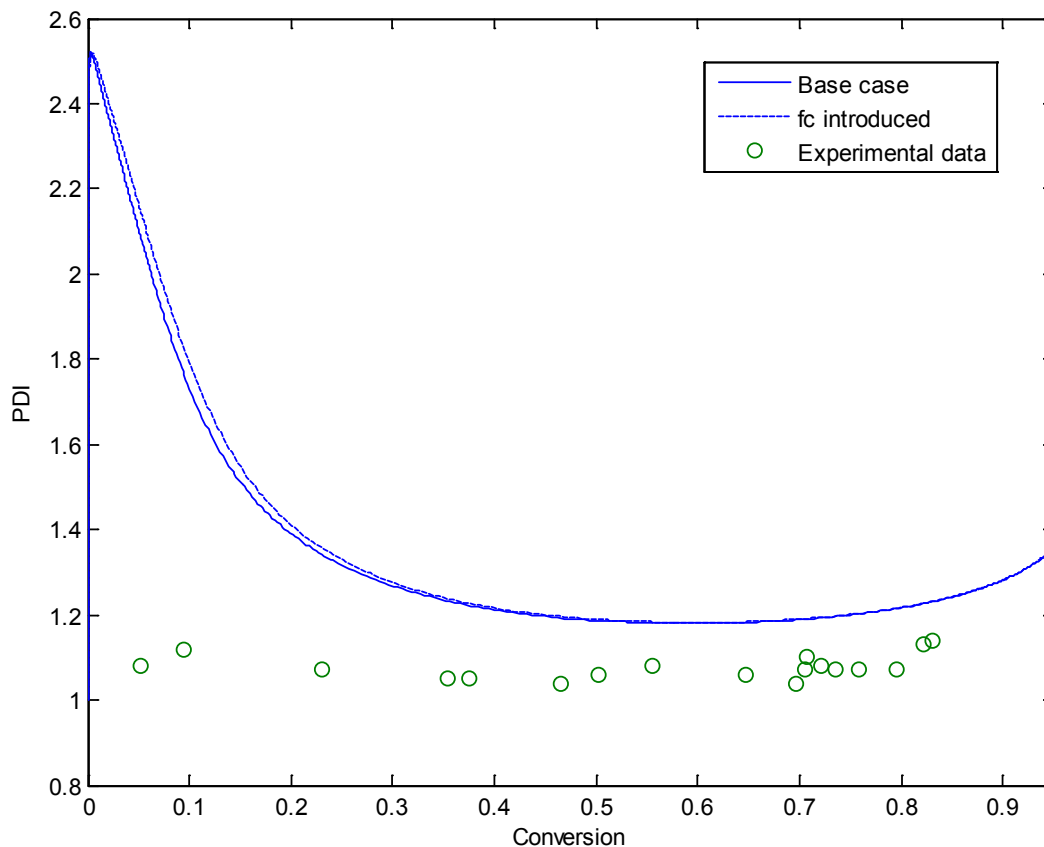
Figure 4-26- Impact of introducing fc on the unimolecular PDI profile (T = 120 °C)

These figures have demonstrated an overall negligible impact of the addition of the controller efficiency term on the overall model performance in the unimolecular case. It then follows that the variation of f and f_c with conversion, as discussed in Section 4.1.2 for the bimolecular case, will similarly have negligible impact on the reaction profiles, as demonstrated in Figures 4-27 through 4-29. The f and f_c changes implemented are the same as those from the bimolecular approach, and are described in Table 4-1.
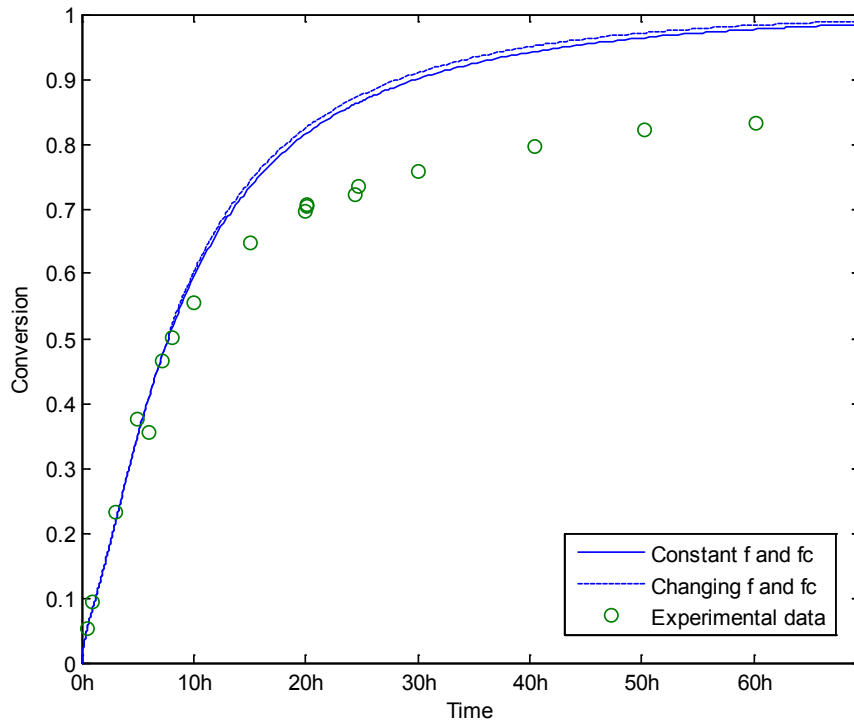
Figure 4-27 - Impact of varying f and fc profiles on unimolecular conversion profile (T = 120 °C)
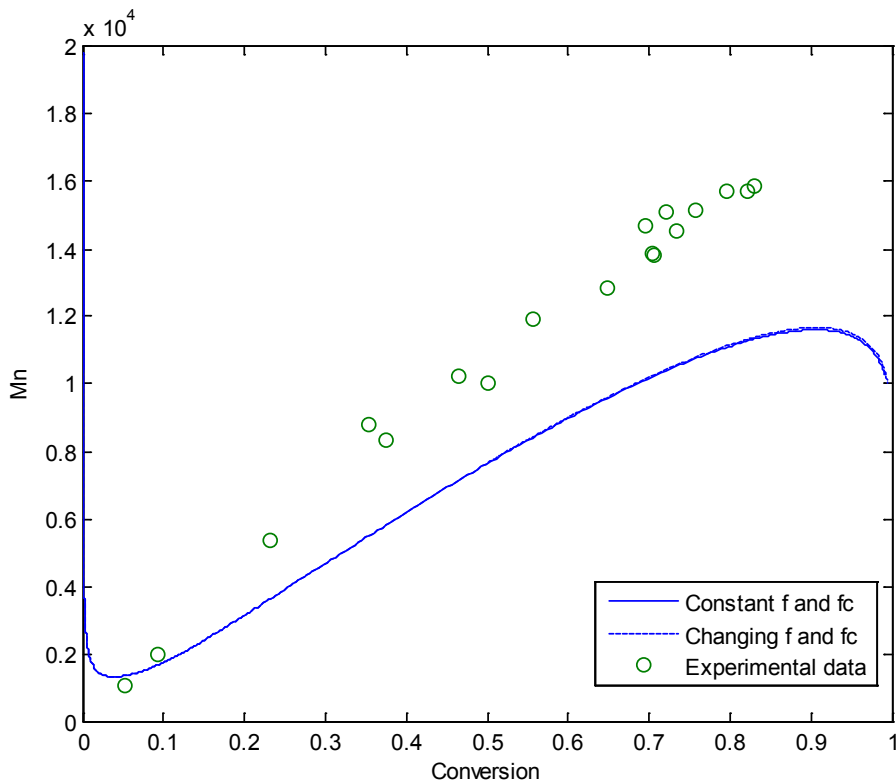
Figure 4-28 - Impact of varying f and fc profiles on unimolecular M_n profile (T = 120 °C)
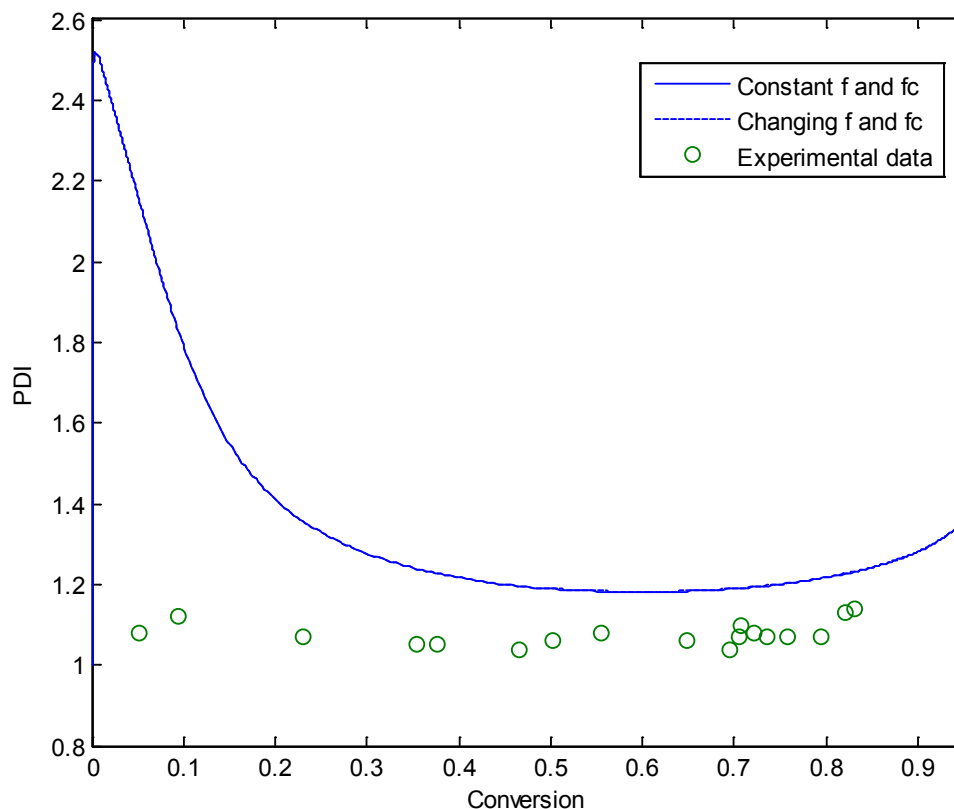
Figure 4-29 - Impact of varying f and fc profiles on unimolecular PDI profile (T = 120 °C)

As seen in these figures, there is no practical upside or downside to introducing a controller efficiency term or implementing these variations with conversion as far as model fit, therefore they will be included in future stages, so as to maintain consistency with what was done in the bimolecular case, as well as to facilitate greater simplicity in the mechanistic model.

4.3.2   Rate of Dimerization

The next step that was taken in the unimolecular case was the reduction of the rate of dimerization, k_{dim}.   The impact of this change should be similar to that seen in the bimolecular case, as discussed in Section 4.2.1.   Figure 4-30 illustrates the effect of this change on the conversion profile for the unimolecular case. The rate of conversion is modestly lowered, which was also seen in the bimolecular case.
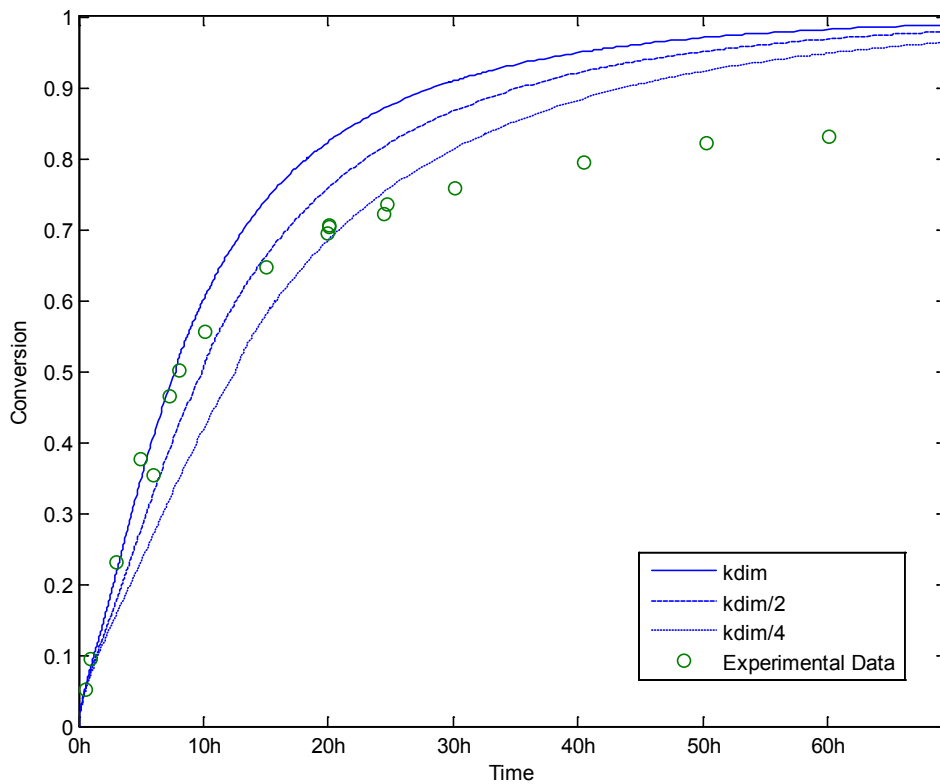
Figure 4-30 – Impact of reducing k$_{dim}$ on the unimolecular conversion profile, T = 120 °C
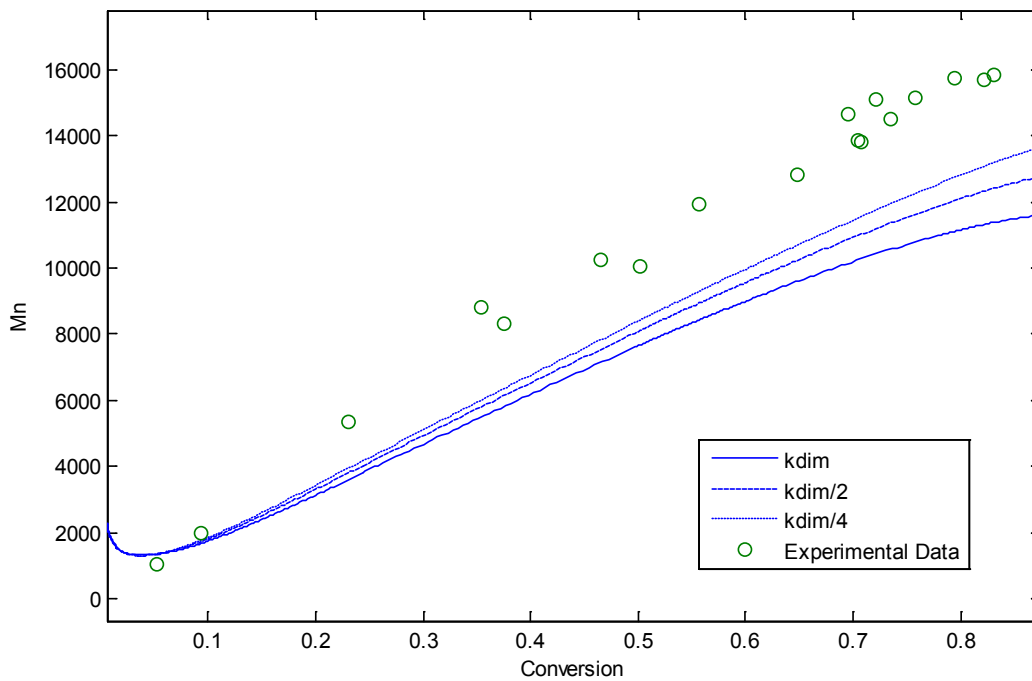
Figure 4-31 – Impact of reducing k$_{dim}$ on the unimolecular $\underline{M}_n$ profile, T = 120 °C

78
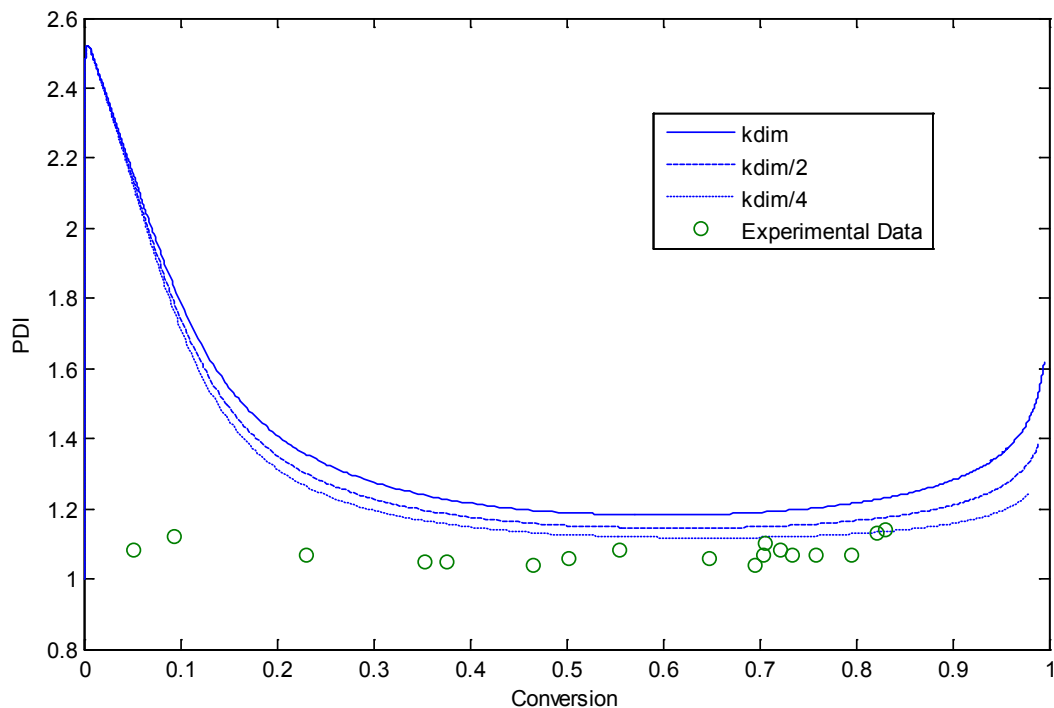
Figure 4-32 – Impact of reducing k_{dim} on the unimolecular PDI profile, T = 120 °C

Figure 4-31 shows the impact of these changes on the number-average molecular weight profile, which is seen to grow more quickly when the rate of this dimerization is reduced. In Figure 4-32, the predicted polydispersity index is seen to lower with k_{dim} as well – indicating that the weight-average molecular weight has seen less of an increase than $\underline{M}_n$. These trends all agree with what was seen in the bimolecular case.

4.3.3   Transfer to Dimer and Transfer to Monomer (k_{fD} and k_{fM})

The last two steps taken towards the goal of improving model fit in the unimolecular case were the removal of the chain transfer to monomer and dimer reactions. This led to much greater agreement between the model and data in the bimolecular case, and it will be interesting to see if this is also the case in the unimolecular process. Figure 4-33 shows the impact of the removal of first the transfer to dimer, and then the transfer to monomer reactions from the model in the unimolecular case.
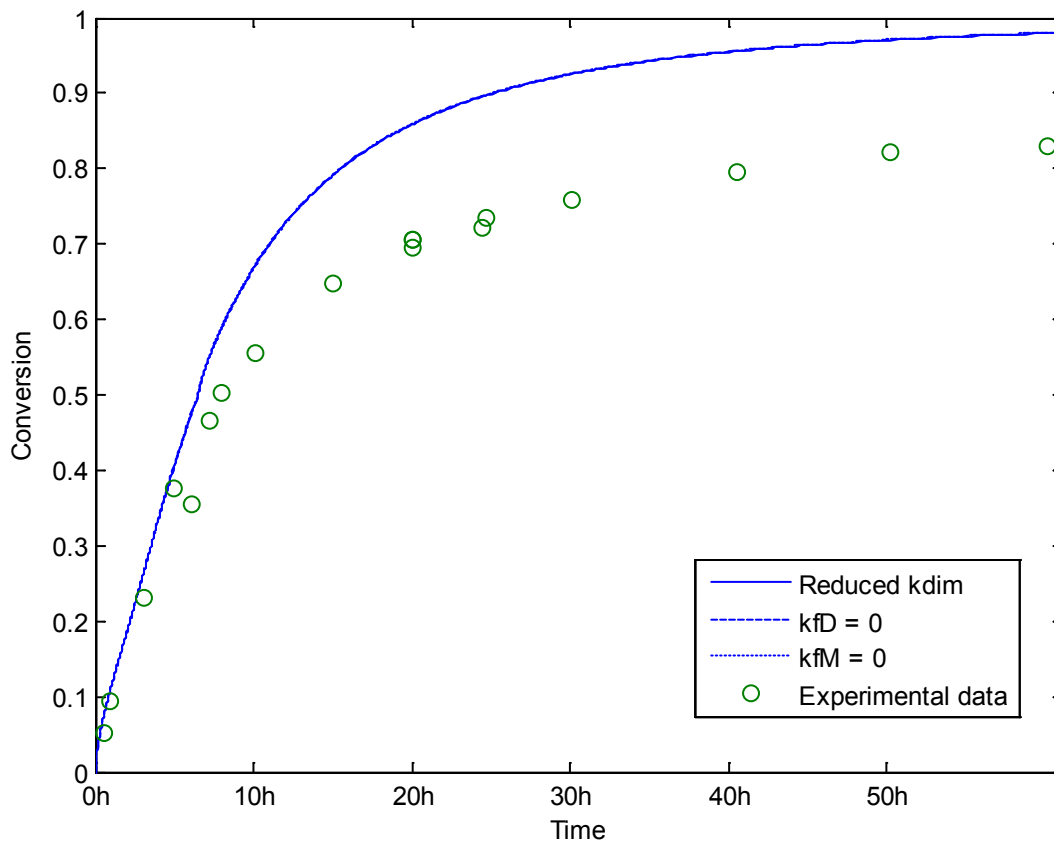
Figure 4-33 – Impact of the removal of kfD and kfM on the unimolecular conversion profile, T = 120 °C

As can be seen, the impact of the removal of these chain transfer terms is insignificant in this case, which is consistent with the results of the bimolecular case, as discussed in Sections 4.2.2 and 4.2.3. Figure 4-34 shows the results of these removals on the number-average molecular weight profile, where a more pronounced straightening of the profile is seen, and the line takes on more of the shape that it should. Worth noting is that at high conversion values, the data values are actually lower than those predicted by the model, as a slight nonlinearity is seen in the molecular weight development of this dataset. Figure 4-35 illustrates the impact of these removals on the predicted PDI profile, where much greater agreement is seen with the experimental data, and the erroneous upswing in PDI at high conversion is no longer predicted.
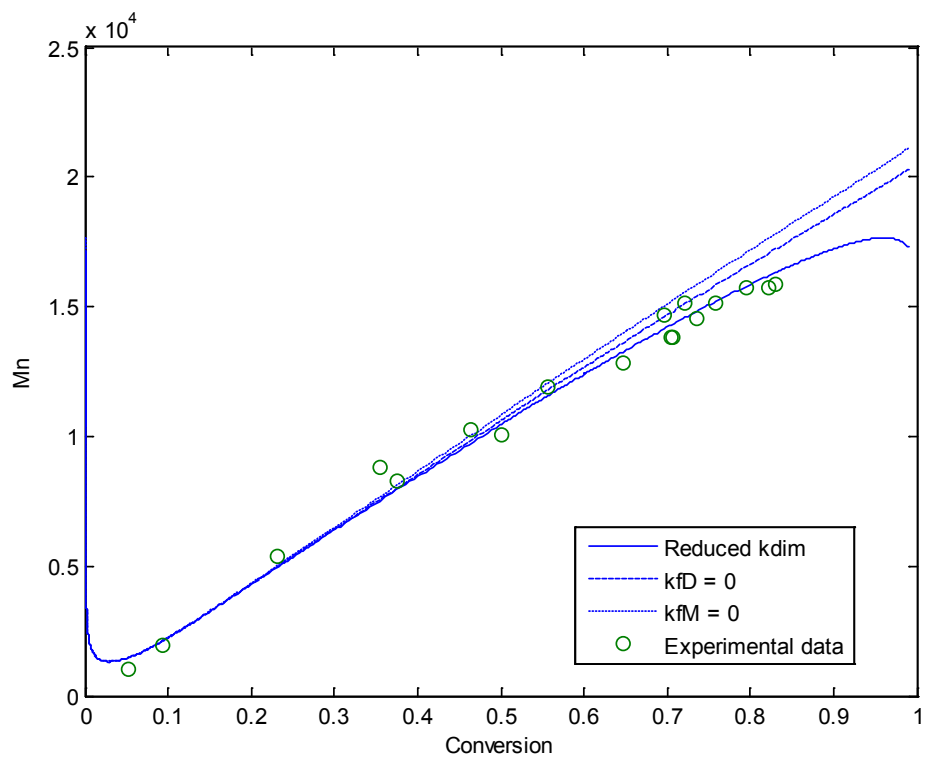
Figure 4-34 – Impact of the removal of kfD and kfM on the unimolecular $\underline{M}_n$ profile, T = 120 °C
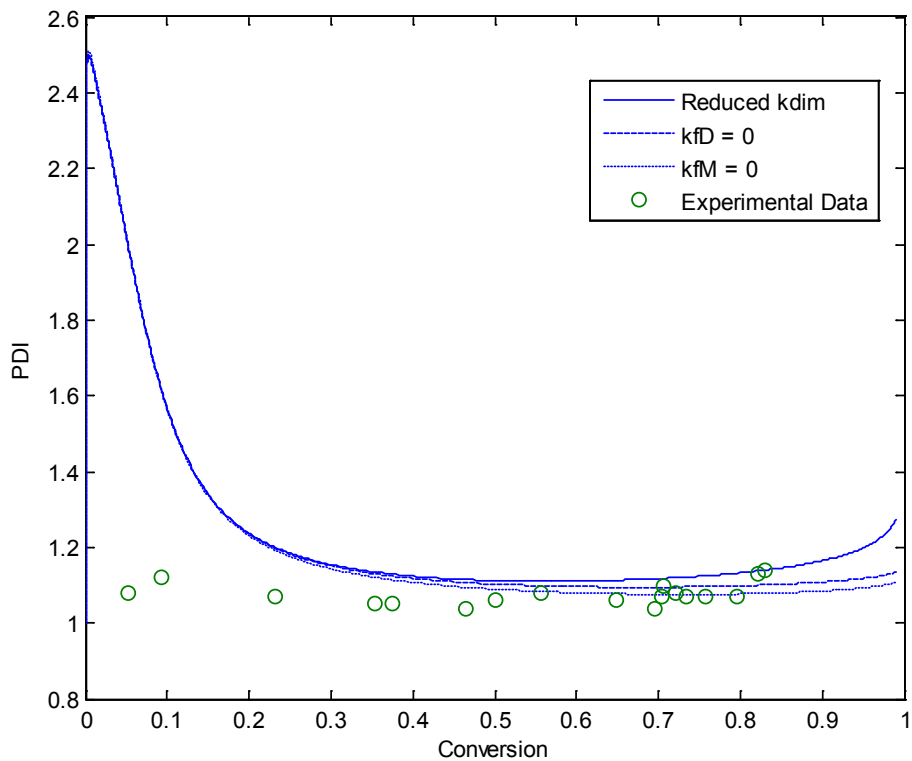
Figure 4-35 – Impact of the removal of kfD and kfM on the unimolecular PDI profile, T = 120 °C

From these results, one can conclude that there is now a very well-fitting model for the unimolecular case as well, across the full conversion range. The adoption of the changes as implemented for the bimolecular case were generally positive for this case, and facilitated much improvement in model fit when it came to prediction of molecular weight values.

4.4 Impact on the TIPNO Case

In Section 3.6 of this thesis, use of the model with a different nitroxide controller radical, TIPNO, was discussed. Rate constants for the new nitroxide were determined from a literature survey and ultimately rate constants for the impacted reactions were selected [7]. Model predictions were obtained, and were similar in accuracy as the predictions in the unrefined TEMPO case, therefore also leaving some room for improvements to be made. In this section, some parameter sensitivity and improvements will be investigated, taking a look at the effects of some of the changes that have been made in the TEMPO case on the TIPNO modeling effort in order to evaluate whether or not they should be adopted in this case.

4.4.1 Efficiency Factors

An investigation into the impact of the efficiency factors for initiator and controller radicals on the model for the TIPNO case was performed. Using the efficiency factors as determined for the TEMPO case, $f = 0.37$ and $f_c = 0.7$, Figures 4-36 through 4-38 illustrate the impact of these efficiencies being implemented into the model for the TIPNO case. Figure 4-36 shows the impact of these changes on the conversion profile – a minor increase in the rate of conversion that causes the predicted profile to show a slightly worse fit to the data. This is the opposite of what was seen in the bimolecular TEMPO case, and in the unimolecular TEMPO case, a negligible impact was seen.
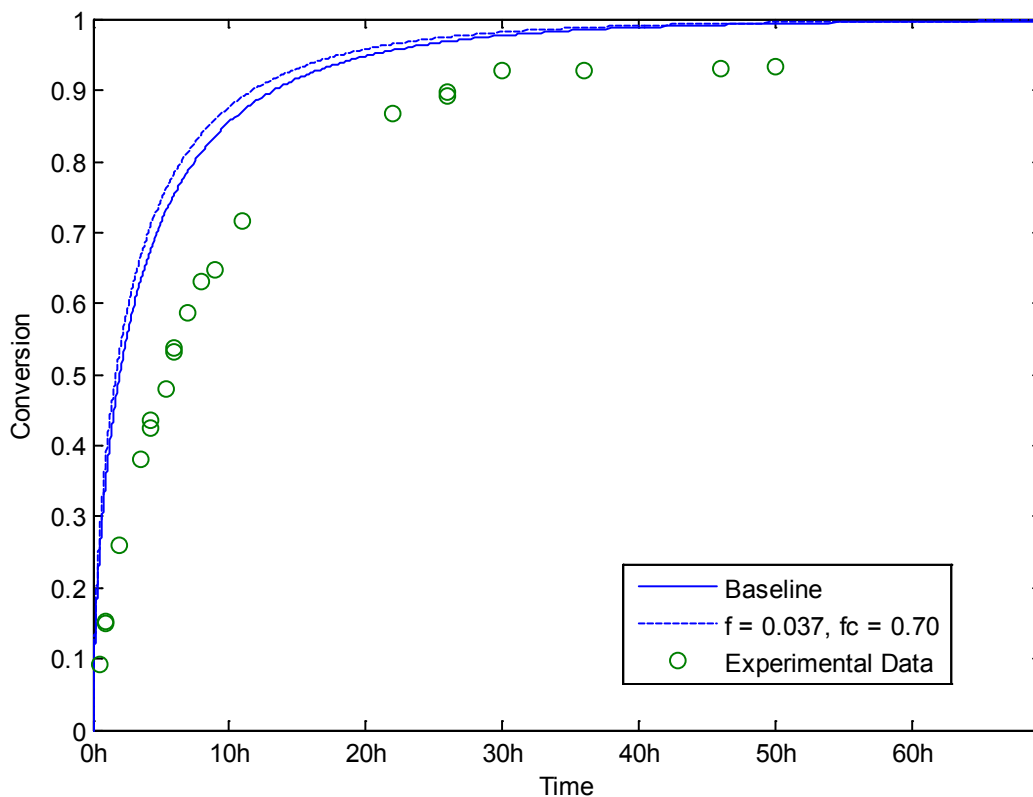
Figure 4-36- Conversion profile incorporating the controller efficiency term for TIPNO, T = 120 °C

This impact is not seen to be great however, so judgment as to whether this change is positive or negative will be reserved until after further analysis. Figure 4-37 illustrates how the introduction of these f and f_c values affect the number-average molecular weight profile. The molecular weight is seen to be higher for a given conversion, bringing it into somewhat better agreement with the experimental data. Figure 4-38 illustrates the effect on the weight-average MW profile, which sees similar gains as those of the number-average MW profile. This leads one to conclude that there will be a minimal impact on the PDI profile, as the ratio between these values appears more or less unchanged.
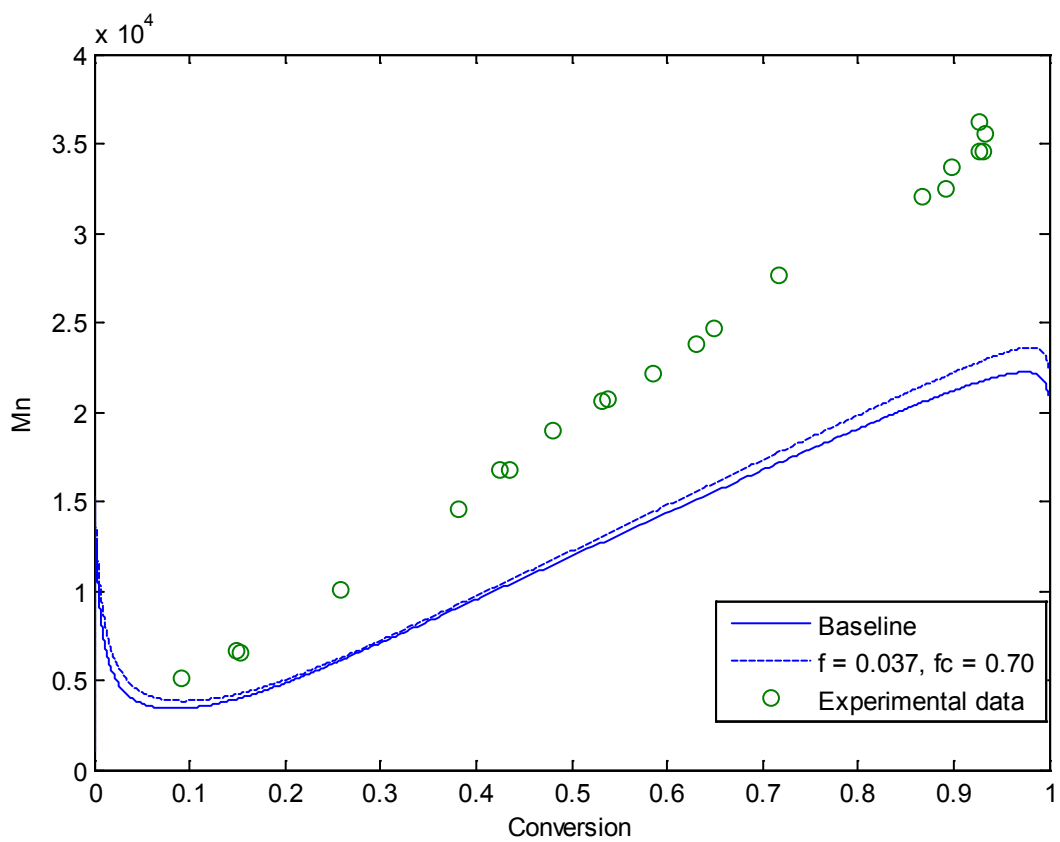
Figure 4-37 $\underline{M}_n$ profile incorporating the controller efficiency term for TIPNO, T = 120 °C
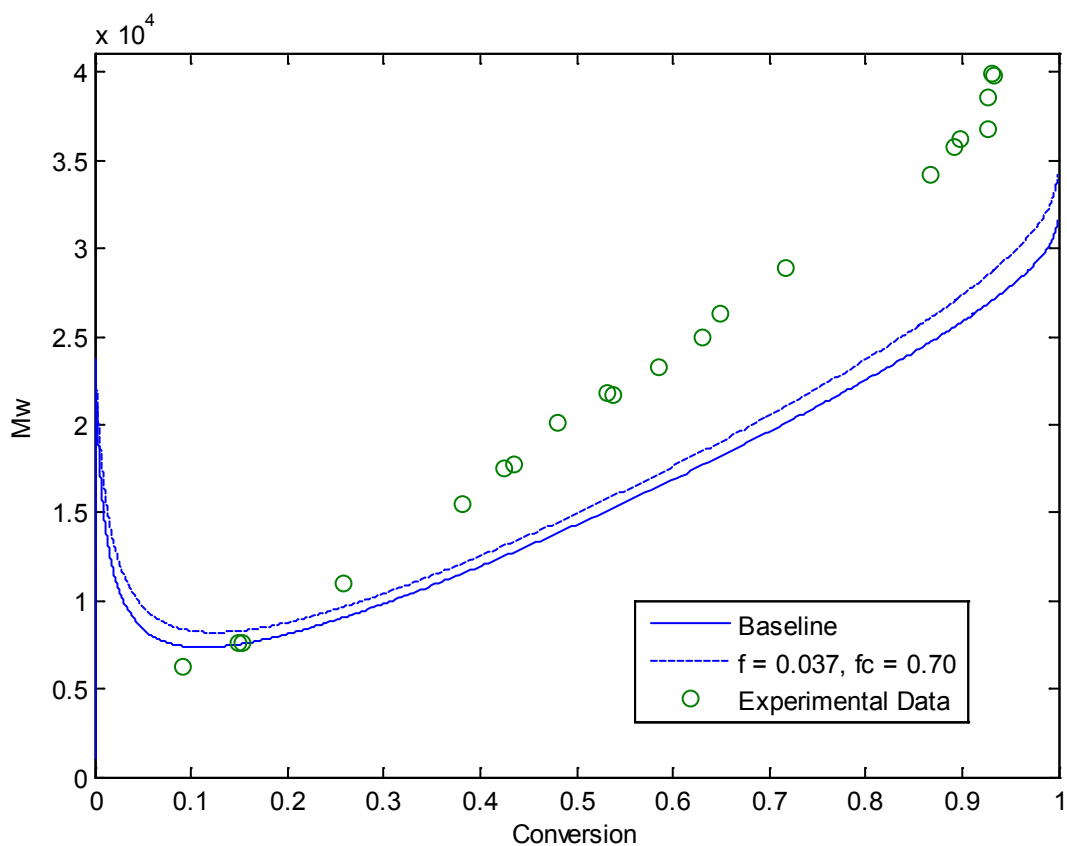
Figure 4-38 $\underline{M}_w$ profile incorporating the controller efficiency term for TIPNO, T = 120 °C

The improvement in the predictive power of the molecular weight profiles may very well be worth the minor loss in fit seen for the conversion profile. Additionally, the impact of changing these efficiencies with conversion was discussed in earlier cases, and may be of use in this case. Figure 4-39 illustrates the implementation of the changes described in Section 4.1.2 on the conversion profile. It is seen that the changes further accelerate this profile in the early phases, and then have a slight reducing effect at higher conversion, again somewhat worsening the fit of this profile. This is comparable to what was seen in the bimolecular TEMPO case, as illustrated in Figure 4-5, where the effect is seen to be more significant than in the unimolecular TEMPO case shown in Figure 4-27. The f and f_c changes again mirror those implemented earlier, and described in Table 4-1.
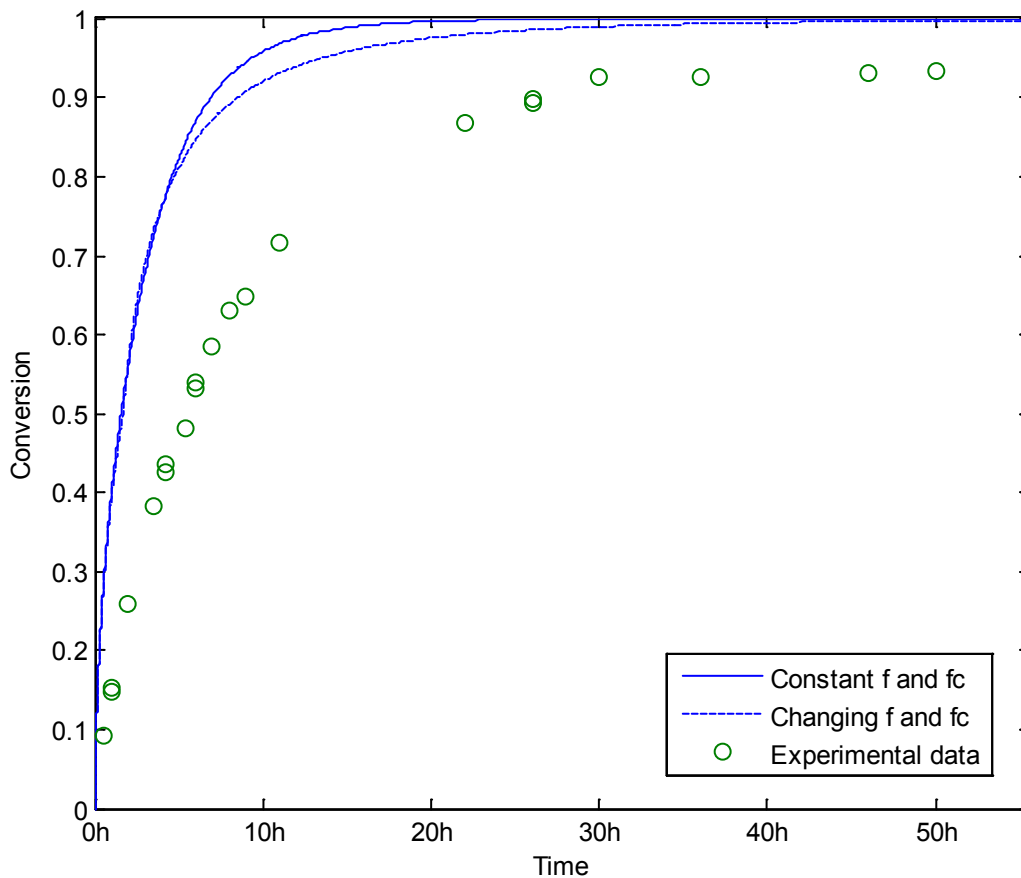
Figure 4-39 - Impact of changing f and f_c on conversion profile, TIPNO case, T = 120 °C

The number-average molecular weight profile was more positively impacted in this case, showing a straighter growth trend and somewhat improved model fit. This is illustrated in Figure 4-40. The weight-average molecular weight profile, Figure 4-41, saw similar gains - though it is now showing more significant curvature as it reaches higher conversion values. This curvature would adversely impact the PDI profile at higher values, as the curvature would be reflected.
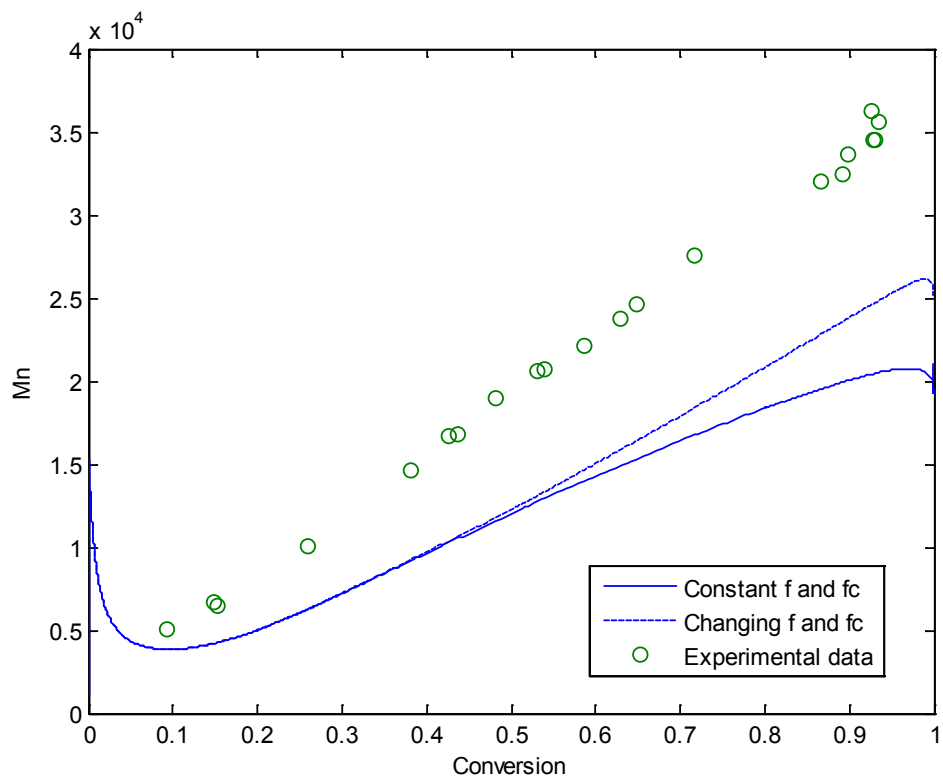
Figure 4-40 – Impact of changing f and f$_c$ on $\underline{M}_n$ profile, TIPNO case, T = 120 °C
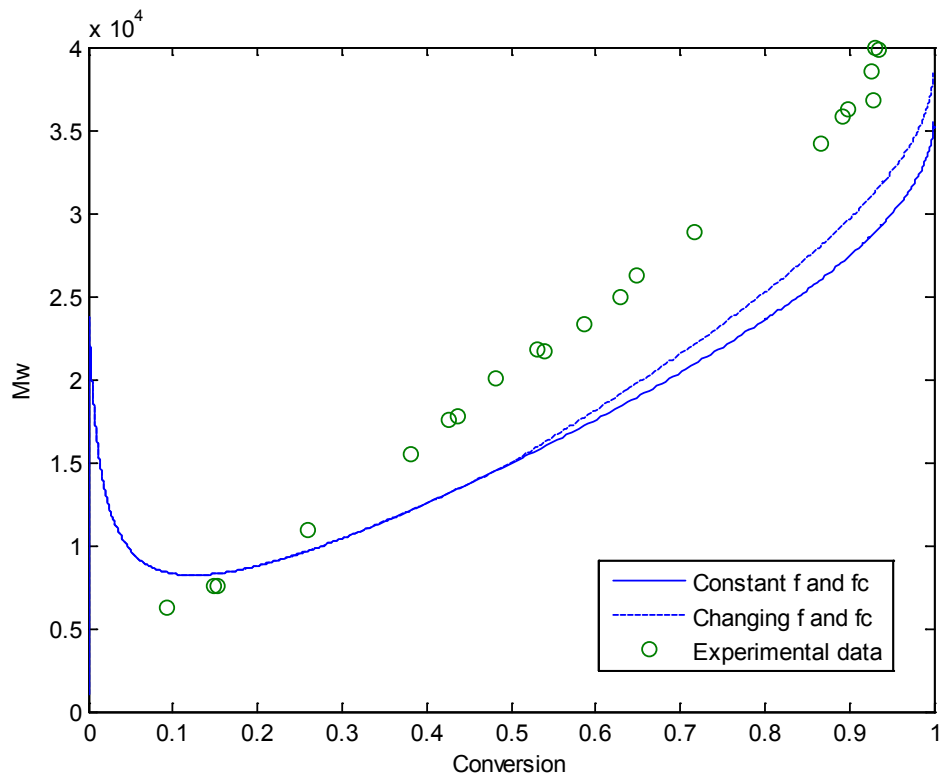
Figure 4-41 - Impact of changing f and f$_c$ on $\underline{M}_w$ profile, TIPNO case, T = 120 °C

Again, the gains in predictive power for the MW estimates may make the minor losses as far as fit of the conversion profile worthwhile. To facilitate consistency with what was done in the earlier cases, these changes will be carried forward as we investigate the other changes to the model.

4.4.2   Rate of Dimerization

Next, the impact of reducing the rate of dimerization in this case is investigated. Figure 4-42 shows the conversion profile as affected by the reduction of k_{dim} as discussed earlier for the unimolecular and bimolecular cases. In this profile, one can see that there is a negligible impact.
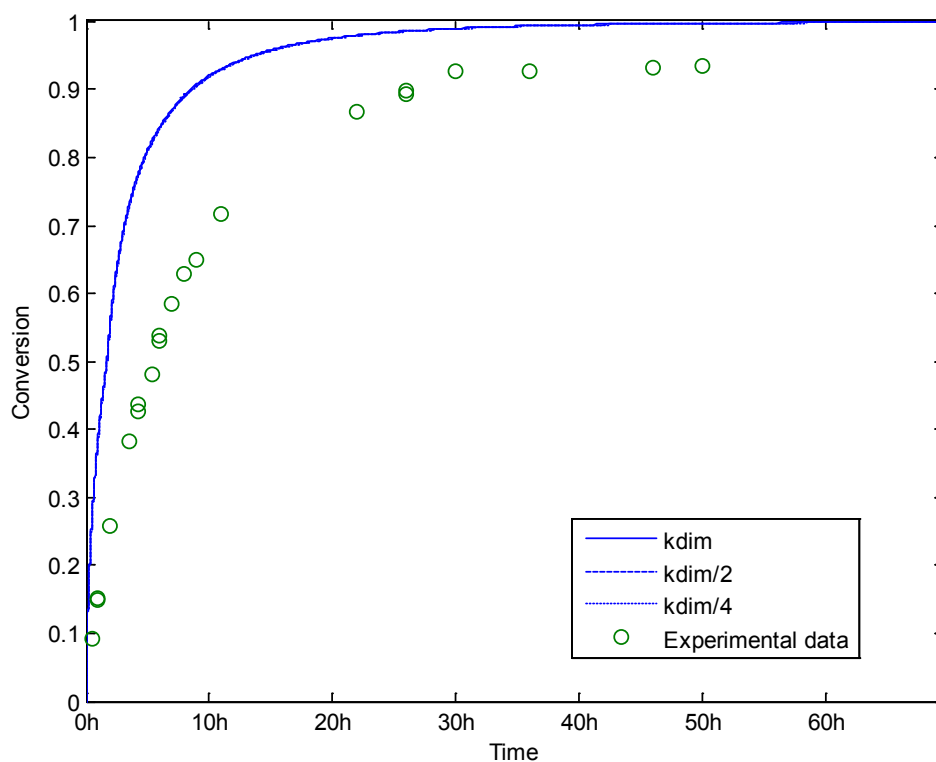
Figure 4-42 – Impact of the reduction of dimerization rate on the conversion profile, TIPNO case, T = 120 °C

The molecular weight profiles show a larger change with this reduction, predicting higher values, more in line with the data. Figure 4-43 shows the impact on the number-average

MW profile, with increased predicted values, especially at higher conversion, and without the downward curvature to this profile. However, a slight upward curvature is seen to have formed at high conversion with the largest reduction in k_{dim}.
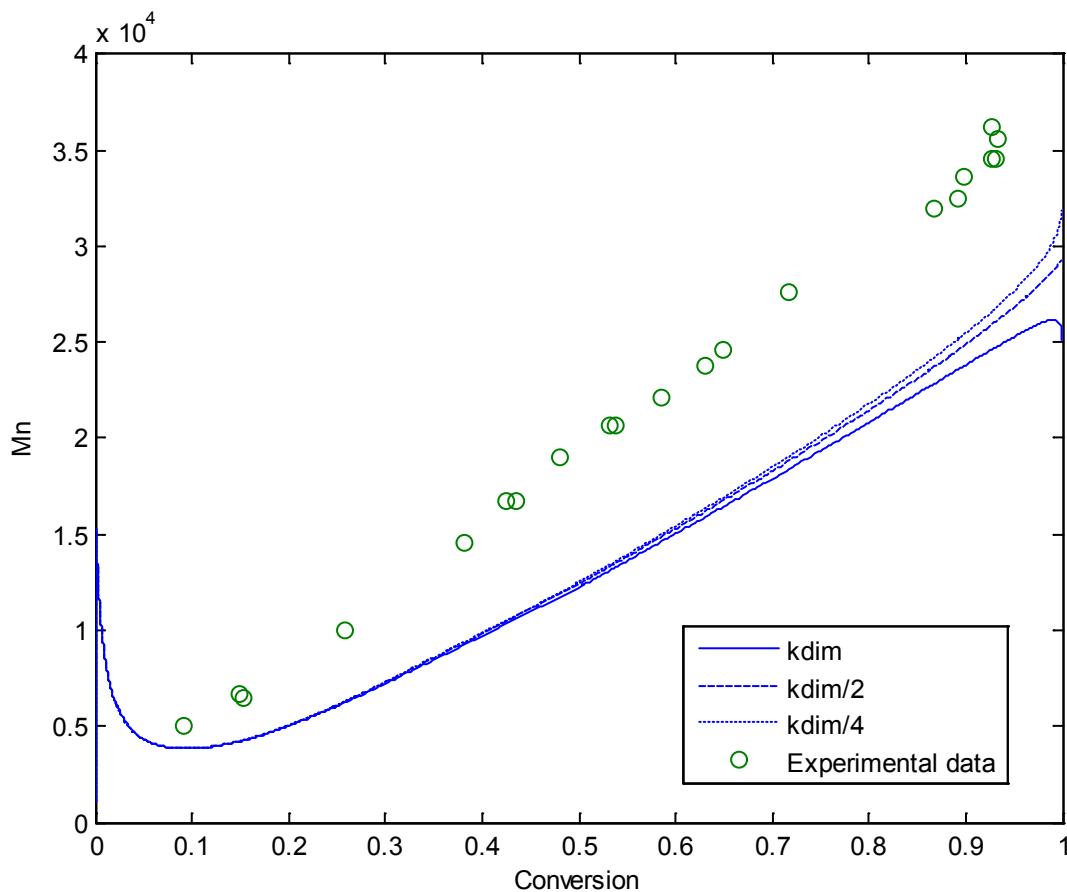
Figure 4-43 – Impact of the reduction of dimerization rate on the $\underline{M}_n$ profile, TIPNO case, T = 120 °C

Figure 4-44 shows the results with the weight-average molecular weight profile, which shows a similar trend; modest increases to predicted molecular weights and some additional curvature introduced to the profile's overall shape as high conversions are reached.
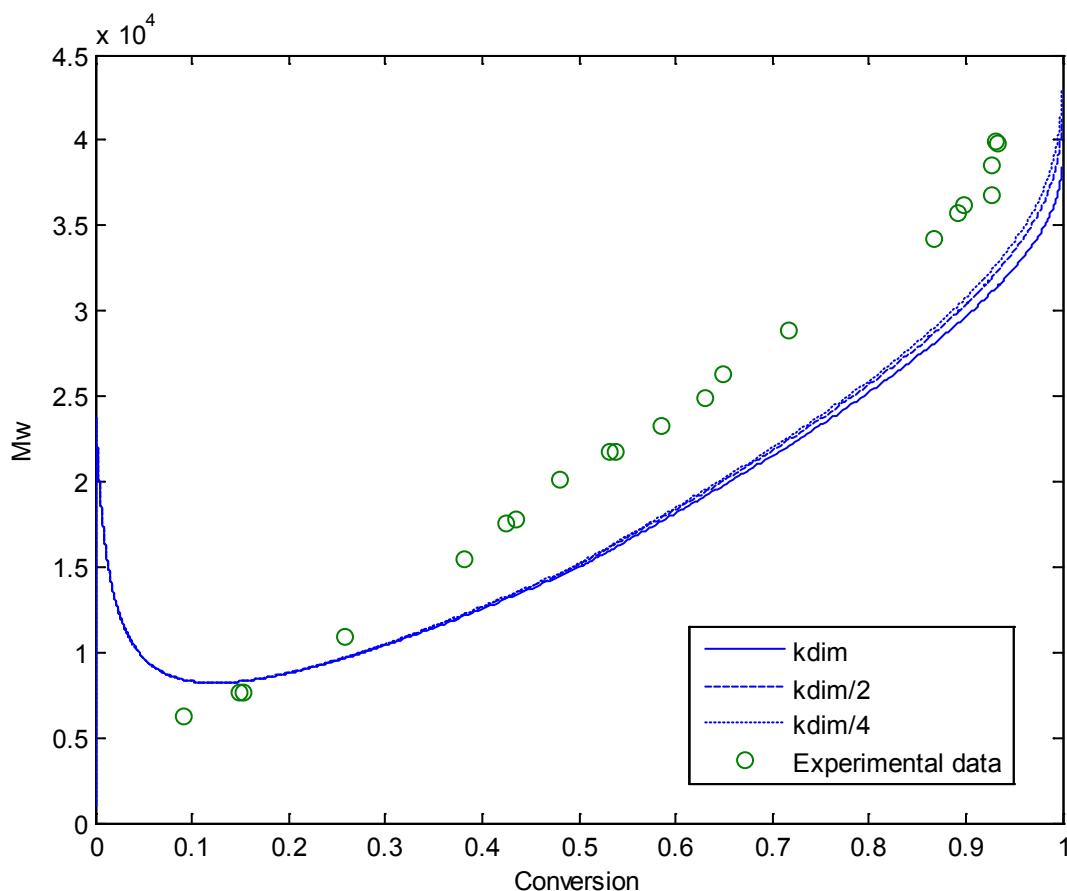
Figure 4-44 – Impact of the reduction of dimerization rate on the $\underline{M}_w$ profile, TIPNO case, T = 120 °C

Overall, these changes have resulted in a slightly better agreement with data, which is consistent with what was seen in the unimolecular TEMPO case. Interesting to note is the lessened impact on conversion, which makes sense, as the higher equilibrium rate between the controller and initiator radicals will make the conversion less sensitive to adjustments in the other rate constants. The changes seen here are very small, and possibly not significant, but it has been demonstrated that the gains in the other cases are more substantial – the adoption of this reduced k_{dim} going forward is planned, in order to ensure greater consistency between what was done in these different cases.

4.4.3 Transfer to Dimer and Transfer to Monomer (k_{fD} and k_{fM})

Finally, the removal of the chain transfer to monomer and chain transfer to dimer reactions will be investigated for the TIPNO case. It is expected that the profiles will be impacted in a manner consistent to the previously discussed cases. Figure 4-45 illustrates the conversion-time profiles generated by the model for this case, with the previous reduction to k_{dim}, the removal of the chain transfer to dimer reaction, and then finally the removal of the chain transfer to monomer reaction as well again plotted with relevant experimental data for comparison.
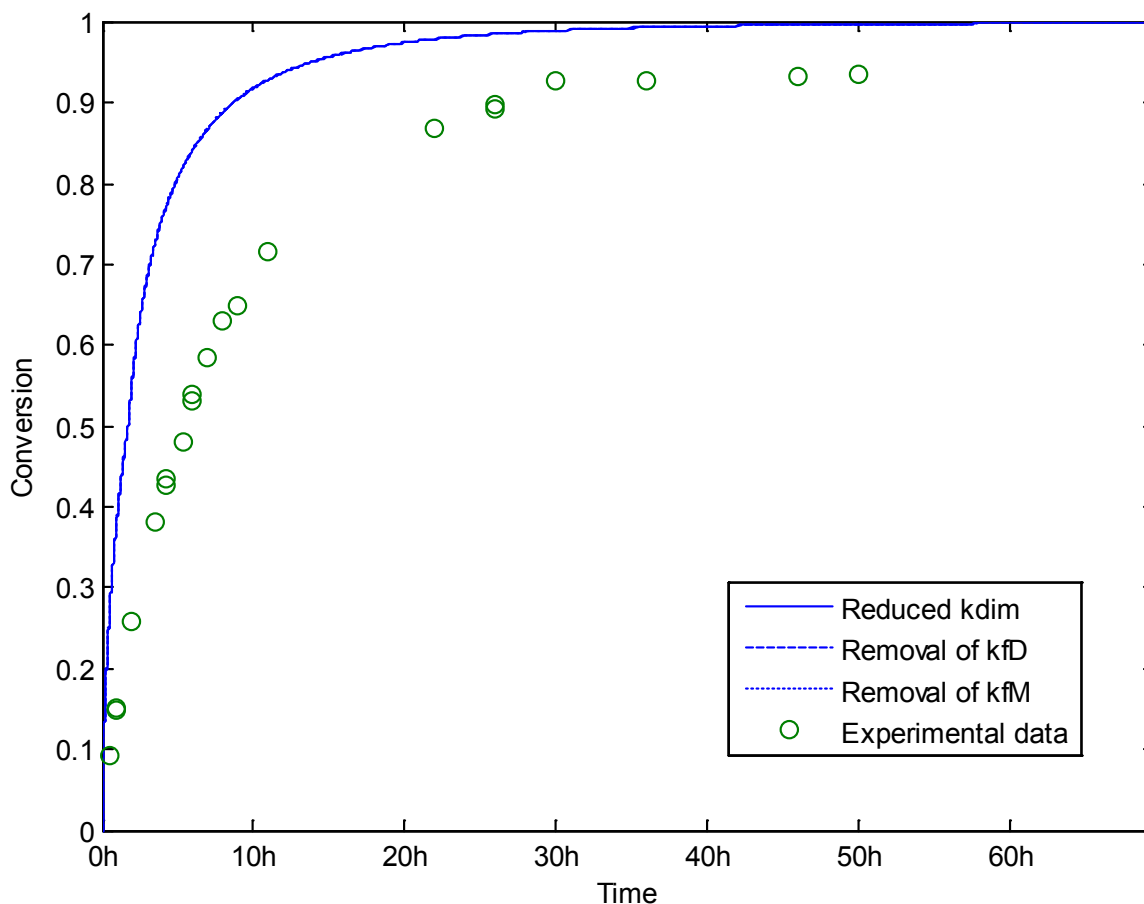
Figure 4-45 – Impact of the removal of k_{fD} and k_{fM} terms for the conversion profile, TIPNO case, T = 120 °C

From this profile, it can be seen that the removal of these reactions has a negligible impact on the conversion profile. This is consistent with what was seen in the unimolecular case with TEMPO. The impacts on the cumulative number-average molecular weight profiles are more promising, with increases in these values, bringing them more in line with the data values. Figure 4-46 illustrates the number-average molecular weight profile for this case, where there is a modest gain in predicted MW values, bringing them somewhat closer to the data values. A similar result is seen in the weight-average MW profile illustrated in Figure 4-47.
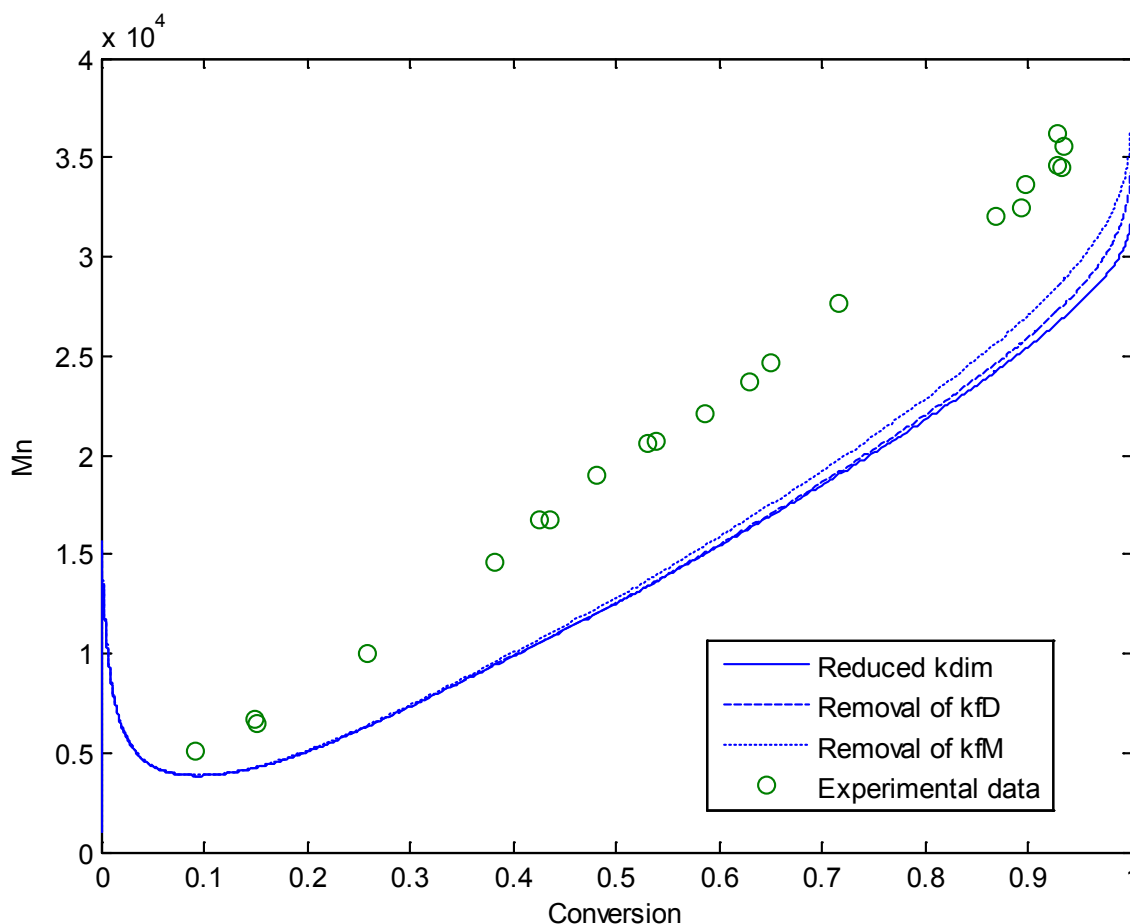
Figure 4-46 – Impact of the removal of k_{fD} and k_{fM} terms for the $\underline{M}_n$ profile, TIPNO case, T = 120 °C
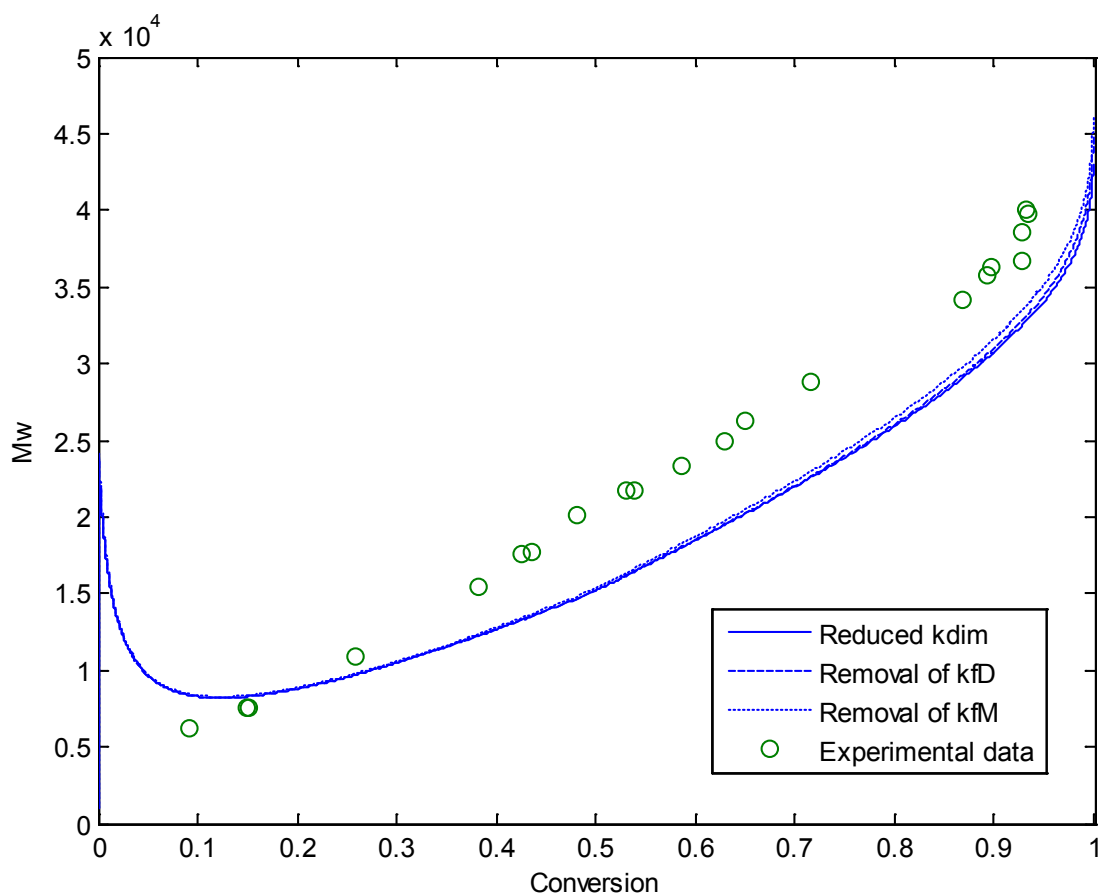
Figure 4-47 – Impact of the removal of k_{fD} and k_{fM} terms for the $\underline{M}_w$ profile, TIPNO case, T = 120 °C

4.5   Concluding Remarks

In essence, this sensitivity study not only revealed interesting trends in the model responses and improved model performance when compared to experimental data, but also indicated a mechanistic model reduction approach. The model at this level is still fully mechanistic, but contains fewer terms, hence it is somewhat reduced. It also provides overall good predictions over the full conversion range and over a wide range of operating conditions for the bimolecular process.

Implementing these reductions and changes in the various applicable cases that were discussed in Chapter 3, including the unimolecular TEMPO and TIPNO cases, yielded similarly interesting results. The unimolecular case was very successful in mirroring the

high level of predictive power, especially when it comes to molecular weight data. More modest gains to model performance were seen in the TIPNO case; however the model still provides fairly good predictions across the full conversion range.

Table 4-3 provides a summary of the changes to the parameter values between the initial model from Chapter 3 (referred to in future chapters as the FMM) and the model incorporating all the changes as discussed in this chapter (referred to in future chapters as the RMM).

Table 4-3 - Summary of the changes to parameter values made in Chapter 4

Parameter	FMM Value	RMM Value
f	0.54-0.55	If conversion <= 0.5, f = 0.4
		If conversion > 0.5, f = 0.37
f_c	Nonexistent (essentially, f_c = 1)	If conversion <= 0.5, f_c = 0.7
		If conversion > 0.5, f_c = 0.35
k_{h3}	0.001 L mol^{-1} s^{-1}	0 (i.e., reaction removed from model)
k_{dim}	$188.97 \exp\left(-\dfrac{16185.1}{RT}\right)$ L mol^{-1} s^{-1}	$188.97 \exp\left(-\dfrac{16185.1}{RT}\right)/4$ L mol^{-1} s^{-1}
k_{fD}	50 L mol^{-1} s^{-1}	0 (i.e., reaction removed from model)
k_{fM}	$9.376 \times 10^6 \exp\left(-\dfrac{13372}{RT}\right)$ L mol^{-1} s^{-1}	0 (i.e., reaction removed from model)

The next chapter (Chapter 5) will attempt a much more significant model reduction, which will lead to a simplified model, which will hopefully capture the main process effects but with highly simplified equations. If the predictions prove satisfactory, these simplified equations, will be easier to use for process design of experimental scenarios and other process optimization applications.

Chapter 5: Model Reduction

5.1   Rationale

At this point, we have developed a quite accurate, though still very complex, fully mechanistic model (FMM). The FMM consists of thirteen differential mass balances (for all of the different species present in the batch NMRP of styrene), nine moment equations (for moments zero, one, and two of each of the living polymer radicals, dormant polymer, and dead polymer species), and several algebraic equations (e.g., to use the moment equations for the formulation of average molecular weights and polydispersity index). This full model could prove too complex for use in certain optimization and design situations, as it requires a non-trivial effort to evaluate numerically/computationally.

To this end, a substantially reduced model was developed by returning to elementary rate expressions, as discussed by Fukuda and Goto [1]. This section will discuss the development of this model, as well as comparisons to experimental data and to the predictions of the fully mechanistic models from Chapters 3 and 4.

5.2   Substantially Reduced Modelling Effort

The guiding idea for developing the reduced model is to try and describe with mathematical equations the minimum number of responses one is interested in from a typical polymerization (i.e., the ones one can measure/quantify), namely, conversion, average molecular weights and polydispersity. Hence, the fully mechanistic model of Chapters 3 and 4 represents one extreme of the spectrum: detailed and comprehensive but complex. It can give information about the main variables of interest (e.g., conversion molecular weights, etc.) and also about intermediate variables that may not be measured or tracked easily experimentally (e.g., concentration profiles of dormant species, moments of molecular weight distribution, concentration profiles of initiator and controller, etc.). However, the numerical computations using the FMM may be prohibitive, if one would like to use the model on-line or for design purposes, since so many higher order derivatives and

sensitivity functions may have to be evaluated over time, with some of these functions being highly non-linear, hence often resulting in numerically unstable or infeasible/impractical solutions.

The substantially reduced model lies on the other end of the spectrum: highly simplified; covers the minimum key process variables; gives sufficient information about main effects (hence, loss of detail and often loss of generality); easy to manipulate, it leads to simpler solutions numerically or computationally, whether efforts for on-line applications or off-line design calculations (or the derivation and evaluation of other optimal trajectories).

If one can show that the reduced (simplified) model can capture not only the main trends but also the trajectories of the main responses quantitatively, then one could use the two extreme mathematical model types interchangeably and in a highly complementary way. In addition, since the highly reduced model is still based on mechanistic first principles, it will be at any time superior to any simpler empirical model.

5.3   Derivation of Substantially Reduced Model

In the derivation of the reduced model, we consider systems where:

1) The quasi-equilibrium is reached so fast that the main body of polymerization occurs in the time range of quasi-equilibrium and the pre-equilibrium stage has no significant effect on the polymerization kinetics.
2) The cumulative number of dead chains by termination and initiated chains by initiation are sufficiently small compared with the number of dormant chains.
3) The initiation rate (R_i) is constant.
4) All possible reactions other than those indicated in what follows are neglected.
5) All the rate constants are assumed to be independent of chain length.

The analysis below will follow the developments in [1, 2, 3, 4]. Translating the above statements into equations, we have the following two differential equations [2]:

$$\frac{d[X\bullet]}{dt} = k_a[R-X] - k_d[R\bullet][X\bullet] \qquad \text{Eq. 5-1}$$

$$\frac{d[R\bullet]}{dt} = k_a[R-X] - k_d[R\bullet][X\bullet] + R_i - k_t[R\bullet]^2 \qquad \text{Eq. 5-2}$$

where $[X\bullet]$ is the concentration of active controller radicals, $[R\bullet]$ is the growing polymer radical concentration, and $[R-X\bullet]$ is the concentration of the dormant species formed by the coupling of the two radicals.

The sum of these Equations, 5-1 and 5-2, gives [3]:

$$\frac{d[R\bullet]}{dt} = \frac{d[X\bullet]}{dt} + R_i - k_t[R\bullet]^2 \qquad \text{Eq. 5-3}$$

The quasi-equilibrium ($\frac{d[X\bullet]}{dt} \approx 0$) with negligible fraction of dead chains is represented by the following, where $I_0 = [R-X]_0$ [4].

$$[R\bullet][X\bullet] = K[R-X] = K I_0 \qquad \text{Eq. 5-4}$$

where $\quad K = \dfrac{k_a}{k_d}$

Since it usually holds that $[R\bullet] << [X\bullet]$, we may neglect $\frac{d[R\bullet]}{dt}$ as compared with $\frac{d[X\bullet]}{dt}$ in the above two equations, giving [1]:

$$\frac{d[X\bullet]}{dt} = \frac{k_t K^2 I_0^2 - R_i[X\bullet]^2}{[X\bullet]^2} \qquad \text{Eq. 5-5}$$

This can then be solved to provide radical concentrations and subsequently the rate of polymerization. However, only the case of stationary-state systems (systems with Ri >>0) will be discussed here.

When R_i is sufficiently large, the stationary state ($\frac{d[R\bullet]}{dt} = \frac{d[X\bullet]}{dt} = 0$) is reached at an early stage of polymerization and we obtain [2]:

$$R_i = R_t = k_t[R\bullet]^2$$

Eq. 5-6

Therefore, the following equations can be used to describe the system.

$$[R\cdot] = (\frac{R_i}{k_t})^{1/2}$$

Eq. 5-7

$$R_p = k_p[M](\frac{R_i}{k_t})^{1/2}$$

Eq. 5-8

$$[X\cdot] = KI_0(\frac{k_t}{R_i})^{1/2}$$

Eq. 5-9

$$\ln\left(\frac{[M]_0}{[M]}\right) = k_p(\frac{R_i}{k_t})^{1/2}t$$

Eq. 5-10

From these equations, the following expressions, Equations 5-11 and 5-12, can be obtained for conversion and rate of initiation:

$$x = 1 - \exp(-k_p(\frac{R_i}{k_t})^{\frac{1}{2}}t)$$

Eq. 5-11

$$R_i = k_{ia}k_{dim}(-[M_0](1-x)^3\,t) + 2fk_dI_0\exp{(k_dt)}$$

Eq. 5-12

Coupled with Arrhenius expressions – as previously discussed in Chapter 3, and reiterated here in Table 5-1 – for the rate constants involved, it is then possible to solve the system of equations 5-7 to 5-12.

Table 5-1 - Arrhenius expressions and values for rate constants required for simplified model

Rate Constant	Units	Bimolecular	Unimolecular
k_d	s^{-1}	$1.7 \times 10^{15} \exp\left(-\dfrac{30000}{RT}\right)$	$1.7 \times 10^{15} \exp\left(-\dfrac{30000}{RT}\right)$
f		0.54-0.55	1
k_{dim}	L mol^{-1} s^{-1}	$188.97 \exp\left(-\dfrac{16185.1}{RT}\right)$	$188.97 \exp\left(-\dfrac{16185.1}{RT}\right)$
k_{ia}	L mol^{-1} s^{-1}	$6.359 \times 10^{12} \exp\left(-\dfrac{36598.55}{RT}\right)$	$6.359 \times 10^{12} \exp\left(-\dfrac{36598.55}{RT}\right)$
k_p	L mol^{-1} s^{-1}	$4.266 \times 10^{7} \exp\left(-\dfrac{7769.17}{RT}\right)$	$4.266 \times 10^{7} \exp\left(-\dfrac{7769.17}{RT}\right)$
k_t	L mol^{-1} s^{-1}	$2.002 \times 10^{10} \exp\left(-\dfrac{3081.84}{RT}\right)$	$2.002 \times 10^{10} \exp\left(-\dfrac{3081.84}{RT}\right)$

Combining this solved conversion profile with the expression for number-average molecular weight (Equation 5-13), predictions for this key process response can also be obtained.

$$M_n = \frac{MW_{Sty}[M_0]}{[TEMPO]_0} \times (x)$$

Eq. 5-13

Estimates for the polydispersity index (PDI) for the final conversion can be determined using the following expression obtained from Grezta and Matyjaszewski, labeled Equation 5-14 [5].

$$PDI = \frac{M_w}{M_n} = 1 + \frac{k_p[I]_0}{k_d[TEMPO]_0}$$

Eq. 5-14

From these, we can now estimate four of the most important process responses for any polymerization process; conversion, number-average molecular weight, weight-average molecular weight, and polydispersity index. However, it is worth noting that the values obtained for PDI and M_w (as calculated from known values using Equation 5-14) are only valid for the final conversion, so profiles cannot be generated for these responses.

5.4   Evaluating the Reduced Model

Now that a simplified model has been proposed, it only makes sense to evaluate its performance. To this end, some comparisons with experimental data, the full mechanistic model (FMM) and the refined mechanistic model (RMM) – as defined in Chapter 4's conclusions – will be discussed here. Also, some investigation into how well this model captures temperature and ingredient (i.e., TEMPO/BPO ratio) changes is needed in order to evaluate this model's performance.

5.4.1   Comparison with Experimental Data

First, for some preliminary results, the simplified model will be solved and compared with some of the experimental data that is available for this process. The data used in this case is for the unimolecular case, taken from Zhou [6] and is the same as was used in earlier chapters when discussing unimolecular initiation.
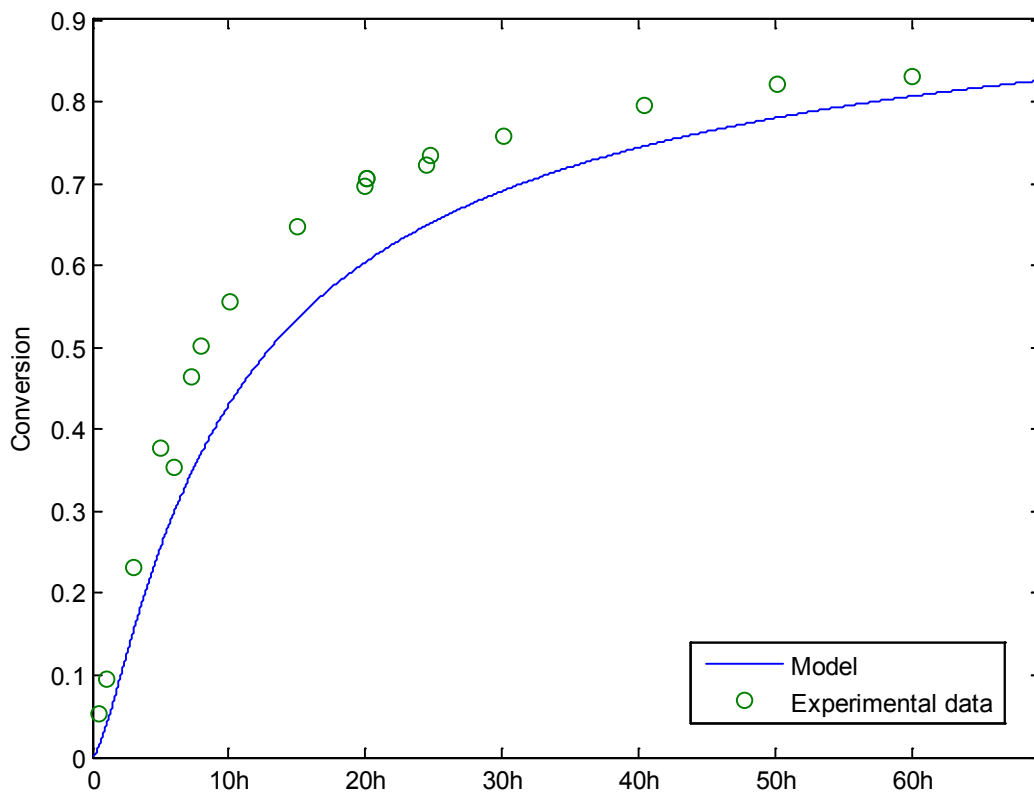
Figure 5-1 – Conversion profile generated by simplified model, T= 120 °C, unimolecular case

Figure 5-1 illustrates the conversion profile generated by this modeling effort, compared with the experimental data for the unimolecular case. The profile generated provides a generally acceptable trend, with a reasonably good fit. The conversion values predicted by this model are seen to be somewhat lower than those obtained experimentally, but the overall shape is good, with slightly better agreement seen at low and high conversion.
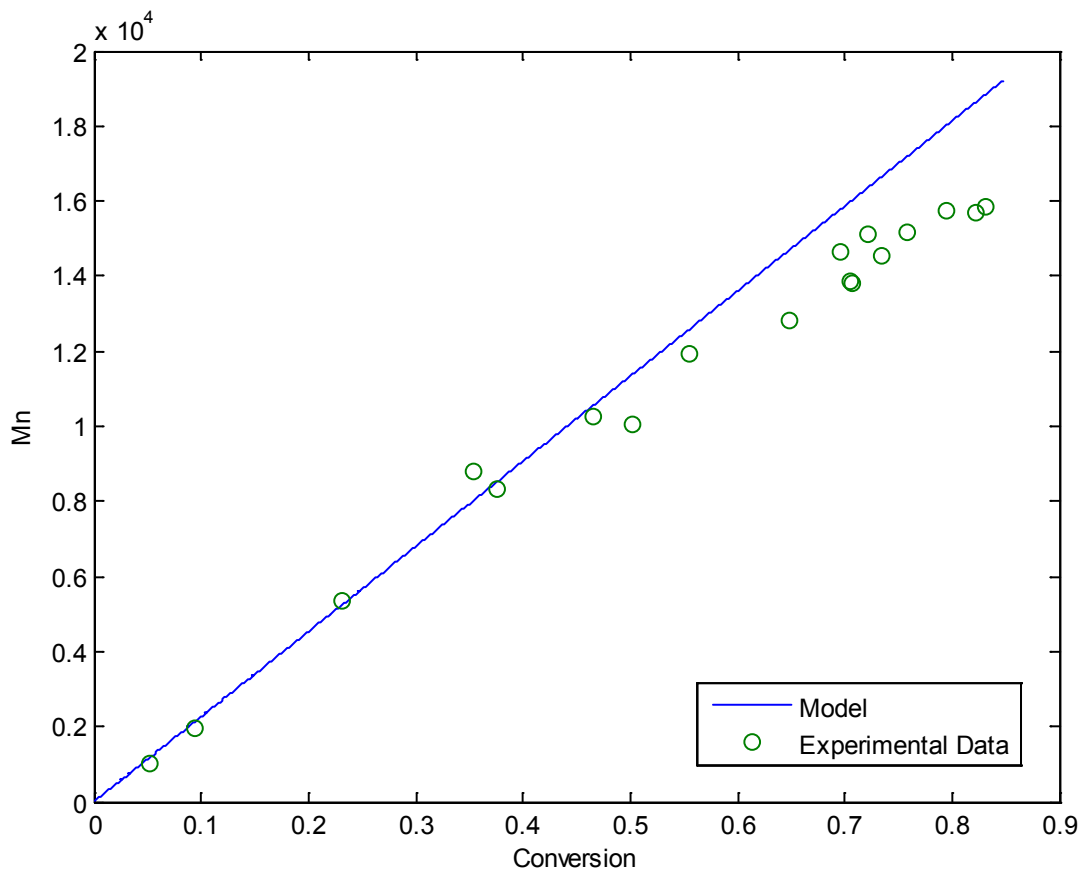
Figure 5-2- Mn profile generated by simplified model, T = 120 °C, unimolecular case

Figure 5-2 depicts the M_n profile generated using this simplified model. Again, general trend agreement is seen, and the predicted values fit the experimentally obtained values very well until high conversion, where the predicted values are seen to somewhat exceed those of the data.

In the bimolecular case, comparing with data from Nabifar [7], similar results are seen, with Figure 5-3 depicting the conversion profile generated by the simplified model for this case. As can be seen, the rate of conversion is again somewhat underestimated, with predicted conversion values being slightly lower than the experimental data throughout the conversion range, and the largest disagreement in the middle of the time range.
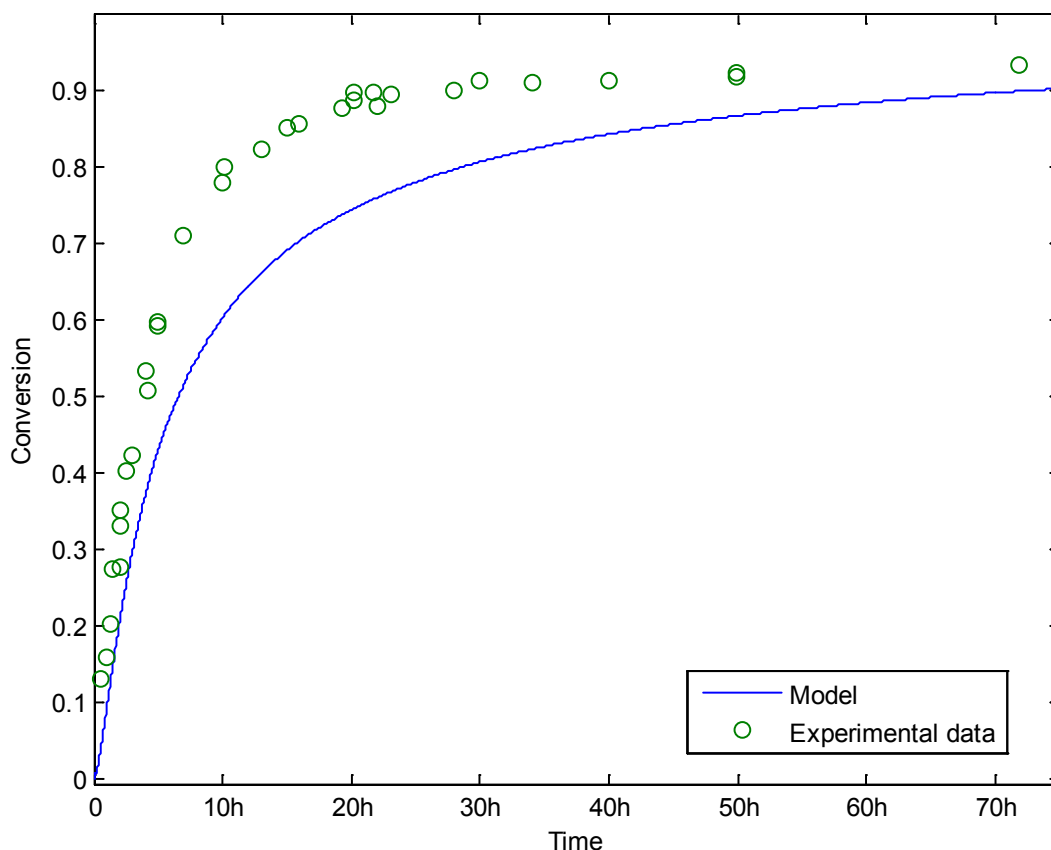
Figure 5-3 Simplified model conversion profile, bimolecular case, T = 130 °C, R = 1.1

Figure 5-4 illustrates the number-average molecular weight profile generated for this case, where generally good agreement is seen with the data, though instead of the predicted values seen to be at the high end of the data range, the predicted values are toward the low end. This compares favourably with the results of the fully mechanistic model prior to its refinement, where similarly low predictions were seen (refer to figure 3-3), however the

current reduced model has the major advantage of not exhibiting the erroneous curvature at high conversion values.
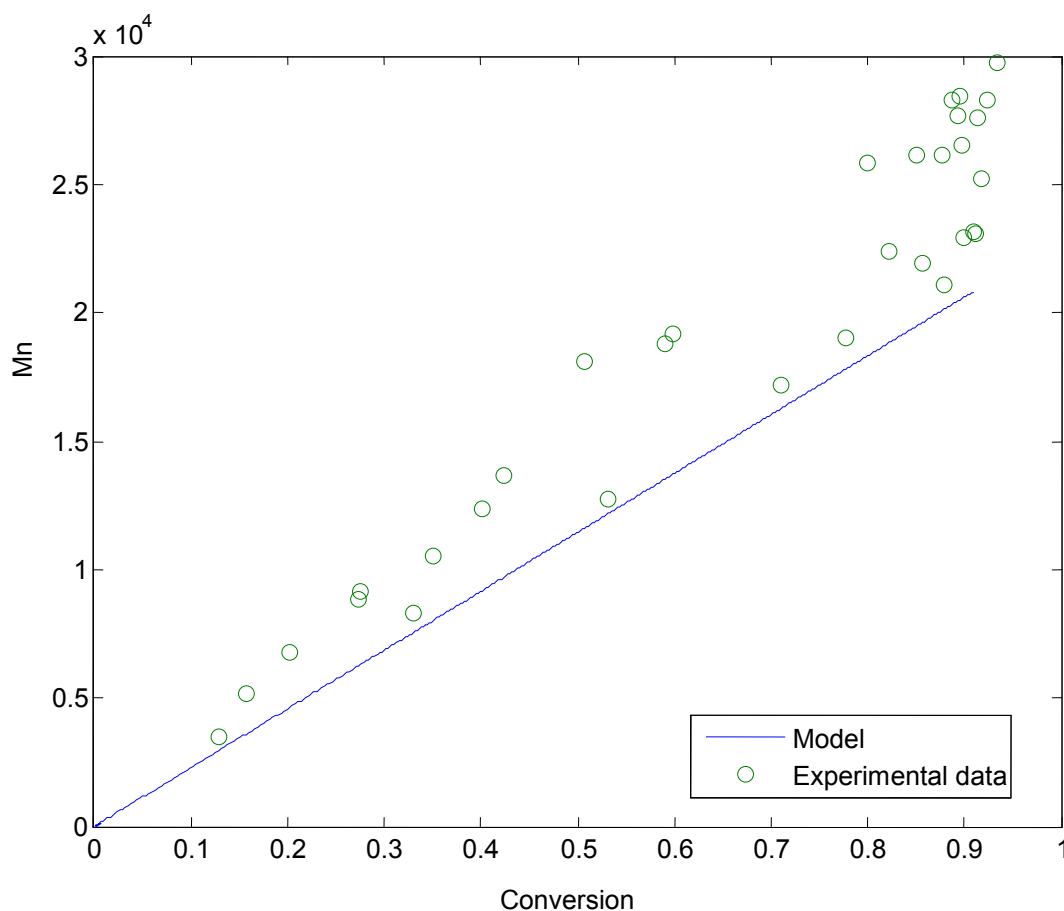
Figure 5-4 – Simplified model $\underline{M}_n$ profile, bimolecular case, T = 130 °C, R = 1.1

5.4.2   Temperature Effects

At this point, now that the reduced model has been shown to be satisfactory at predicting values for both the unimolecular and bimolecular cases, some brief analysis of how the model is impacted by changes to temperature is in order.   Figure 5-5 illustrates the profiles generated by this model with temperatures set at 120 °C and 130 °C. As expected, the conversion rate is seen to be considerably higher with the higher temperature setting, which is comparable to the trend that was seen in the earlier discussion with temperature variation of the FMM, as shown in Figure 3-7. Figure 5-6 shows the impact of changing

temperature on the generated molecular weight profile, which is seen to be mostly negligible.
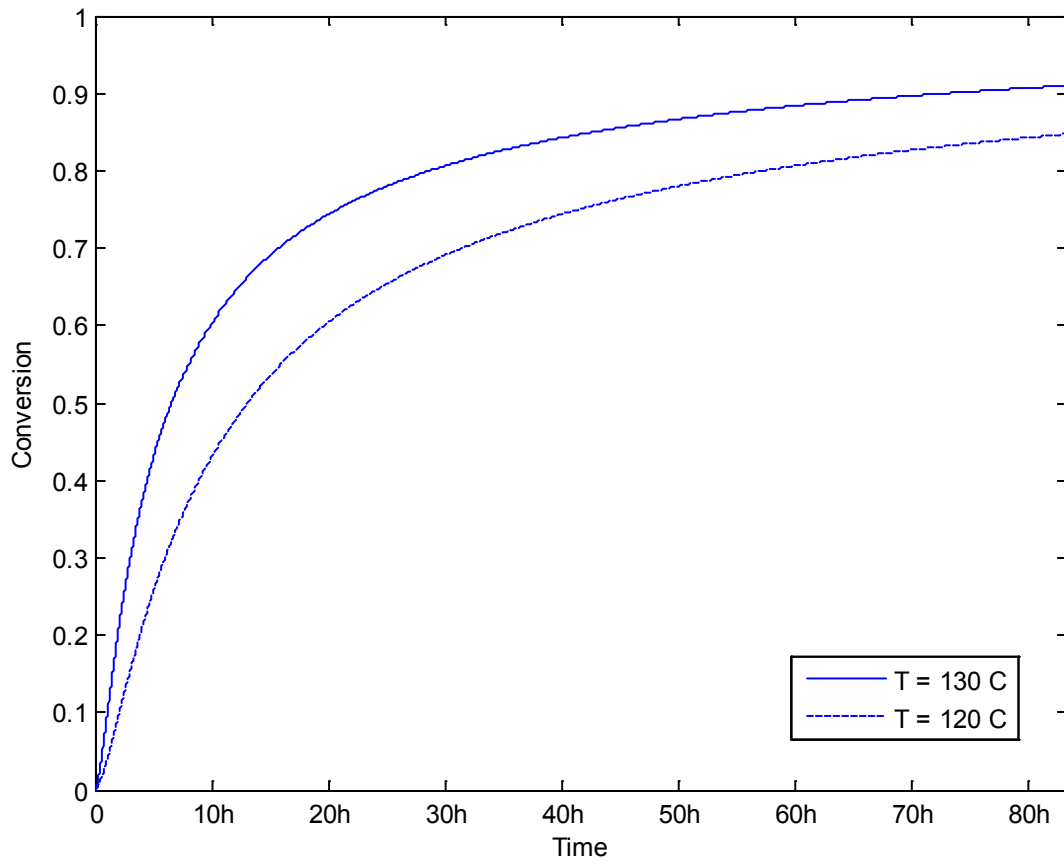
Figure 5-5 – Temperature effects on simplified model conversion profile, bimolecular case, R = 1.1
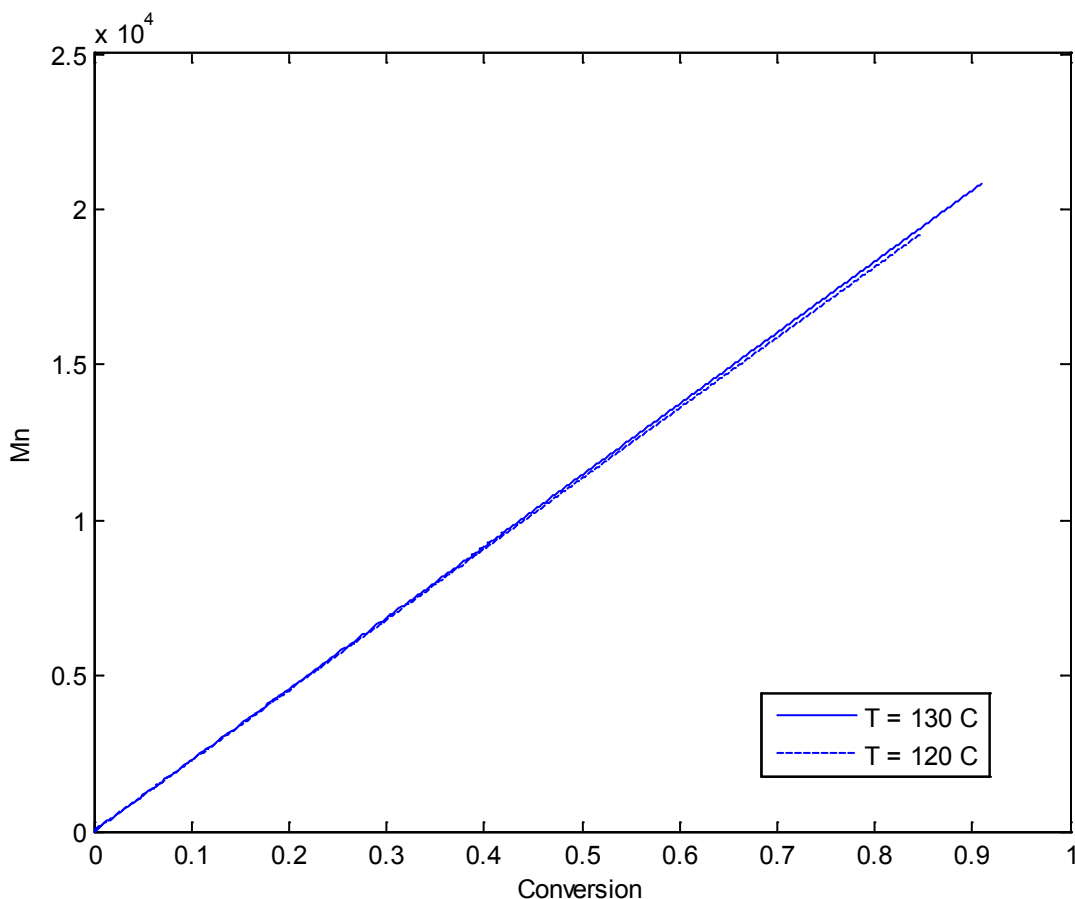
Figure 5-6 – Temperature effects on simplified model $\underline{M}_n$ profile, bimolecular case, R = 1.1

5.4.3   Ratio Effects

The impacts of changes to the TEMPO/BPO ratio, R, on the simplified model are also of interest.   Figure 5-7 illustrates the negligible impact of this ratio on the generated conversion profile.   Contrary to what was seen with the FMM earlier (see Figure 3-13), where lower values of R were seen to greatly slow down the rate of reaction, especially early on in the reaction, the change in ratio is seen to have a negligible impact on the conversion profile generated by the simplified model.   This should be noted as a disadvantage of the reduced model.
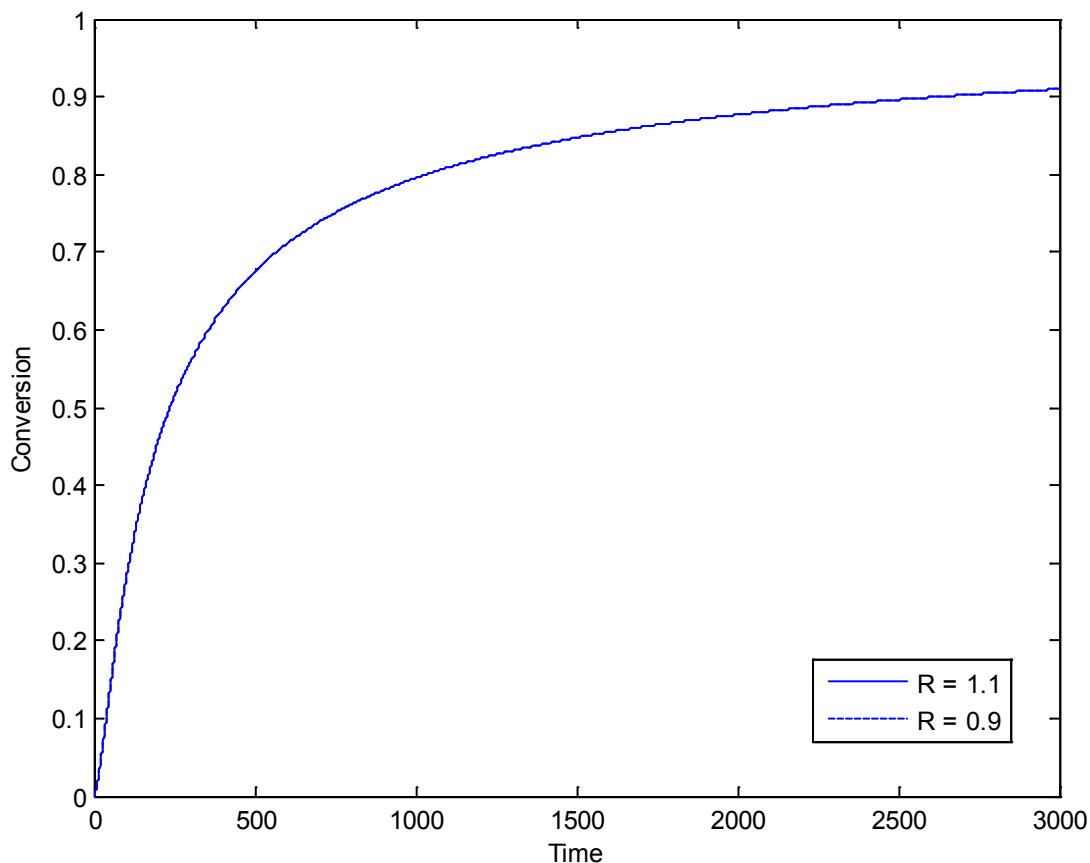
Figure 5-7 Effect of variation of TEMPO/BPO ratio on simplified model conversion profile, T = 130 °C

Figure 5-8 illustrates the impact of changes to R on the molecular weight profile generated using the simplified model. As was seen in the earlier discussion involving the FMM (and as shown in Figure 3-14), the molecular weight prediction is seen to substantially increase with a reduction in the TEMPO/BPO ratio. This is also in line with what was seen with the data, in the discussion of Section 3.4.3, which leads us to believe that the model is again performing satisfactorily.
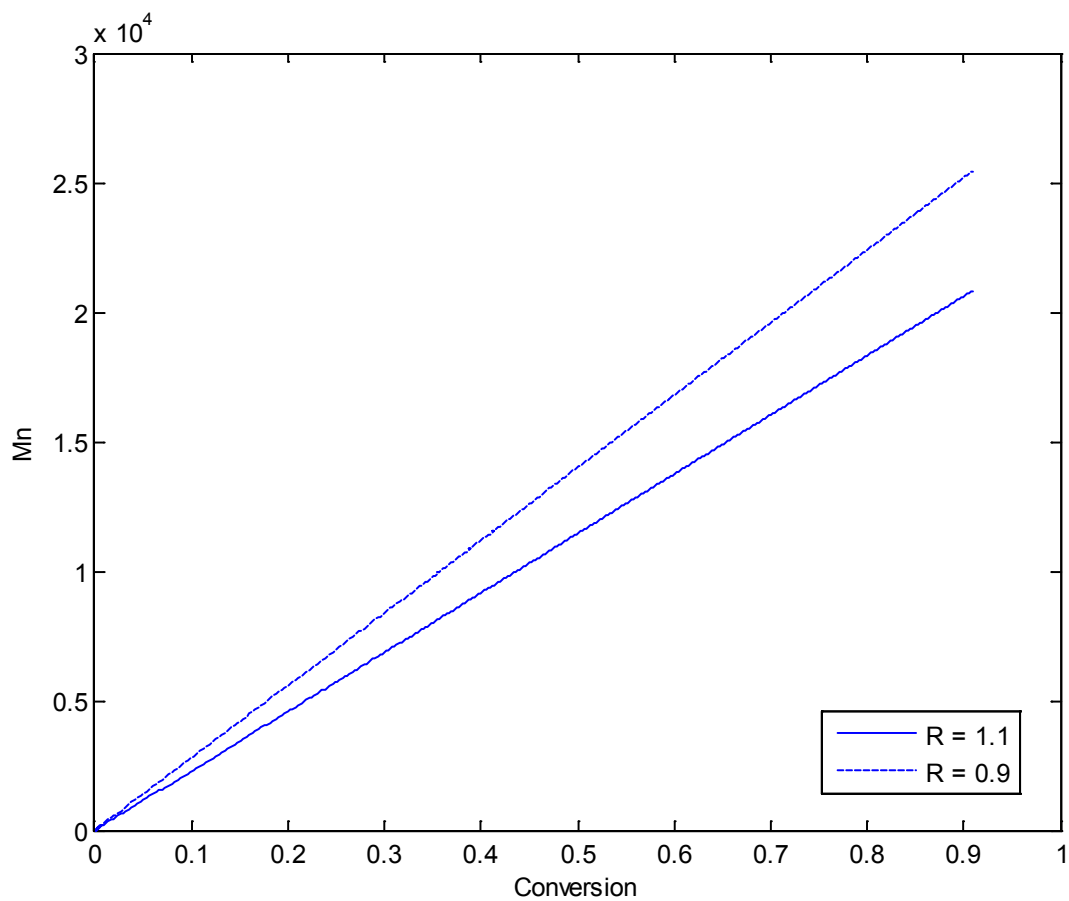
Figure 5-8 – Effect of variation of TEMPO/BPO ratio on simplified model $\underline{M}_n$ profile, T = 130 °C

5.5   Concluding Remarks

The efforts to create a much simpler, easier to implement, yet still mechanistic model of the process have been largely successful. The simplified model as presented in this chapter has been demonstrated to provide a good picture of the trends of the key measurable responses of such a polymerization; namely, the number-average molecular weight and conversion.

This model appears to be a reasonably effective option for capturing main trends, and as such, can be used interchangeably and in conjunction with the more complex fully mechanistic or refined mechanistic models in a variety of applications – for instance, with the simplified model providing on-line estimates of molecular weight averages and conversion while the FMM is used off-line to verify or to estimate those responses that are not easily measureable. If used in cases where only these main process responses are of interest, the simplified model could suffice.

Chapter 6: D-Optimal Design of Experiments

An application of these models was their use in the D-optimal design of experiments. D-optimal design of experiments is a method for choosing a set of experiments to run that are most valuable (i.e., maximize the information obtained by running them) [1]. Chemical engineering applications of these experimental designs have been discussed in the literature since the 1960's [2], [3], but with the ever improving state of computers, can be performed much more easily and with more complex models than ever before. Some more recent work has been done with the design of experiments related to polymerizations, including that done by Nabifar et al. [4], [5], [6] as well as others by Dube et al. [7] and Vivaldo-Lima et al. [8].

6.1   Background on the Statistical Design of Experiments

Statistical designs of experiments have become increasingly common in order to maximize the information content about the process [2]. This is important, as without properly selected experiments, there is a good likelihood that experimental data might be highly correlated or imprecise. Once such data are collected, no amount of statistical analysis can correct this [3]. To this end, a properly selected experimental design can be instrumental in avoiding these kinds of shortcomings.

Further, in the majority of polymerization processes, mathematical models do exist – albeit often with a good deal of uncertainty in their parameter values, and sometimes even in their mechanistic bases [4]. In the cases of complex polymerizations, or those for which less research has been performed (i.e., newer technologies like the different CRP variants) this problem can be even more significant [5]. Hence, the idea of applying methods from the statistical design of experiments to help clarify polymerization kinetics appears of interest, in order to help decrease these amounts of uncertainty. Figure 6-1 shows the overall scheme for an experimental design.
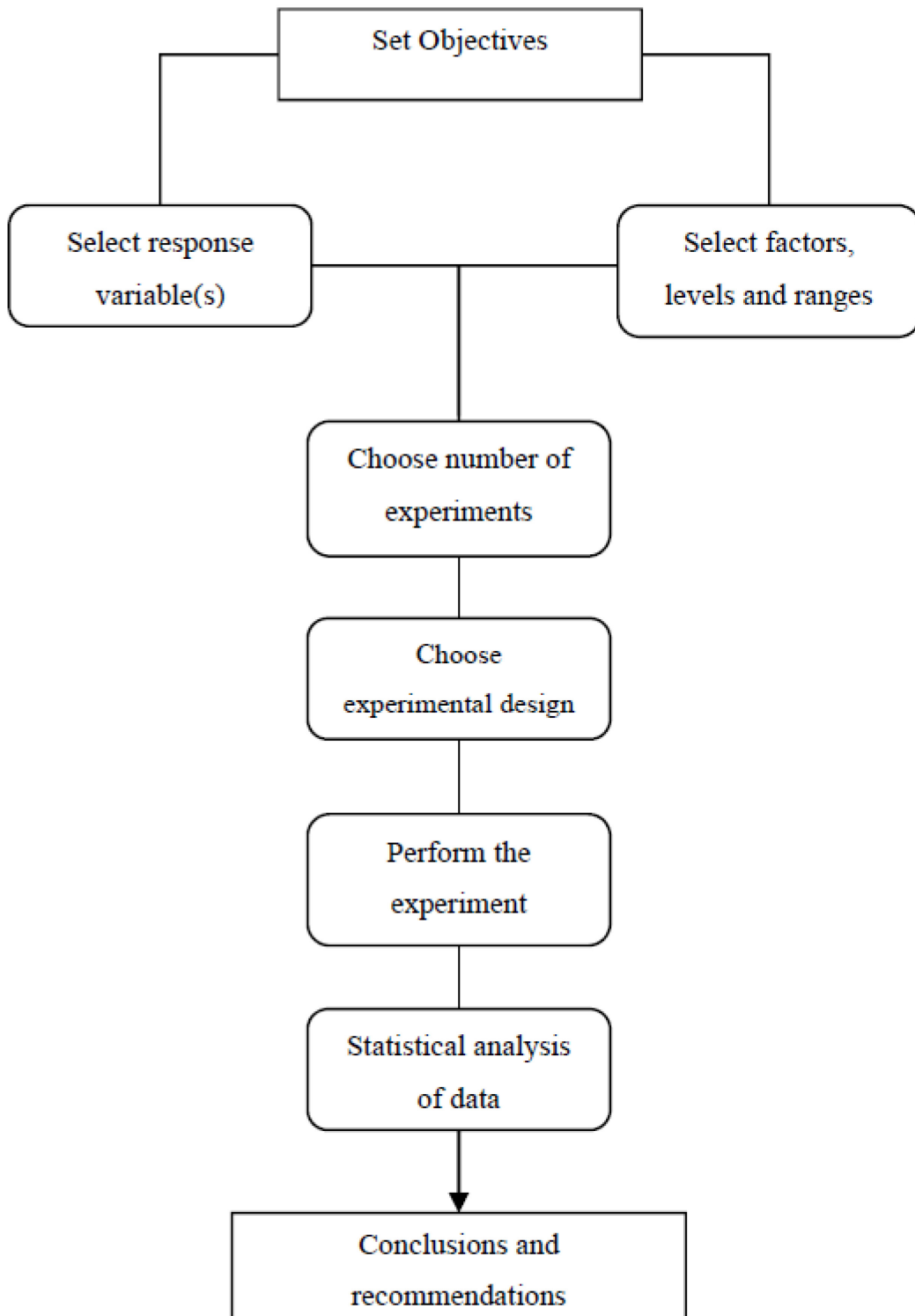
Figure 6-1: Guidelines for Designing an Experiment [1]

6.1.1   Factorial Designs

Full and fractional factorial designs are probably the most commonly used types of experimental designs in science and engineering [1]. However, quite often these elegant and very useful techniques cannot satisfy several practical needs. For instance, most of the experiments are strictly limited in the time and material resources that are available. These types of experimental designs do provide fractional factorial experiments to economize on effort but often the resources available do not match the number of trials which must be run for a specific fraction.

Further practical difficulties involve impractical treatment combinations, experiments which go astray because of missing observations, redefinition of factor levels as the experiment proceeds, factors which require different numbers of levels, and dropping/adding factors [4]. Several of these very practical needs simply cannot be accommodated by standard factorial designs. While some of the above issues have solutions which are known to experts in the design of experiments, it often happens that the practicing scientist or engineer cannot handle them and gives up on the use of statistical designs.

Finally, and more importantly, in the standard experimental designs minimal amount of prior knowledge is taken into account [4]. Most of the time, if experiments are to be conducted, there is some prior knowledge available about the process under study and the purpose of the statistical analysis is to strengthen/clarify a hypothesis already present. Ignoring the prior information, which can often lead to wasted experimental resources (i.e., time and materials), does not sound like a correct or reasonable thing to do!

6.1.2   Bayesian Designs

Bayesian design is a powerful experimental design method, which can accommodate practical limitations encountered in conventional factorial designs. This approach incorporates prior knowledge about a process into the design in order to suggest a set of future experiments in an optimal, sequential, and iterative fashion. Thus, it can be used to

determine the relative importance of different operating factors and also to identify optimal experiments [4].

In addition, Bayesian design allows the use of a nonlinear (fully mechanistic) model along with experimental information. It is essentially an optimal model-based design of experiments. Hence, this approach can shed light on the most uncertain parts of our process understanding, identify the least reliable parameters (e.g., uncertain values of kinetic rate constants), and further guide sensitivity analysis studies focusing on key uncertain parameters in one's model [6].

The Bayesian design of experiments combines both prior and new experimental data with modeling information, thus leading to model parameter updates and the selection of optimal experimental conditions aimed at achieving a certain goal [9]. There is not a large volume of literature dealing with the Bayesian design of experiments applied to polymerizations. Dube et al. [7] were the first to present a systematic study of emulsion terpolymerization using the Bayesian design technique. Subsequently, Vivaldo-Lima et al. [8] used this technique to determine the relative importance of process factors in suspension copolymerization.

Nabifar et al. ([4], [5], [6]), investigated the Bayesian design of experiments as applied to the case of nitroxide-mediated radical polymerization (NMRP). The papers discuss the application of the Bayesian design methodology to both the unimolecular and bimolecular NMRP processes. They also consider several case studies, where, for instance, four optimal runs are designed and contrasted with two sequences of 2-trials each. Comparisons are offered with fractional factorial designs and different ways of incorporating prior knowledge are discussed. These case studies exhibit significant advantages of Bayesian design over standard experimental design techniques and illustrate the application of the Bayesian design framework in order to enhance our understanding of important process characteristics. Of course, since the technique is general, it could potentially be applied to a wide variety of other polymerization and chemical engineering processes [9]. The basic procedure for the Bayesian design of experiments is outlined in Figure 6-2, where α is the vector of prior parameters (estimates), U is the parameter variance/covariance matrix, and θ is the vector of the unknown parameters of interest.
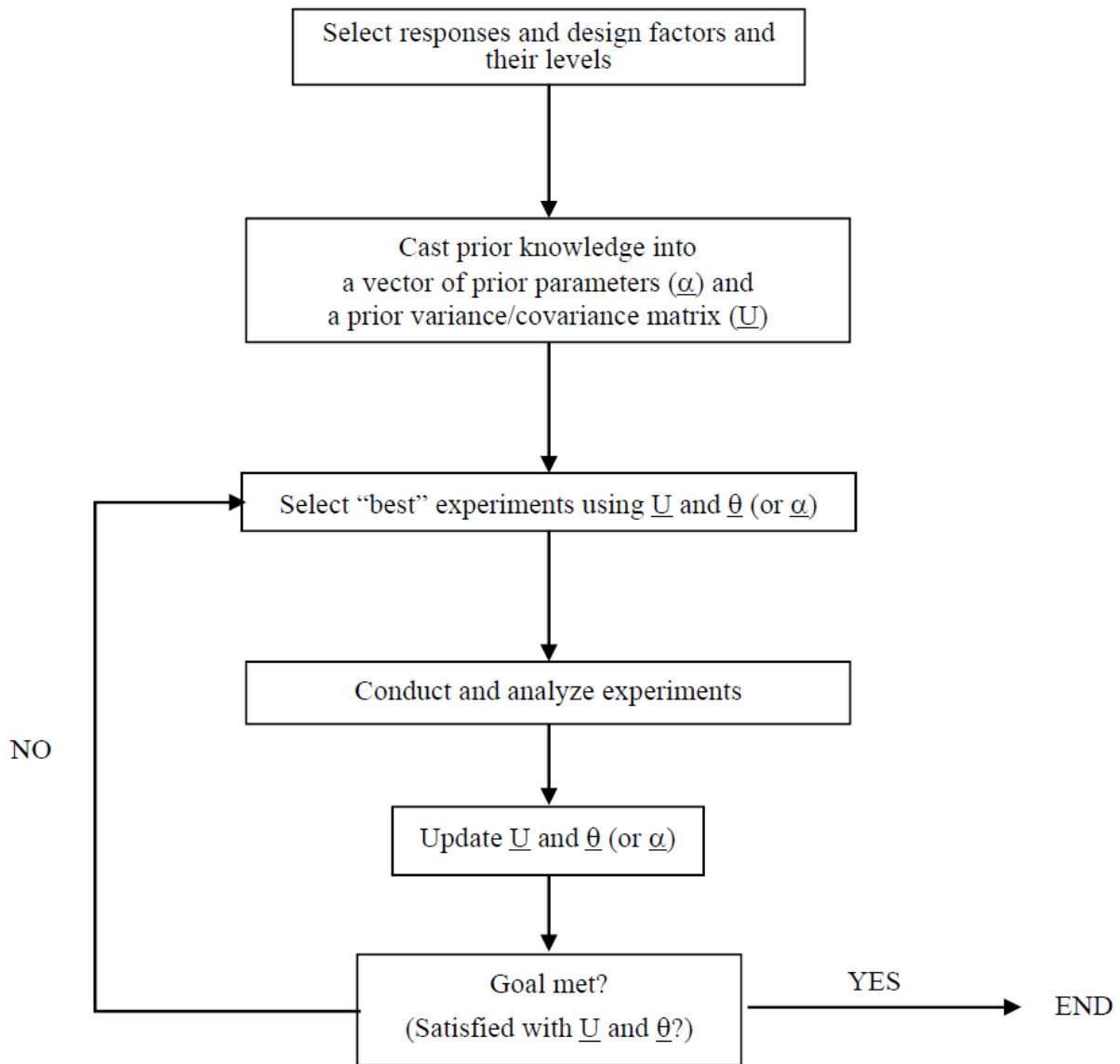
Figure 6-2: Procedure for the Bayesian Design of Experiments [9]

From this figure, Bayesian designs may seem relatively simple and straightforward, however, results are highly dependent on prior knowledge as well as the selection of responses and their levels. Therefore, extended thought or "brainstorming" must be put into the design's selection and implementation [5]. Additionally, the steps that require iteration each require a good deal of time, effort and sophisticated thought/analysis, which combined with the need for considerable thought about the early steps, make this type of experimental design more onerous to implement than it may at first seem [9].

6.1.3 Model-Based D-Optimal Designs

Traditional experimental designs (i.e., Full Factorial Designs, Fractional Factorial Designs, and Response Surface Designs) are appropriate for calibrating linear models. In some cases, however, models are necessarily nonlinear. D-optimal designs are model-specific designs that address these limitations of traditional designs [1]. A D-optimal design is generated by an iterative search algorithm and seeks to minimize the covariance of the parameter estimates for a specified model. This is equivalent to the maximization of the determinant described in Equation 6-1.

$$D = |\underline{X}'\underline{X}|$$

Eq. 6-1

Henceforth this determinant will be referred to as the D-optimality criterion, where $\underline{X}$ is the design matrix of model terms (the columns) evaluated at specific treatments in the design space (the rows). Unlike traditional designs, D-optimal designs do not require orthogonal design matrices, and as a result, parameter estimates may be correlated [1]. Parameter estimates may also be locally, but not globally, D-optimal.

A key component of implementing a D-optimal design is the determination of the design matrix ($\underline{X}$). For a nonlinear system of equations, the $\underline{X}$ matrix is described in Equation 6-2 [1].

$$\underline{X} = \begin{bmatrix} \dfrac{\partial f(x_1, \hat{\theta})}{\partial \theta_1} & \cdots & \dfrac{\partial f(x_1, \hat{\theta})}{\partial \theta_j} \\ \vdots & \ddots & \vdots \\ \dfrac{\partial f(x_i, \hat{\theta})}{\partial \theta_1} & \cdots & \dfrac{\partial f(x_i, \hat{\theta})}{\partial \theta_j} \end{bmatrix}$$

Eq. 6-2

This is the matrix of the partial derivatives of the responses $f(x_i, \theta)$ for the required levels of the factors/variables (x's) (i.e., a full factorial of the possible combinations) with respect to the j parameters (θ's). Given a nonlinear model of any real complexity (i.e., our RMM has 18 parameters, many possible variables, and several possible measurable responses), this

quickly becomes mathematically quite intensive to determine – however, with the ready availability of computational power, it is possible.

Once the $\underline{X}$ matrix has been determined, it is simply a matter of performing the row exchange of the rows pertaining to the combinations of experiments of interest (i.e., how many experiments, other restrictions), evaluating the determinant $|\underline{X}'\underline{X}|$, and comparing the results to the other possible permutations. Selecting the maximum value of the determinant gives you the optimal set of experiments.

Therefore, it is a reasonable extension to perform an optimal design of experiments using a complex nonlinear model using the D-optimal design criterion. This involves a great deal of computational effort, replacing some of the extended thought that was necessary in the aforementioned Bayesian designs using a linear model, with a more "brute force" computational approach. In this type of design, prior knowledge is not incorporated in the prior parameters vector ($\underline{\alpha}$) and the prior variance/covariance matrix ($\underline{U}$), but rather in that a more complex, or mechanistic model is used in the computation of the design, rather than a linear empirical one.

6.2 D-optimality Using the Substantially Reduced Model

The model-based D-optimal design of experiments can be quite a computationally intensive and mathematically onerous task. Therefore it was decided that starting with the most simplified model, as discussed in Chapter 5, would be ideal, in order to obtain some preliminary results on these experimental designs before the more onerous task of designs using the fully mechanistic models of Chapters 3 and 4 was taken on.

The greater level of simplicity of this model makes it possible to compute the $\underline{X}$ matrix analytically, rather than relying on a numerical method. This will save significant computational power, as the one-time analytical solution saves the numerical computation of the matrix of partial derivatives upon each of the program's iterations. In order to help validate the results of this analysis, work was done to replicate some of the Bayesian design case studies from Nabifar et al. [5].

6.2.1   Preliminary Results

In order to get a preliminary idea, a simple, straightforward situation was considered initially. Using a starting set of experiments, the next optimal experiments to be run were selected. Additionally, visual interpretations of this data were created – Figure 6-3 shows a contour plot generated via this process, showing the relative information content (i.e., D-optimality) for the number-average molecular weight responses that are provided by measurements across the viable data range for conversion and [TEMPO]/[BPO] ratio. The inputted experiments (i.e., levels) that were used in this case can be found in Table 6-1.

Table 6-1- Input experiments for preliminary results using simplified model to generate Figure 6-3

Experiment	Conversion	Ratio
1	0.538	0.9
2	0.536	1.1
3	0.688	1.1
4	0.489	1.2

The values were selected to be of a moderate conversion level, the same temperature, and varying yet typical controller/initiator ratios. As expected, the program suggested that data from experiments outside of this preliminary data range would be more informative, as indicated by higher values of the D-optimality criterion. The simulation was run across a range of conversion values, varied from 27% to 90% and controller/initiator ratios between 0.9 and 1.65.

The ideal next experiment according to the program would be that run at the two highest extremes, which can be seen in the upper right corner of Figure 6-3, corresponding to values of approximately 90% conversion and a ratio of 1.65 (i.e., maximizing both ratio and conversion within the possible range). This behavior makes sense, intuitively, as that is the furthest from the area where the preliminary experiments were located.
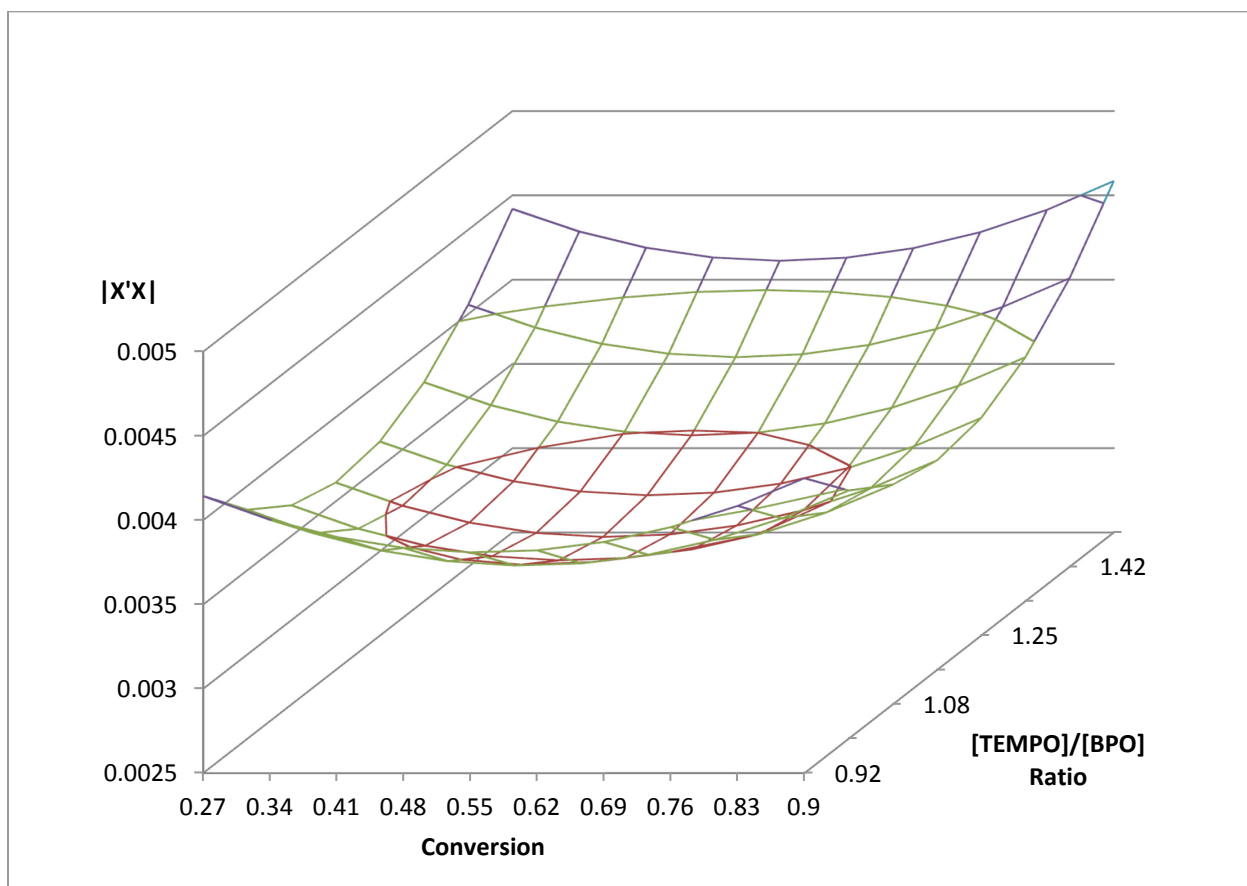
Figure 6-3 - Contour plot of |$\underline{X}'\underline{X}$| across viable conversion and Ratio ranges for M_n response, T = 120 °C

Because of results like these, there was reasonable confidence that the program was performing adequately. Therefore, it was deemed appropriate to perform further tests of this design program, comparing it with some case studies performed with a Bayesian design framework [5].

6.2.2   Case Study 1: Selection of a Sequence of Two Experiments

From here, the D-optimal design was compared with a case presented by Nabifar et al. [5, 6]. In this case, the FMM is used to generate the prior information for a Bayesian design scheme using a linear model as described in [4] with the 2^3 factorial design for the levels shown in Table 6-2, where T is the temperature, [I] is the initiator concentration, and [N] the nitroxide concentration.

Table 6-2 - Selected factors and their levels [5]

Level	T (°C)	$[I]_0$ (M)	$[N]_0$ (M)
Low	120	0.0305	0.0324
High	130	0.036	0.0396

The Bayesian design scheme was then used to suggest a set of two experimental trials. In this case, a single response was selected, that of the reaction time required to reach 75% conversion. Applications of this approach in cases with other and more responses are indeed possible [9], however the cases discussed all involve the conversion time response. Nabifar et al. [6] suggested that four 2-trial sets were equally desirable for the first sequence of experiments. These sets are shown in Table 6-3, where -1 represents the low level and 1 represents the high level. As can be seen, the only change between the two runs for each set is that of the temperature level, and the nitroxide and initiator levels were maintained from the first to second chosen run.

Table 6-3 - Possible 2-trial experiments selected by Bayesian design for Case 1 [6]

Set Number	T	$[I]_0$	$[N]_0$
1	-1	-1	-1
	1	-1	-1
2	-1	-1	1
	1	-1	1
3	-1	1	-1
	1	1	-1
4	-1	1	1
	1	1	1

The results of this indicate that the previous Bayesian design methodology had placed the most importance on temperature. The results from the D-optimal design program do also suggest this temperature change, but in addition suggest changing the value of the initiator, and therefore the controller to initiator ratio. This suggests that the variation of this ratio

is seen to be of similar importance by our simplified model using the D-optimality criterion. These results are displayed in Table 6-4.

6-4 – Trials selected by D-optimal design program using simplified model for Case 1

Experiment	T	$[I]_0$	$[N]_0$
1	1	1	1
2	-1	-1	1

6.2.3 Case Study 2: Selection of Two Additional Experiments

The next case from Nabifar et al. [6] was a continuation of the first case, where a further two experiments were chosen from where Case 1 left off. Now, a second set of experiments is to be calculated, given one of the first sets as an input. This time, the Bayesian design was able to settle on only one optimal pair of experiments, switching the controller levels from high to low. The chosen experiments are shown in Table 6-5. From this it can be concluded that the Bayesian design viewed the controller level of the next importance after the temperature, with the third variable, initiator level, of the least importance of the three.

Table 6-5 - Four trials selected for Case 2 by the Bayesian design [6]

Sequence	T	$[I]_0$	$[N]_0$
1	-1	1	-1
	1	1	-1
2	-1	1	1
	1	1	1

The experiments used as inputs for our D-optimality comparison will be those selected by the Bayesian design. The D-optimality program incorporating the simplified model was run, given this first set of experiments, and returned the following plot, Figure 6-4. As can be seen by the values with the highest peaks, the two additional experiments chosen were not the same two as were selected in the Bayesian design; however the chosen trials do follow the general trend of selecting a change to both the controller/initiator ratio and temperature levels.
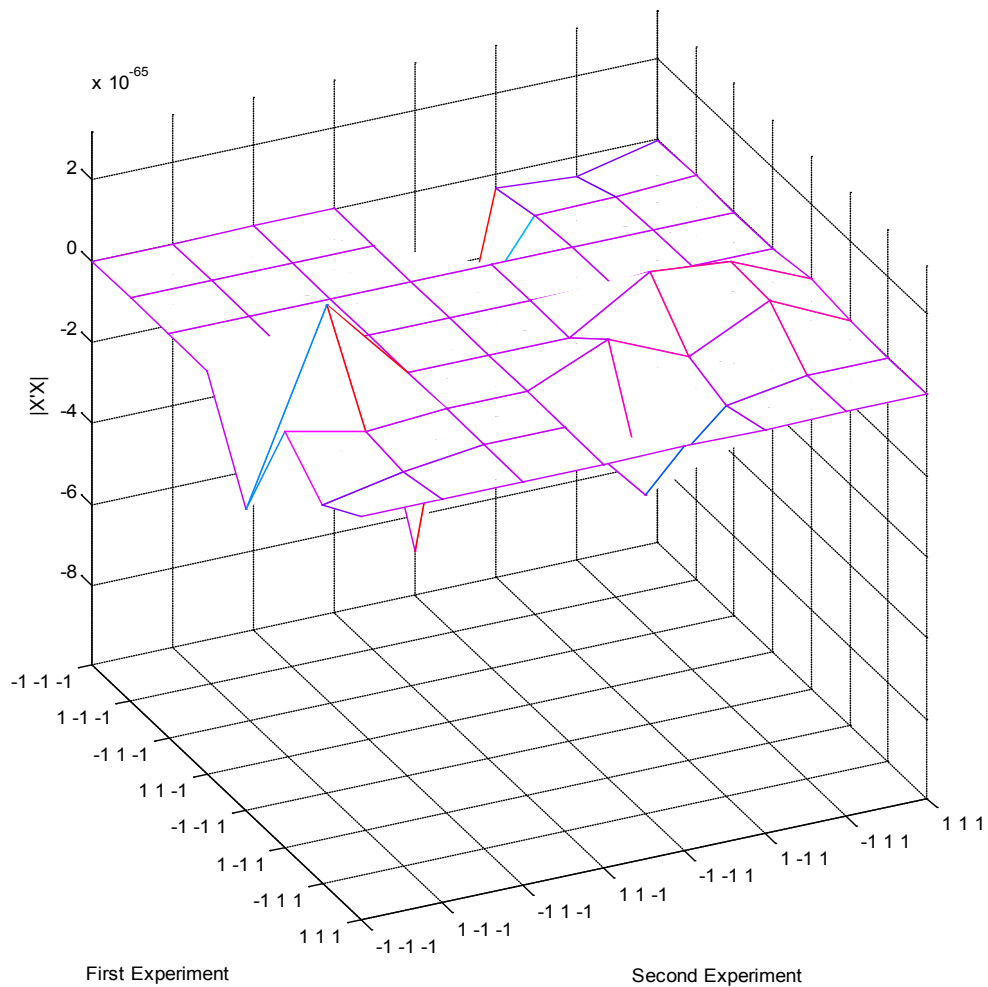
Figure 6-4 - Contour plot of |X'X| for simplified model, Case 2

The values selected by the D-optimal design are presented in Table 6-6 below. The key difference between these results and those of the Bayesian design is that these suggest changing the initiator level as well, which would serve to help in isolating that effect. Also, this is consistent with the different experiments that were chosen for Case 1 in that $[I]_0$ was changed. Again, this suggests that the simplified model places a higher value on the information gained by varying the initiator level than the linear model as used in the Bayesian design does.

	T	$[I]_0$	$[N]_0$
2	-1	-1	1
	1	-1	-1

6.2.4   Change of Constraints

In Section 6.2.3, the levels available to the Bayesian design were simply the high and low values for each factor. This was done to more exactly match the conditions of the sample case. An analysis was performed using this case as a basis, but allowing more levels to be evaluated. Instead of only high and low values, the range was incremented into ten levels. Some interesting results were found. A new constraint was added, that the ratio must be maintained at a more reasonable level, not higher than 1.2. Table 6-7 shows the results from this analysis, which resulted in the maintenance of the Ratio chosen by the Bayesian design, but chose new temperatures and controller and initiator amounts. It is interesting to note that the signs of the respective values were maintained (i.e., high and low levels are basically maintained).

Table 6-7 - Results of permitting more levels to be considered in Case 2, D-optimal design, simplified model

		Bayesian Design				D-Optimal Design			
	Run	T	$[I]_0$	$[N]_0$	Ratio	T	$[I]_0$	$[N]_0$	Ratio
First Sequence of Two Runs	1	-1	1	-1	0.81	-1	1	-1	0.81
	2	1	1	-1	0.81	1	1	-1	0.81
Second Sequence of Two Runs	3	-1	1	1	1.19	-0.6	1	1	1.19
	4	1	1	1	1.19	0.2	0.6	0.4	1.19

This appears to make sense with what was seen in the earlier case, as the D-optimal design of experiments using the simplified model still seeks to vary both initiator and controller designs as with the previous cases, but now was seen to seek out the controller/initiator ratio that the Bayesian design did.

6.3   D-optimality Using the Refined Mechanistic Model

6.3.1   Implementation

Due to the larger, more complex nature of the RMM when compared to the simplified model used in Section 6.2, the implementation of this model was a more difficult undertaking. First of all, the design matrix for this model is rather intensive to compute, as the nonlinear system of differential equations is quite large, and there is no analytical solution to the system (this will be discussed in more detail in Section 6.4.2). Therefore, finite differences must be used to compute the partial derivatives required to populate the $\underline{X}$ matrix as described in Equation 6-2 previously. This means that the model must be solved for both high and low values of each of the parameters (θ's), for each combination of variable levels to be evaluated, and then the values used in the following finite difference equation, Equation 6-3.

$$\frac{\partial x_i}{\partial \theta_j} \cong \frac{f\left(x_i, \theta_j + h\right) - f\left(x_i, \theta_j\right)}{h}$$

Eq. 6-3

where $f(x_i, \theta_j)$ is the value of the response of interest, x_i, is the variable level, θ_j is the parameter being perturbed for the finite difference, and h is the increment between the high and low values for the parameter (i.e., degree of this perturbation). The value of h must be tuned for each parameter so as to provide for a stable solution. A representative sample of the MATLAB code (and some pseudo-code) used to compute these derivatives for the X matrix is available as described in Appendix B.

Once these finite differences are computed for each of the variable levels that are of interest, the $\underline{X}$ matrix can be constructed as was shown in Equation 6.1 in Section 6.1.3. From here it's simply a matter of combining these variable levels and finding which yield

124

the optimal result , indicated by the maximization of the D-optimality criterion (i.e., max(D $= |\underline{X}'\underline{X}|$).

6.3.2   Comparisons with Bayesian Design Results

From here, as with the earlier investigation of the D-optimal design program using the simplified model, the D-optimal design program using our refined (fully) mechanistic model will be compared with the Bayesian design case studies mentioned earlier in Section 6.2, as well as others from the literature [4, 5, 6].

6.3.3   Case Study 1 – Selection of two experiments

This first case study is the same as was discussed in Section 6.2.2, where a sequence of two experiments was chosen by the Bayesian design. In this case, the chosen sequence of experimental runs did not match those suggested with the simplified model. The results are shown in Table 6-8.

Table 6-8 - Trials selected by D-optimal design using RMM for Case Study 1

	Bayesian Design				D-Optimal Design			
Run	T	$[I]_0$	$[N]_0$	Ratio	T	$[I]_0$	$[N]_0$	Ratio
First Sequence of Two Runs								
1	-1	1	-1	0.81	-1	1	-1	0.81
2	1	1	-1	0.81	1	1	1	1.19

Interestingly, the D-optimal design chose one of the two runs suggested by the Bayesian design, -1 1 -1, but on the other run varied the controller level in addition to the temperature level. The second experiment chosen by the D-optimality program is in fact one of the ones that was selected for the second set of two experiments using the Bayesian design, as discussed in Section 6.2.3.

That the results differ is reasonable, as the two designs are based on completely different models and are therefore not necessarily expected to yield the same results. This difference in selected sequence of runs could suggest that the model-based design using the RMM and the D-optimality criterion places a higher importance on the controller to initiator ratio than the Bayesian design did. This is in line with what was seen in Section 6.2.2, where this case study was investigated using the simplified model, in that both of these model-based designs seem to place a higher importance on the variation of the controller/initiator ratio than the model in the Bayesian design did.

6.3.4   Case Study 2 – Selection of four experiments

Next, the case study where an additional two experiments were selected is considered. This case was previously discussed using the simplified model in Section 6.2.2. Initially, the set of experiments chosen by the D-optimal design was seen to be different from that chosen by the Bayesian design, however once the second sequence of runs was selected, three of the four experiments were seen to have been chosen to be the same, albeit in a different order. The key difference in the results from the D-optimal design in this case is seen to be that it places a larger importance on changing the initiator level (and therefore having another, higher TEMPO/BPO ratio).

Table 6-9 - Trials selected by D-optimal design using RMM for Case Study 2

		Bayesian Design				D-Optimal Design			
	Run	T	$[I]_0$	$[N]_0$	Ratio	T	$[I]_0$	$[N]_0$	Ratio
First Sequence of Two Runs	1	-1	1	-1	0.81	-1	1	-1	0.81
	2	1	1	-1	0.81	1	1	1	1.19
Second Sequence of Two Runs	3	-1	1	1	1.19	-1	1	1	1.19
	4	1	1	1	1.19	1	-1	1	2.39

However, this does not shed light into how the D-optimal design behaves given the same inputs as the Bayesian Case Study 2. Using the first sequence that was selected using the Bayesian design from Nabifar et al. [6] yielded some interesting results. In fact, when using the first set of two experiments chosen by the Bayesian design as the inputs for the D-optimal design to select the second sequence, the results are seen to agree completely (i.e., in both additional experiments chosen and their sequence). Table 6-10 shows the results from this analysis.

Table 6-10 - Trials selected by D-optimal design using RMM for Case Study 2, and first sequence from Bayesian design

		Bayesian Design				D-Optimal Design (Fixing 1st sequence)			
	Run	T	$[I]_0$	$[N]_0$	Ratio	T	$[I]_0$	$[N]_0$	Ratio
First Sequence of Two Runs	1	-1	1	-1	0.81	-1	1	-1	0.81
	2	1	1	-1	0.81	1	1	-1	0.81
Second Sequence of Two Runs	3	-1	1	1	1.19	-1	1	1	1.19
	4	1	1	1	1.19	1	1	1	1.19

Interesting to note here is that three of the four runs selected in these last two D-optimal designs are the same, with the less constrained model-based D-optimal design (results shown in Table 6-9) choosing to run an experiment with a much higher controller to initiator ratio instead of investigating the effect of the temperature level on the lower ratio as in the Bayesian case.

6.3.5   Case Study 3 – Changing variable levels

Similar to the previous case, using the trials selected by the Bayesian design as past experiments and adding two new experiments, this time with an expanded range for temperature, also yielded interesting results. Table 6-11 shows the results generated by

the D-optimal design for this case. There is perfect agreement with the sequence of runs chosen by the Bayesian design. This is consistent with both of the observed behaviours in previous cases discussed with this model – the tendency to vary the controller/initiator ratio in chosen runs, and choosing the same runs when given the first two runs from the Bayesian design.

Table 6-11 - Trials selected by D-optimal design using RMM for Case Study 3

		Bayesian Design				D-Optimal Design			
	Run	T	$[I]_0$	$[N]_0$	Ratio	T	$[I]_0$	$[N]_0$	Ratio
First Sequence of Two Runs	1	-0.33	1	-1	0.81	-0.33	1	-1	0.81
	2	0.33	1	-1	0.81	0.33	1	-1	0.81
Second Sequence of Two Runs	3	-1	-1	-1	1.61	-1	-1	-1	1.61
	4	1	-1	-1	1.61	1	-1	-1	1.61

Figure 6-5 shows the contour plot of the determinants (D = $|\underline{X}'\underline{X}|$) for the combinations of two experiments, where it is seen that the chosen combination of experiments is indeed the best by this criterion, by quite a substantial margin. It does indicate, interestingly, that there is another set of experiments that stands out from the bulk of the combinations, that of -1 1 1 and 1 -1 -1, which similarly seek to test the new temperature extremes, but also want to investigate another [TEMPO]/[BPO] ratio, of 1.19. These second-best choices also follow one of the trends we have seen in this analysis – that of suggesting changes to the controller/initiator ratio to investigate in the experiments.
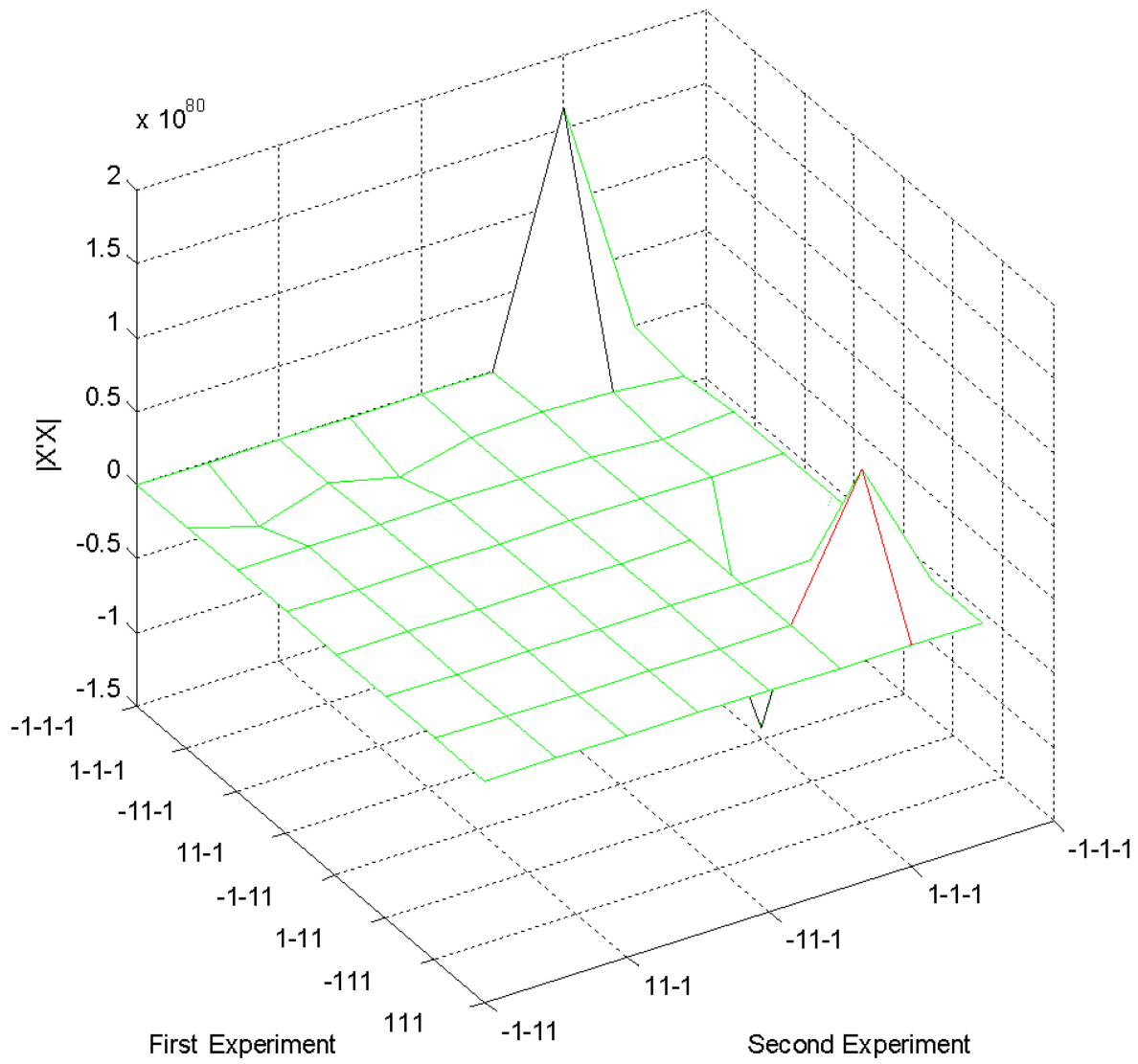
Figure 6-5 - Using RMM for Case Study 3

6.4   Comparisons Between Model Levels

6.4.1   Results and Trends

There were some differences seen between the recommendations made when using the simplified model and when using the RMM, though the trends largely seemed to agree. In general, the RMM is expected to provide more accurate and informative results since it takes more of what is truly going on in the process into consideration. In a practical application, the speed and simplicity of the simplified model makes it a likely candidate for on-line applications where delays could mean lost productivity, whereas off-line verification using the RMM could be quite appealing in cases where time allows.

Interestingly, when making comparisons between our designs and the Bayesian design, it was worth noting that both the simplified model and RMM displayed the tendency to place a higher importance on varying the controller/initiator ratio than the Bayesian design did. This trend could suggest a good deal of agreement between the model levels.

6.4.2   Practical Considerations

The much more complex nature of the RMM/FMM makes for a considerably more computationally intensive design of experiments where it is used. For the relatively simple comparisons that were made with the cases in the previous sections, runtime of the FMM/RMM was in the order of 5 minutes compared with the nearly instantaneous returns from the simplified model.

However, when designs considering more variables or levels are considered, the amount of computation required grows exponentially. For instance, a design that considered 3 variables with ten levels using the RMM had a runtime of nearly four hours. Similar designs with the simplified model took a fraction of the time, as the simpler solution does not require the solution of the large system of equations repeatedly. When the design program was given multiple responses, variables, and levels to evaluate, runtimes could be even longer still. The longest run of the D-optimality program that has been made to date,

looking for the impact on both the conversion time and number-average molecular weight responses using the RMM with 10 levels of three variables took approximately 8 hours to complete.

Despite this greater time investment, the use of the higher-level model may be worthwhile, as it takes a much more complete, mechanistic view of what is going on in the process, and provides more process information (i.e., can predict information about species concentrations, M_w, and PDI) than the simplified model can.

6.5   Changes to the Optimality Criterion

6.5.1   Rationale and Methodology for Implementation

Model parameter correlations can prevent the solution of experimental design calculations, make parameter isolation/identification more difficult, and even decrease the statistical validity of the design of experiments and the resulting models [10, 11]. In order to try to combat this more aggressively than in a D-optimal design, Fransceshini and Macchietto proposed some anticorrelation criteria for model-based experiment design [10, 11, 12]. One of their proposed anticorrelation criteria was adopted for comparison with our D-optimal designs using the RMM. The criterion is given by the following, Equation 6-4 [10].

$$\min_{\varphi \in \Phi} \sum_{i=1}^{p-1} \sum_{j=2}^{p} C_{ij}^2(\theta, \varphi)\big|_{i \neq j} \qquad \text{Eq. 6-4}$$

In the above, φ is the design vector, Φ is the design space, θ is the vector of the best currently available parameter estimates and C_{ij} is the correlation matrix given by Equation 6-5 [11].

$$C_{ij} = \frac{V_{ij}}{\sqrt{V_{ii}}\sqrt{V_{jj}}}$$

<div align="right">Eq. 6-5</div>

In equation 6-5, V is the variance-covariance matrix, which is the inverse of X'X. Substituting this in gives us the following expression for C_{ij}, Equation 6-6.

$$C_{ij} = \frac{(X'X)_{ij}^{-1}}{\sqrt{(X'X)_{ii}^{-1}}\sqrt{(X'X)_{jj}^{-1}}}$$

<div align="right">Eq. 6-6</div>

That is, the criterion is the minimization of the sum of the squared values of all of the correlation coefficients given by Equation 6-6. Implementing this criterion into the design of experiments program in MATLAB was relatively simple, and just involved the replacement of the final evaluation of the D-optimality criterion for the chosen sets of experiments with the new anticorrelation criterion.

6.5.2   Comparison with Case 2

The implementation of this criterion had some interesting effects on the results of the design of experiments. Often the same combinations of experiments would not be selected for the two criteria.

Comparisons were made with one of the case studies discussed previously in this Chapter, namely Case 2, as originally discussed in Sections 6.2 and 6.3 for the simplified and refined mechanistic models, respectively. The results of the anticorrelation design are compared with those from the D-optimal design (which matched the earlier Bayesian design) in Table 6-12.

Table 6-12 - Trials selected using anticorrelation criterion and RMM for Case 2

	D-Optimal Criterion (RMM)				Anticorrelation Criterion			
	Run	T	$[I]_0$	$[N]_0$	Ratio	T	$[I]_0$	$[N]_0$	Ratio

	Run	T	$[I]_0$	$[N]_0$	Ratio	T	$[I]_0$	$[N]_0$	Ratio
First Sequence of Two Runs	1	-1	1	-1	0.81	-1	1	-1	0.81
	2	1	1	-1	0.81	1	1	-1	0.81
Second Sequence of Two Runs	3	-1	1	1	1.19	1	-1	1	2.39
	4	1	1	1	1.19	-1	-1	1	2.39

As can be seen, the anticorrelation criterion did not choose the same additional experiments as the D-optimal criterion using the RMM (and therefore the Bayesian design), as discussed in Section 6.3.4. The difference is that the anticorrelation design suggests the lowering of the initiator level along with the increase of the nitroxide level, or rather, that this design chose the experiments with both extremes of the controller/initiator ratio. This is illustrated in Figure 6-6, where the best set of experiments is indicated by the smallest (i.e., largest downward) peak.

Interestingly, when not constrained by being made to use the first two experimental inputs from the Bayesian case, the D-optimality-based design chose to recommend all three of these initiator/controller ratio values (i.e., 0.81, 1.19 and 2.39). Also interesting to note is that the next best or second-best choice peak contains one of the experiments contained in the other (Bayesian/D-optimal) design, namely 1 1 1, but the second chosen experiment opts to test the impact of the low initiator value as well with the chosen values of 1 -1 -1, which would correspond to an initiator/controller ratio of 1.61.
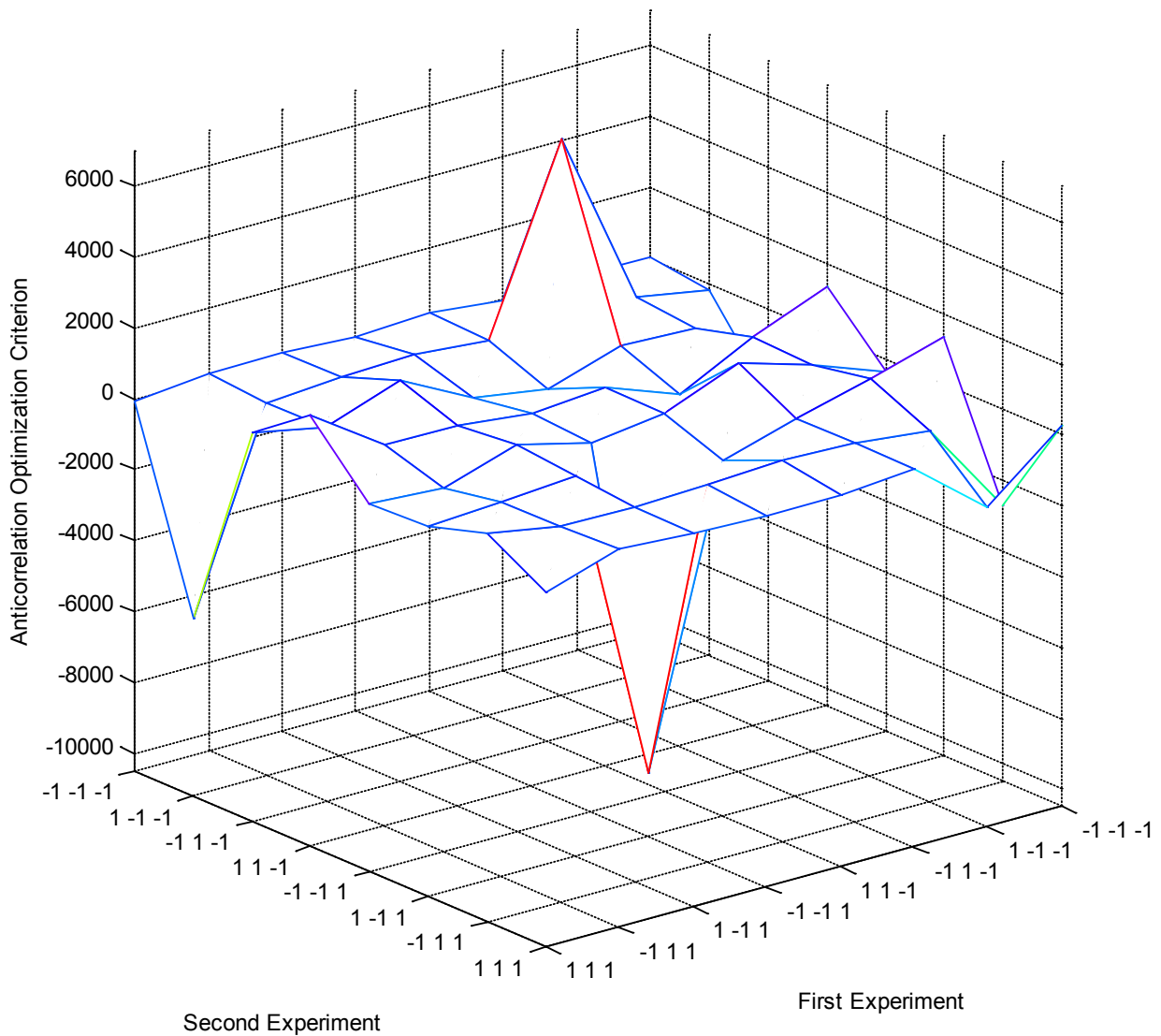
Figure 6-6 - Anticorrelation results for the conditions of Case Study 2 using RMM

6.5.3   Comparison with Case Study 3

Another analysis using this criterion was made in comparison with Case Study 3 as was discussed earlier for the D-optimality criterion using the RMM in Section 6.3.5. The results are displayed in Table 6-13, where it can be seen that the two approaches are in perfect

agreement. Since the D-optimal design was in agreement with the Bayesian design in this case as well, it can be said that all three experimental designs were in agreement for this case. This suggests that the increase in information content gained by the evaluation of these new temperatures and ratios is able to overcome that obtained in the previous case (Section 6.5.2) by changing both the initiator and controller levels. A possible explanation is that changing all three variable levels would provide less insight into the parameter interactions/correlation than leaving one constant.

Table 6-13 - Trials selected using anticorrelation criterion and RMM for Case 3

		D-Optimal Criterion				Anticorrelation Criterion			
	Run	T	$[I]_0$	$[N]_0$	Ratio	T	$[I]_0$	$[N]_0$	Ratio
First Sequence of Two Runs	1	-0.33	1	-1	0.81	-0.33	1	-1	0.81
	2	0.33	1	-1	0.81	0.33	1	-1	0.81
Second Sequence of Two Runs	3	-1	-1	-1	1.61	-1	-1	-1	1.61
	4	1	-1	-1	1.61	1	-1	-1	1.61

Figure 6-7 shows the pictorial results of this experimental design, where the selected combination of experiments (-1 -1 -1 and 1 -1 -1) is seen to stand out from the group as the lowest value of the optimality criterion (i.e., the deepest valley). The second choice as was identified in Figure 6-5 for the D-optimality approach, -1 1 1 and 1 -1 -1, is not seen to stand out in this case, suggesting that perhaps it failed to address the problem of parameter correlation that this criterion seeks to reduce.
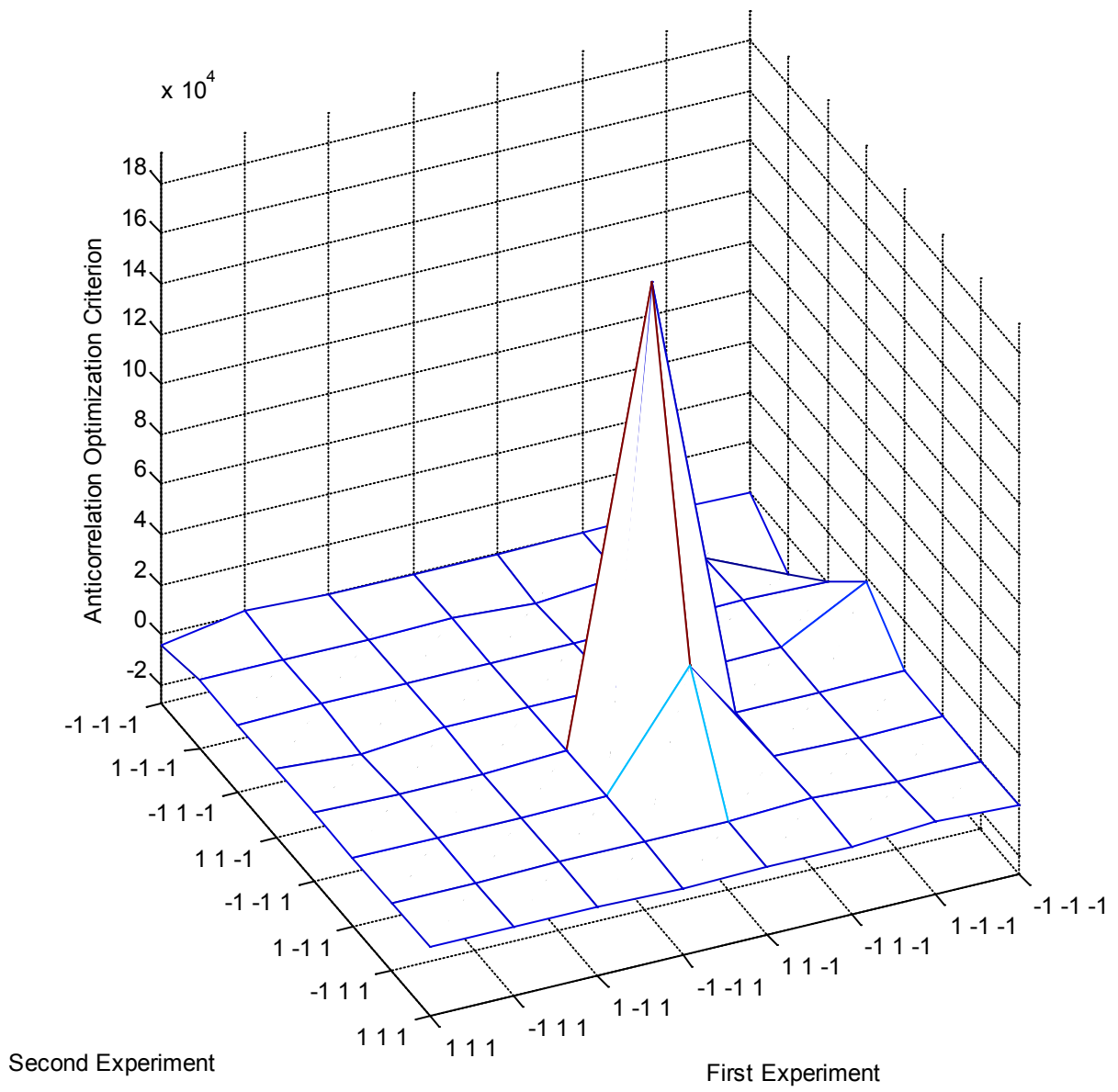
Figure 6-7 - Anticorrelation results for the conditions of Case Study 3 using RMM

6.6   Concluding Remarks

We have studied three different model-based optimal experiment designs, all with quite reasonable results. Comparisons of these different designs to each other and a previously explored Bayesian design have yielded some interesting results.

The D-optimality-based experiment designs using both the RMM and the simplified model are seen to select similar sets of experiments under similar conditions, however some of the results were seen to differ between the two (as were highlighted in the discussion). Therefore, in practical applications, one could use the simplified model when the computation time is a factor (i.e., on-line applications) and the higher-level mechanistic models when time permits (i.e., off-line applications). Also, it may be worth using the different model levels in conjunction – for instance, using the simplified model on-line or for quick estimates and the higher level model for off-line verification.

Implementation of the anticorrelation criteria discussed by Franceshini and Macchieto [10, 11] was then completed, and applied to the case studies using the RMM. Comparable (although not always identical) results were seen to when the D-optimal designs were used. In cases where there is a suspicion that parameters may be correlated, the use of this criterion could be of benefit, as it is aimed at the reduction of such correlations.

Finally, comparisons between results obtained from using the regular D-optimality criterion and those from using the anticorrelation criterion could be of value, as any differences in these results could help clarify the role of parameter correlations in the process model.

Chapter 7:   Concluding Remarks, Main Contributions, and Recommendations for Future Work

7.1   Concluding Remarks

As per Chapter 3, we have a fully functioning mechanistic model that captures the overall trends of styrene NMRP, with unimolecular and bimolecular TEMPO as well as unimolecular TIPNO controllers. There is evident room for improvement as far as the model's fit, and this is a very complex and difficult to solve model, involving a large, stiff system of differential equations. This system must be solved together with numerous Arrhenius expressions for the various rate constants contained within it. On top of all this, further calculations must be done in order to generate the cumulative molecular weight averages and polydispersity index.

Therefore, from this point, two main priorities are clear: model refinement and model reduction – that is, improving the predictive power and reducing the amount of computation required to generate model profiles.

Chapter 4 of this discussion examined the first goal, model refinement – seeking to improve the agreement between these models and experimental data. In essence, this sensitivity study not only revealed interesting trends in the model responses (and improved model performance versus experimental data), but also generated a mechanistic model reduction approach. The model at this level is still fully mechanistic, but with fewer terms, hence somewhat reduced, and it still provides good predictions over the full conversion range and over a wide range of operating conditions for the bimolecular process.

Implementing these reductions and changes in the unimolecular TEMPO and TIPNO cases yielded similarly interesting results.   The unimolecular case was very successful in mirroring the high level of predictive power, especially for the molecular weights. More modest gains to model performance were seen in the TIPNO case; however, the model still provides fairly good predictions across the full conversion range.

Chapter 5 attempted a much more significant model reduction, which led to a simplified model, which captured the main process effects but with highly simplified equations (which are easier to use, if the model predictions are satisfactory, for process design of experiments scenarios).

The efforts to create a much simpler, easier to use model of the process have been largely successful. The simplified model as presented in Chapter 5 has been demonstrated to provide a good picture of the trends of the key measurable responses of such a polymerization; namely, the number-average molecular weight and conversion.

This model appears to be a reasonably effective option for capturing main trends, and as such, can be used interchangeably and in conjunction with the more complex fully mechanistic or refined mechanistic models in a variety of applications. For instance, with the simplified model providing on-line estimates of MW and conversion with the FMM used off-line to verify or to estimate those responses that are not (easily) measureable. If used in cases where only these main process responses are of interest, the simplified model could suffice.

An application of these models – that of their use in the design of experiments, was investigated in Chapter 6. The work in this chapter yielded 3 different model-based optimal experiment designs, all with quite reasonable results. Comparisons of these different designs to one another and a previously explored Bayesian design have yielded some interesting results.

When comparing the D-optimality-based experiment designs using both the RMM and simplified model – both performed adequately, however some of the results differed between the two. It therefore makes sense to potentially use the simplified model when the computation time is a factor (i.e., on-line applications) and the higher-level mechanistic models when time permits (i.e., off-line applications). Additional work was done, implementing another optimality criterion with and anti-correlation component, aimed at reducing the impact of model parameter correlation.

 These experimental designs can be used in a variety of situations, for a variety of responses and can be compared with one another when questions such as the role of parameter correlations or the results yielded from the use of the simplified model are

suspected to be less accurate (i.e., the use of the higher-level model for off-line verification when primarily using the simplified model could then be of interest).

7.2   Main Contributions

- A working, fully mechanistic model for the NMRP of styrene, with an analysis of its performance compared to experimental data, with both unimolecular and bimolecular initiation options and both TEMPO and TIPNO as controller radicals. This work is detailed in Chapter 3.

- A refined, yet still fully mechanistic model for the NMRP of styrene, shown to work with two different nitroxides and both the unimolecular and bimolecular options was developed and analyzed in Chapter 4.

- A substantially reduced model derived and tested in Chapter 5, which captures the main trends, and while still nonlinear, much simpler than the fully mechanistic model.

- Computer code and programs in Chapter 6, to perform model-based D-optimal design of experiments using these models with comparisons to other experimental designs as well as between levels.

- In Section 6.5, modifications to the optimal design criterion using a different criterion, tailored to further reduce correlation between parameters.

- In Section 7.3.2, a detailed discussion of work that can be done using these or similar models in the optimal selection of sensors for CRP, including a basic strategy for implementation of various measures of information content.

7.3   Recommendations for Future Work

7.3.1   Bayesian Designs using FMM

A logical extension to this work would be to use a non-linear model in the Bayesian design to replace the linear model that was used. Initially, and for practical purposes, one can start with the simplified non-linear model, as discussed in Chapter 5, in order to begin with a simpler case.

Eventually, incorporating the fully mechanistic model into this design could capture the benefits of both the Bayesian design process and the more complex models used in the designs from this thesis. Further, the Bayesian design methodology using the refined (fully) mechanistic model could be used with the anticorrelation criterion, which would be expected to provide advantages to the selection of experiments with the downside of lengthening runtimes further.

Once the step on nonlinear Bayesian designs is completed, comparisons between the different model levels (linear, RMM, and simplified) and design types (D-optimal, anticorrelation, and Bayesian) warrant further study as well. This could lead to greater model refinements (through improvement of parameter estimates and better data).

7.3.2   Applications to Sensor Selection

Another interesting use of these models would be their use in the selection and placement of sensors for these process measurements. Quality control is of the utmost importance in any industrial process. However, plants experience disturbances from numerous sources which often are not possible to anticipate and can impact the final product's quality [1]. To combat this, accurate and complete measurements must be taken to monitor the output variables and identify when and if these disturbances are impacting the process. These measurements can be used in a process control scheme to dictate the required adjustments to ensure that the final product meets or exceeds quality requirements.

The performance of any process monitoring or control system is strongly dependent on the available measurements, and the absence of sufficient measurements can significantly complicate any attempt to control an industrial process [2]. It is therefore important to ensure that the appropriate sensor configuration is in place to maximize the information content of the gathered measurements.

One way of performing such a sensor selection was suggested by Penlidis and Duever for a styrene/methyl methacrylate copolymerization process, using a Kalman Filter approach [1]. Consider the process model in a linearized, discretized form, given by Equations 7-1 and 7-2 [1]:

$$X_{k+1} = \Phi_k X_k + \Delta_k u_k + w_k$$

Eq. 7-1

$$y_k = H_k X_k + v_k$$

Eq. 7-2

X_k is the (n x 1) state variable vector at time k, u_k the (r x 1) manipulated input variable vector, y_k the (m x 1) measurement vector, H_k the measurement matrix and w_k and v_k are independent Gaussian white noise vectors with zero mean representing the process and measurement noises, respectively.

First the deterministic and stochastic state vectors are predicted by Equations 7-3 and 7-4 [1]:

$$\hat{X}_{k+1/k}^d = \hat{X}_{k/k}^d + \int_{t_k}^{t_k+1} f\left(\hat{X}^d(t), u(t), t\right) dt$$

Eq. 7-3

$$\hat{X}_{k+1/k}^s = \Phi^s \hat{X}_{k/k}^s$$

Eq. 7-4

$\hat{X}_{k+1/k}^d$ and $\hat{X}_{k+1/k}^s$ are the one step ahead predictions for the deterministic and stochastic state vectors, respectively. $\hat{X}_{k/k}^d$ and $\hat{X}_{k/k}^s$ are the corresponding filtered estimates from the prior step, and $f\left(\hat{X}^d(t), u(t), t\right)$ is the right hand side of the general nonlinear state differential equation description of the process. The inclusion of stochastic states in the Kalman Filter formulation is necessary to eliminate offset in the state estimates when

143

chemical processes experience nonstationary stochastic disturbances. The augmented state vector, composed of both the deterministic and stochastic states, is then used in Equations 7-5 through 7-8 [1].

$$P_{k+1/k} = \Phi_k P_{k/k} \Phi_k^T + R_w \qquad \text{Eq. 7-5}$$

$$\hat{X}_{k+1/k+1} = \hat{X}_{k+1/k} + K_k(y_{k+1} - h(\hat{X}_{k+1/k}, t)) \qquad \text{Eq. 7-6}$$

$$P_{k+1/k+1} = P_{k+1/k} - K_k H_{k+1} P_{k+1/k} \qquad \text{Eq. 7-7}$$

$$K_k = P_{k+1/k} H_k^T (H_k P_{k+1/k} H_k^T + R_v)^{-1} \qquad \text{Eq. 7-8}$$

$P_{k+1/k}$ is the covariance matrix for $\hat{X}_{k+1/k}$, $P_{k+1/k+1}$ is the covariance matrix for $\hat{X}_{k+1/k+1}$, K_k the Kalman gain matrix, R_w the process noise covariance matrix, R_v the measurement noise covariance matrix, and $h(X, t)$ the nonlinear measurement model.

Competing sensor designs can be evaluated by their effect on the computed covariance matrices, which give a measure of the quality of information in the corresponding state estimates, much as the optimality criteria served as indicators of the quality of information gained from a set of experiments. Equations 7-5 through 7-8 are independent of the process observations (y_k) and can therefore be calculated iteratively until the covariance matrices converge.

For completely observable systems with positive definite $P_{0/0}$, both $P_{k+1/k}$ and $P_{k+1/k+1}$ will converge to unique, steady-state positive definitive matrices denoted by $P_{k+1/k}^{\infty}$ and $P_{k+1/k+1}^{\infty}$. The optimal sensor design, then, is that which minimizes a scalar function of P. The square root of the determinant of P is the scalar function chosen, as it is scale invariant and proportional to the hypervolume of the approximate joint confidence region of the state estimates [1]. The D-optimality criterion for this design is defined as follows in Equation 7-9 [1]:

$$\min\left(D_i = \sqrt{\det\left(P_i^\infty\right)}\right), \qquad i = 1, 2 \qquad\qquad \text{Eq. 7-9}$$

where P_1 is $P_{k+1/k}^\infty$ and P_1 is $P_{k+1/k+1}^\infty$.

A model of a process like the RMM developed for the NMRP of styrene could be used as the basis for such a sensor selection/design program. As with the design of experiments, this criterion can be used to evaluate sets of measurements that maximize the information content (minimize the criterion) for a given set. This criterion is quite similar to the D-optimality and anticorrelation criteria for design of experiments that were discussed in Chapter 6 of this thesis.

Implementation of such a program would take a similar form to the work of Chapter 6, but with the responses (i.e., f(x, θ)'s) being the rows that are exchanged in the formulation of the X matrices being compared, rather than the process conditions (i.e., x's). Therefore one could compare the impact on information content of different combinations of measurements by comparing the values obtained for the derivative. For example, an X matrix constructed for the responses of number-average molecular weight and controller concentration could be compared with one for monomer conversion and initiator concentration responses. The set of responses evaluated that optimizes this criterion could then be said to provide the optimal sensor configuration.

Another approach proposed by Duever and Penlidis [1] was that of maximizing the observability of the system. The observability of a system is a measure of the degree to which a transition of states impacts measured responses [3]. The observability matrix (n x mn) is given by Equation 7-10 [1]:

$$Q = (H^T, \Phi^T H^T, (\Phi^T)^2 H^T, \dots, (\Phi^T)^{n-1} H^T) \qquad\qquad \text{Eq. 7-10}$$

Using this matrix, one can tell if a system is mathematically observable if and only if it has rank equal to n [1]. From this viewpoint, whether or not a system is observable is a yes or no question, but there has to be a way to quantify the degree to which an observable

system is in fact observable. In this case, one could use this degree of observability to evaluate competing experiment designs.

For a system to be observable, the columns of Q must be linearly independent [3]. That is, any measure of how far the matrix Q is from singularity can be taken as a degree of observability for the system. The optimal set of sensors would therefore be the one that maximizes this observability [1]. Penlidis and Duever [1] went on to suggest a number of criteria to use as measures of observability, which are to be maximized by an optimal sensor design, as given in Equations 7-11 through 7-14 [1].

$$\mu_1 = cond(Q) = \frac{\sigma_{max}}{\sigma_{min}} \qquad \text{Eq. 7-11}$$

$$\mu_2 = \lambda_{min}(QQ^T) \qquad \text{Eq. 7-12}$$

$$\mu_3 = \frac{n}{trace((QQ^T)^{-1})} \qquad \text{Eq. 7-13}$$

$$\mu_4 = \sqrt[n]{det(QQ^T)} \qquad \text{Eq. 7-14}$$

σ_{max} and σ_{min} are the maximum and minimum square roots of the eigenvalues of the product of Q and Q^T. The condition number approaches infinity as Q becomes singular, thus the expression in Equation 7-11 is to be minimized for an optimal selection. The expressions in Equations 7-12 through 7-14 are to be maximized by the optimal choice of sensor design.

Again, sensor selection studies could be performed through using a model like the RMM to generate the information required for these measures for different sets of measured responses, and selecting the optimal set of sensors. The approach to take in such a case would be similar to that with the optimal designs in Chapter 6, however instead of changing which parameter values are being evaluated, one would change the subset of potential responses that are to be measured. Results would then be compared between different sets of responses, and the one resulting in the maximized criterion of choice would then be called the optimal configuration.

References

References for Chapter 2

1. Priddy, D. B. and Updated by Staff **2006**. "Styrene Plastics." Kirk-Othmer Encyclopedia of Chemical Technology; John Wiley and Sons, Inc.: Hoboken, NJ.

2. Odian, G. **2004** "Radical Chain Polymerization", In *Principles of Polymerization*; John Wiley & Sons, Inc.: Hoboken, NJ; p 198.

3. Matyjaszewski, K. **2002** "General Concepts and History of Living Radical Polymerization", In *Handbook of Radical Polymerization*; Matyjaszewski, K., Davis, T. P., eds. John Wiley and Sons, Inc.: Hoboken, NJ; pp 361-406.

4. Matyjaszewski, K. **1997** "Overview: Fundamentals of Controlled/Living Radical Polymerization", In *Controlled Radical Polymerization*; Matyjaszewski, K., ed. American Chemical Society: Washington, DC; pp 2-30.

5. Shipp, D. A. **2005** "Living radical polymerization: controlling molecular size and chemical functionality in vinyl polymers" *Polymer Reviews*, *45*, 171-194.

6. Matyjaszewski, K. **2002** "Fundamentals of Atom Transfer Radical Polymerization", In *Handbook of Radical Polymerization*; Matyjaszewski, K., Davis, T. P., eds. John Wiley and Sons, Inc.: Hoboken, NJ, pp 523-628.

7. Moad, G.; Barner-Kowollik, C. **2008** "The Mechanism and Kinetics of the RAFT Process: Overview, Rates, Stabilities, Side Reactions, Product Spectrum and Outstanding Challenges", In *Handbook of RAFT Polymerization*; Barner-Kowollik, C., ed. John Wiley and Sons, Inc.: Hoboken, NJ, pp 105-149.

8. Chiefari, J.; Chong, Y. K.; Ercole, F.; Krstina, J.; Jeffery, J.; Le, T. P. T.; Mayadunne, R. T. A.; Meijs, G. F.; Moad, C. L.; Moad, G.; Rizzardo, E.; Thang, S. H. **1998** "Living free radical polymerization by reversible addition fragmentation chain transfer : the RAFT process" *Macromolecules*, *31*, 5559-5562**.**

9. Fukuda, T.; Terauchi, T.; Goto, A.; Ohno, K.; Tsujii, Y.; Miyamoto, T.; Kobatake, S.; Yamada, B. **1996** "Mechanisms and kinetics of nitroxide-controlled free radical polymerization" *Macromolecules*, *29*, 6393-6398.

10. Hawker, C.J. **2002** "Nitroxide Mediated Living Radical Polymerization", In *Handbook of Radical Polymerization*; Matyjaszewski, K., Davis, T. P., eds. John Wiley and Sons, Inc.: Hoboken, NJ, pp 463-522.

11. Braunecker, W. A.; Matyjaszewski, K. **2007** "Controlled/living radical polymerization: Features, developments, and perspectives" *Progress in Polymer Science*, *32*, 93-146.

12. Pirrung, F. O. H.; Aushra, C. **2005** "Nitroxide-mediated synthesis of acrylic block copolymers- and their use as coating additives" Polymer Preprints, 46, 316-317.

13. Ho, K.; Lapitsky, Y.; Shi, M.; Shoichet, M. S. **2009** "Tunable immunonanoparticle binding to cancer cells: thermodynamic analysis of targeted drug delivery vehicles" Soft Matter, 5, 1074-1080.

References for Chapter 3

1. Nabifar, A. **2007** "Investigations of kinetic aspects in nitroxide-mediated radical polymerization of styrene" MASc Thesis, Department of Chemical Engineering, University of Waterloo.

2. Nabifar, A., McManus, N., Vivaldo-Lima, E., Lona, L. M. F., and Penlidis, A. **2008**. A replicated investigation of nitroxide-mediated radical polymerization of styrene over a range of reaction conditions. *Canadian Journal of Chemical Engineering*, 86, 879-892.

3. Bonilla, J.; Saldivar, E.; Flores-Tlacuabuac, A.; Vivaldo-Lima, E.; Pfaendner, R.; Tiscareno-Lechuga, F. **2002** "Detailed modeling, simulation, and parameter estimation of nitroxide mediated living free radical polymerization of styrene" *Polymer Reaction Engineering Journal*, *10*, 227-263.

4. Belincanta-Ximenes, J.; Mesa, P. V. R.; Lona, L. M. F.; Vivaldo-Lima, E.; McManus, N. T.; Penlidis, A. **2007** "Simulation of styrene polymerization by monomolecular and bimolecular nitroxide-mediated radical processes over a range of reaction conditions" *Macromolecular Theory and Simulations*, *16*, 194-208.

5. Roa-Luna, M.; Nabifar, A.; Diaz-Barber, M. P.; McManus, N. T.; Vivaldo-Lima, E.; Lona, L. M. F.; Penlidis, A.; **2007** "Another perspective on the nitroxide mediated radical polymerization (NMRP) of styrene using 2,2,6,6-tetramethyl-1-piperidinyloxy (TEMPO) and dibenzoyl peroxide (BPO)" *Journal of Macromolecular Science Part A: Pure and Applied Chemistry*, *44*, 337-349.

6. Zhou, M.; **2009** "Investigation of kinetics of nitroxide mediated radical polymerization of styrene with a unimolecular initiator" MASc Thesis, Department of Chemical Engineering, University of Waterloo.

7. Drache, M. Mandel, K. Schmidt-Naake, G.; **2007** "Kinetics of nitroxide-controlled radical polymerization during the non stationary state" *Polymer, 48, 1875-1883*.

8. Noguiera, T.R., Goncalves, M.C., Lona, L.M., Vivaldo-Lima, E., McManus, N., Penlidis, A.; **2010** "Effect of initiator type and concentration on polymerization rate and molecular weight in the bimolecular nitroxide mediated radical polymerization of styrene" *Advances in Polymer Technology, 29, 1, 11-19.*

9. Nabifar, A.; **2012** '"Bayesian experimental design framework applied to complex polymerization processes" PhD Thesis, Department of Chemical Engineering, University of Waterloo.

References for Chapter 4

1. Murari, A.R., Contant, S., Lona, L.M.F., Vivaldo-Lima, E., McManus, N.T., and Penlidis, A. **2011.** "Modeling insights on the TEMPO mediated radical polymerization of styrene" Journal of Macromolecular Science, Volume 48, Issue 9, 681-687.

2. Nabifar, A. **2007.** "Investigations of kinetic aspects in nitroxide-mediated radical polymerization of styrene" MASc Thesis, Department of Chemical Engineering, University of Waterloo.

3. Bonilla, J.; Saldivar, E.; Flores-Tlacuabuac, A.; Vivaldo-Lima, E.; Pfaendner, R.; Tiscareno-Lechuga, F. **2002** "Detailed modeling, simulation, and parameter estimation of nitroxide mediated living free radical polymerization of styrene" *Polymer Reaction Engineering Journal*, *10*, 227-263.

4. Belincanta-Ximenes, J.; Mesa, P. V. R.; Lona, L. M. F.; Vivaldo-Lima, E.; McManus, N. T.; Penlidis, A. **2007** "Simulation of styrene polymerization by monomolecular and bimolecular nitroxide-mediated radical processes over a range of reaction conditions" *Macromolecular Theory and Simulations*, *16*, 194-208.

5. Greszta, D.; Matyjaszewski, K. **1996.** "Mechanism of Controlled/"Living" Radical Polymerization of Styrene in the Presence of Nitroxyl Radicals. Kinetics and Simulations" *Macromolecules, 29,* (24), 7661-7670.

6. Zhou, M.; **2009** "Investigation of kinetics of nitroxide mediated radical polymerization of styrene with a unimolecular initiator" MASc Thesis, Department of Chemical Engineering, University of Waterloo.

7. Drache, M. Mandel, K. Schmidt-Naake, G.; **2007** "Kinetics of nitroxide-controlled radical polymerization during the non stationary state" *Polymer, 48, 1875-1883*

References for Chapter 5

1. Fukuda, T.; Goto, A. **2004** "Kinetics of living radical polymerization" *Progress in Polymer Science*, *29*, 329-385.

2. Fukuda, T.; Terauchi, T.; Goto, A.; Ohno, K.; Tsujii, Y.; Miyamoto, T. **1996** "Mechanisms and Kinetics of Nitroxide-Controlled Free Radical Polymerization" *Macromolecules*, 29, 6393-6398

3. Fischer H. **1997** "The persistent radical effect in "living" radical polymerization" *Macromolecules*, *30*, 5666-5672.

4. Saldivar-Guerra, E.; Bonilla, J.; Becerril, F.; Zacahua, G.; Albores-Velasco, M.; Alexander-Katz, R.; Flores-Santos, L.; Alexandrova, L. **2006** "On the nitroxide quasi-equilibrium in the alkoxyamine-mediated radical polymerization of styrene" *Macromolecular Theory and Simulations*, *15*, 163-175.

5. Greszta, D.; Matyjaszewski, K. **1996**. "Mechanism of Controlled/"Living" Radical Polymerization of Styrene in the Presence of Nitroxyl Radicals. Kinetics and Simulations" *Macromolecules*, 29, (24), 7661-7670.

6. Zhou, M.; **2009** "Investigation of kinetics of nitroxide mediated radical polymerization of styrene with a unimolecular initiator" MASc Thesis, Department of Chemical Engineering, University of Waterloo.

7. Nabifar, A. **2007** "Investigations of kinetic aspects in nitroxide-mediated radical polymerization of styrene" MASc Thesis, Department of Chemical Engineering, University of Waterloo.

References for Chapter 6

1. Montgomery, D. C.; **2005** "Design and Analysis of Experiments". Sixth Edition. John Wiley & Sons, Inc.

2. Box, G.E.P; Lucas, H.L.; **1959** "Design of experiments in non-linear situations" *Biometrika*, 46, 77-90.

3. Box, G.E.P.; Hunter, W.G. **1963** "Sequential design of experiments for nonlinear models" IBM Scientific Computing Symposium on Statistics.

4. Nabifar, A., McManus, N.T., Vivaldo-Lima, E., Penlidis, A.; **2010** "A sequential iterative scheme for design of experiments in complex polymerizations" Chemical Engineering Technology, 33, No. 11, 1814-1824.

5. Nabifar, A., McManus, N.T.; Vivaldo-Lima, E.; Reilly, P.M.; Penlidis, A.; **2010** "Optimal Bayesian design of experiments applied to nitroxide-mediated radical polymerization" Macromolecular Reaction Engineering, 4, 387-402.

6. Nabifar, A.; McManus, N.T.; Vivaldo-Lima, E.; Penlidis, A.; **2011** "Diagnostic checks and measures of information in the Bayesian design of experiments with complex polymerizations" Macromolecular Symposia, 302, 90-99.

7. Dube, M. A., Penlidis, A., Reilly, P. M.; **1996** "A systematic approach to the study of multicomponent polymerization kinetics: The butyl acrylate/methyl methacrylate/vinyl acetate example. IV. Optimal Bayesian design of emulsion terpolymerization experiments in a pilot plant reactor" Journal of Polymer Science, Part A: Polymer Chemistry, 34, 811.

8. Vivaldo-Lima, E.; Penlidis, A.; Wood, P. E.; Hamielec, A. E.; **2006** "Determination of the relative importance of process factors on particle size distribution in suspension polymerization using a Bayesian experimental d" Journal of Applied Polymer Science, 102, 5577.

9. Nabifar, A.; **2012** "Bayesian Experimental Design Framework Applied to Complex Polymerization processes" PhD Thesis, Department of Chemical Engineering, University of Waterloo.

10. Franceschini, G.; and Macchietto, S.; **2008** "Novel Anticorrelation Criteria for Design of Experiments: Theory and Formulations" American Institute for Chemical Engineering Journal, 54, 1009-1024

11. Franceschini, G.; and Macchietto, S.; **2008** "Novel Anticorrelation Criteria for Design of Experiments: Algorithm and Application" American Institute for Chemical Engineering Journal, 54, 3221-3238

12. Franceschini, G.; and Macchietto, S.; **2008** "Anti-Correlation Approach to Model-Based Experiment Design: Application to a Biodiesel Production Process" Industrial & Engineering Chemistry Research, 47, 2331-2348

References for Chapter 7

1. Penlidis, A. and Duever, T., **1996** "Optimal sensor selection for copolymerization processes" Macromolecular Symposium, 111, 195-207.

2. Chmielewski, D.J.; Palmer, T.; Manousiouthakis, V., **2002** "On the Theory of Optimal Sensor Placement", American Institute of Chemical Engineering Journal, 48(5), 1001-1012.

3. Gopal, M., **2008** "Control Systems: Principles and Design." 3rd Edition, McGraw Hill. pp 606-615.

Appendix A: Experimental Data Used for Comparisons

Table A-1- R = 0.9, T = 120 C, Bimolecular Process

Time (hr)	Conversion	ln[M]$_0$/[M]	Mn - (Daltons)	Mn*10-3	Mw - (Daltons)	Mw*10-3	Mw / Mn (PDI)
0.5	0.237	0.27	10,213	10.21	16,747	16.75	1.64
1	0.289	0.34	12,318	12.32	17,713	17.71	1.44
1.25	0.326	0.39	11,775	11.78	17,817	17.82	1.51
1.5	0.350	0.43	13,976	13.98	19,648	19.65	1.41
2	0.389	0.49	14,973	14.97	19,731	19.73	1.32
2	0.389	0.49	14,446	14.45	19,488	19.49	1.35
2.53	0.435	0.57	16,517	16.52	21,556	21.56	1.31
3	0.466	0.63	16,517	16.52	22,064	22.06	1.25
4	0.538	0.77	19,597	19.60	23,493	23.49	1.20
5	0.595	0.90	20,842	20.84	24,888	24.89	1.19
5	0.600	0.92	21,075	21.08	25,052	25.05	1.19
10	0.787	1.55	27,551	27.55	31,074	31.07	1.13
15	0.853	1.92	29,541	29.54	33,571	33.57	1.14
20	0.891	2.22	31,696	31.70	35,383	35.38	1.12
20	0.886	2.17	31,168	31.17	35,112	35.11	1.13
34	0.919	2.52	31,360	31.36	35,364	35.36	1.13
50	0.937	2.77	31,547	31.55	35,887	35.89	1.14
70	0.944	2.88	32,598	32.60	36,669	36.67	1.13

Table A-2 - R = 0.9, T = 120 C, Bimolecular Process, Replicates

Time (hr)	Conversion	Mn - (Daltons)	Mn*10-3	Mw - (Daltons)	Mw*10-3	Mw / Mn (PDI)
0.5	0.237	12,766	13	19,273	19	1.51
34	0.919	32,315	32	36,924	37	1.14
70	0.944	33,010	33	36,530	37	1.125

Table A-3 - R = 1.1, T = 120 C, Bimolecular Process

Time (hr)	Conversion	ln[M]$_0$/[M]	Mn - (Daltons)	Mn*10-3	Mw - (Daltons)	Mw*10-3	Mw / Mn (PDI)
2	0.153	0.166	4,990	4.99	6,084	6.08	1.219
3	0.238	0.272	7,256	7.26	8,595	8.60	1.184
6	0.384	0.485	12,056	12.06	13,509	13.51	1.121
9	0.536	0.767	17,412	17.41	19,286	19.29	1.108
14	0.688	1.166	20,613	20.61	23,223	23.22	1.127
24	0.802	1.618	24,450	24.45	27,537	27.54	1.126
40	0.893	2.239	24,857	24.86	28,516	28.52	1.147
9	0.555	0.810	17,358	17.36	19,166	19.17	1.104

Table A-4 - R = 1.1, T = 120 C, Bimolecular Process, Replicates

Time (hr)	Conversion	ln[M]0/[M]
1	0.037	0.037
2	0.108	0.114
3	0.225	0.255
4	0.269	0.314
6	0.392	0.497
9	0.535	0.765
14	0.659	1.077
19	0.779	1.511
24	0.801	1.617
29	0.848	1.882
40	0.894	2.242
50	0.898	2.282

Table A-5 - R = 1.2, T = 120 C, Bimolecular Process

Time (hr)	Conversion	ln[M]$_0$/[M]	Mn - (Daltons)	Mn*10-3	Mw - (Daltons)	Mw*10-3	Mw / Mn (PDI)
1.00	0.0091	0.009	1,016	1.02	3,139	3.14	3.143
1.33	0.0154	0.016	1,480	1.48	2,556	2.56	1.727
1.67	0.0122	0.012	1,906	1.91	2,272	2.27	1.195
2.00	0.0330	0.034	2,134	2.13	2,363	2.36	1.108
2.33	0.0544	0.056	2,192	2.19	2,543	2.54	1.160
2.33	0.0551	0.057	2,291	2.29	2,630	2.63	1.148
2.67	0.1157	0.123	4,060	4.06	4,636	4.64	1.142
3.00	0.0913	0.096	3,460	3.46	3,967	3.97	1.147
3.33	0.1059	0.112	3,986	3.99	4,591	4.59	1.152
3.67	0.1818	0.201	6,598	6.60	7,300	7.30	1.107
4.00	0.2077	0.233	7,230	7.23	8,013	8.01	1.109
5.00	0.2117	0.238	7,842	7.84	8,583	8.58	1.095
6.00	0.3356	0.409	11,661	11.66	12,533	12.53	1.075
8.00	0.3780	0.475	14,691	14.69	14,691	14.69	1.081
10.00	0.4886	0.671	17,046	17.05	18,156	18.16	1.066
14.00	0.6301	0.995	21,125	21.12	23,105	23.11	1.094
14.00	0.6588	1.075	22,212	22.21	23,755	23.75	1.070
18.00	0.7435	1.361	24,236	24.24	26,326	26.33	1.086
22.00	0.7988	1.603	26,789	26.79	28,553	28.55	1.066
26.00	0.8314	1.780	27,800	27.80	30,274	30.27	1.089
40.00	0.8930	2.235	29,193	29.19	31,104	31.10	1.066
49.00	0.9023	2.326	29,355	29.35	31,884	31.88	1.086
72.00	0.9192	2.516	29,358	29.36	32,458	32.46	1.108

Table A-6 - R = 1.2, T = 120 C, Bimolecular Process, Replicates

Time (hr)	Conversion	Mn - (Daltons)	Mn*10-3	Mw - (Daltons)	Mw*10-3	Mw / Mn (PDI)
3.67	0.1818	6,771	6.77	7,637	7.64	1.128
22.00	0.7988	27,955	27.95	30,001	30.00	1.073
72.00	0.9192	31580	31.58	33480	33.48	1.06

Table A-7 - R = 0.9, T = 130 C, Bimolecular Process

Time (hr)	Conversion	ln[M]₀/[M]	Mn - (Daltons)	Mn*10-3	Mw - (Daltons)	Mw*10-3	Mw / Mn (PDI)
0.52	0.281	0.33	9,734	9.73	13,785	13.78	1.42
1	0.346	0.42	12,083	12.08	15,198	15.20	1.26
1.5	0.444	0.59	14,821	14.82	18,037	18.04	1.22
2	0.489	0.67	17,021	17.02	20,014	20.01	1.18
3	0.587	0.88	19,429	19.43	22,972	22.97	1.18
3	0.601	0.92	21,077	21.08	23,939	23.94	1.14
4	0.656	1.07	22,369	22.37	25,560	25.56	1.14
4.95	0.705	1.22	23,159	23.16	26,637	26.64	1.15
8	0.802	1.62	26,872	26.87	30,078	30.08	1.12
8	0.834	1.80	29,191	29.19	32,279	32.28	1.11
10.1	0.852	1.91	29,870	29.87	33,450	33.45	1.12
10.1	0.870	2.04	29,366	29.37	33,425	33.43	1.14
24.05	0.901	2.31	29,110	29.11	33,689	33.69	1.16
24.05	0.916	2.48	30,070	30.07	35,236	35.24	1.17
15	0.876	2.09	27,908	27.91	33,082	33.08	1.19
15	0.876	2.08	27,894	27.89	33,333	33.33	1.20
30.02	0.908	2.39	27,185	27.18	33,108	33.11	1.22
50	0.929	2.65	28,263	28.26	33,972	33.97	1.20
50	0.930	2.67	29,565	29.56	34,791	34.79	1.18

Table A-8 - R = 0.9, T = 130 C, Bimolecular Process, Replicates

Time (hr)	Conversion	Mn - (Daltons)	Mn*10-3	Mw - (Daltons)	Mw*10-3	Mw / Mn (PDI)
1	0.346	12,064	12.06	15,202	15.20	1.260
3	0.587	20,141	20.14	23,175	23.18	1.151
8	0.802	26,395	26.39	29,872	29.87	1.132
8	0.802	26,564	26.56	29,772	29.77	1.121
30.02	0.908	27,906	27.91	33,165	33.17	1.189
50	0.929	27,767	27.77	33,327	33.33	1.201

Table A- 9 - R = 1.1, T = 130 C, Bimolecular Process

Time (hr)	Conversion	ln[M]$_0$/[M]	Mn - (Daltons)	Mn*10-3	Mw - (Daltons)	Mw*10-3	Mw / Mn (PDI)
0.50	0.129	0.14	3,492	3.49	5,146	5.15	1.47
1.00	0.158	0.17	5,168	5.17	6,058	6.06	1.17
1.25	0.203	0.23	6,759	6.76	7,651	7.65	1.13
1.50	0.274	0.32	8,845	8.84	9,861	9.86	1.12
2.00	0.350	0.43	10,552	10.55	11,856	11.86	1.12
2.00	0.276	0.32	9,129	9.13	9,960	9.96	1.09
2.50	0.402	0.51	12,389	12.39	13,711	13.71	1.11
3.00	0.423	0.55	13,623	13.62	14,846	14.85	1.09
4.17	0.508	0.71	18,071	18.07	19,138	19.14	1.06
5.00	0.598	0.91	19,194	19.19	20,698	20.70	1.08
5.00	0.591	0.89	18,816	18.82	20,372	20.37	1.08
10.18	0.799	1.61	25,798	25.80	27,902	27.90	1.08
15.08	0.850	1.90	26,120	26.12	28,604	28.60	1.10
19.23	0.877	2.10	26,105	26.11	28,733	28.73	1.10
20.27	0.897	2.28	26,503	26.50	30,256	30.26	1.14
20.27	0.888	2.19	28,284	28.28	30,868	30.87	1.09
21.72	0.896	2.27	28,447	28.45	30,921	30.92	1.09
23.15	0.894	2.24	27,656	27.66	30,827	30.83	1.12
29.98	0.913	2.44	27,573	27.57	31,231	31.23	1.13
50.00	0.924	2.58	28,251	28.25	31,709	31.71	1.12
71.93	0.934	2.72	29,715	29.72	32,374	32.37	1.09

159

Table A- 10 - R = 1.1, T = 130 C, Bimolecular Process, Replicates

Time (hr)	Conversion	$\ln[M]_0/[M]$	Mn - (Daltons)	Mn*10-3	Mw - (Daltons)	Mw*10-3	Mw / Mn (PDI)
2	0.331	0.40	8,293	8.29	10,669	10.67	1.29
4	0.532	0.76	12,765	12.77	16,765	16.77	1.31
7	0.711	1.24	17,158	17.16	22,038	22.04	1.28
10	0.778	1.51	19,016	19.02	23,989	23.99	1.26
13	0.823	1.73	22,359	22.36	25,149	25.15	1.13
16	0.857	1.95	21,950	21.95	26,255	26.26	1.20
22	0.880	2.12	21,058	21.06	26,519	26.52	1.26
28	0.900	2.31	22,917	22.92	26,485	26.49	1.16
34	0.909	2.40	23,120	23.12	26,863	26.86	1.16
40	0.912	2.43	23,050	23.05	27,356	27.36	1.19
50	0.917	2.49	25,255	25.26	28,010	28.01	1.11

Table A-11- R = 1.2, T = 130 C, Bimolecular Process

Time (hr)	Conversion	$\ln[M]_0/[M]$	Mn - (Daltons)	Mn*10-3	Mw - (Daltons)	Mw*10-3	Mw / Mn (PDI)
1	0.027	0.028	1,147	1.15	2,105	2.11	1.84
2	0.084	0.088	3,404	3.40	3,768	3.77	1.11
3	0.162	0.177	6,440	6.44	6,955	6.96	1.08
4	0.246	0.282	9,016	9.02	9,844	9.84	1.09
5	0.323	0.390	12,650	12.65	13,473	13.47	1.07
5(rep)	0.335	0.407	12,120	12.12	13,120	13.12	1.08
6	0.432	0.566	15,528	15.53	16,489	16.49	1.06
7	0.490	0.673	18,040	18.04	19,164	19.16	1.06
8	0.566	0.834	19,269	19.27	20,992	20.99	1.09
8(rep)	0.543	0.782	19,345	19.35	20,990	20.99	1.09
9	0.622	0.972	21,106	21.11	22,990	22.99	1.09

Table A-12 - R = 1.2, T = 130 C, Bimolecular Process, Replicates

Time (hr)	Conversion	$\ln[M]_0/[M]$	Mn - (Daltons)	Mn*10-3	Mw - (Daltons)	Mw*10-3	Mw / Mn (PDI)
0.5	0.021	0.02	748	0.75	2,254	2.25	3.01
1	0.034	0.03	1,839	1.84	2,398	2.40	1.30
1.25	0.034	0.03	2,134	2.13	2,585	2.59	1.21
2.72	0.148	0.16	5,227	5.23	5,646	5.65	1.08
3.58	0.252	0.29	8,070	8.07	8,675	8.67	1.07
5.5	0.405	0.52	12,638	12.64	13,702	13.70	1.08
6.5	0.468	0.63	15,032	15.03	16,210	16.21	1.08
8	0.579	0.87	17,723	17.72	19,348	19.35	1.09
15.2	0.783	1.53	23,749	23.75	26,336	26.34	1.11
15.2	0.779	1.51	23,218	23.22	26,173	26.17	1.13
18.03	0.810	1.66	24,728	24.73	27,825	27.82	1.13
18.03	0.823	1.73	25,243	25.24	27,941	27.94	1.11
20	0.841	1.84	26,258	26.26	28,730	28.73	1.09
22	0.857	1.95	25,200	25.20	28,085	28.08	1.11
22	0.862	1.98	24,711	24.71	27,080	27.08	1.10
25	0.872	2.06	25,150	25.15	28,406	28.41	1.13
25	0.875	2.08	24,503	24.50	27,438	27.44	1.12
25.52	0.869	2.03	26,163	26.16	29,408	29.41	1.12
25.52	0.881	2.13	25,762	25.76	28,409	28.41	1.10
30	0.891	2.22	26,185	26.19	29,573	29.57	1.13
41.47	0.913	2.44	25,548	25.55	29,581	29.58	1.16
48.05	0.914	2.45	24844.5	24.84	28073.5	28.07	1.13
66.03	0.921	2.54	25820	25.82	30511.5	30.51	1.1815
72.5	0.928	2.63	24937.5	24.94	28818.5	28.82	1.156
72.5	0.926	2.61	26386	26.39	30032	30.03	1.1385

Table A-13- T = 120 C, Unimolecular Process

Time (hr)	Conversion	ln[M]$_0$/[M]	Mn - (Daltons)	Mn*10-3	Mw - (Daltons)	Mw*10-3	Mw / Mn (PDI)
0.55	0.052	0.054	955	0.96	1,031	1.03	1.08
1.00	0.094	0.099	1,751	1.75	1,956	1.96	1.12
3.03	0.231	0.263	5,000	5.00	5,368	5.37	1.07
6.05	0.354	0.438	8,423	8.42	8,818	8.82	1.05
8.03	0.502	0.697	9,486	9.49	10,048	10.05	1.06
24.73	0.735	1.329	13,567	13.57	14,522	14.52	1.07
15.00	0.648	1.044	12,053	12.05	12,828	12.83	1.06
20.07	0.705	1.221	12,884	12.88	13,847	13.85	1.07
20.07	0.707	1.229	12,598	12.60	13,809	13.81	1.10
40.50	0.795	1.586	14,747	14.75	15,743	15.74	1.07
30.12	0.758	1.418	14,161	14.16	15,157	15.16	1.07
60.12	0.831	1.775	13,913	13.91	15,850	15.85	1.14
50.22	0.822	1.724	13,854	13.85	15,706	15.71	1.13

Table A-14 - T = 120 C, Unimolecular Process, Replicates

Time (hr)	Conversion	ln[M]0/[M]	Mn - (Daltons)	Mn*10-3	Mw - (Daltons)	Mw*10-3	Mw / Mn (PDI)
5	0.376	0.471	7,910	7.91	8,310	8.31	1.05
7.27	0.465	0.626	9,869	9.87	10,243	10.24	1.04
10.07	0.556	0.812	11,048	11.05	11,914	11.91	1.08
24.45	0.722	1.281	14,030	14.03	15,110	15.11	1.08
20	0.696	1.190	14,131	14.13	14,673	14.67	1.04

163

Appendix B: MATLAB Code Availability

Code used for the generation of these simulations, designs, results, and figures is available with Professor Alexander Penlidis of the Department of Chemical Engineering at the University of Waterloo.

Some samples of key routines (code and pseudo-code) are provided in what follows.

Fully Mechanistic Model (FMM):

```
function dy = FUNps(t,y)
%mass balances of Tempo mediated radical polymerization
%   Legend of Y's
% Material Balances
% y(1)   [I]
% y(2)   [M]
% y(3)   [NOE]
% y(4)   [M*]
% y(5)   [Rin*]
% y(6)   [D*]
% y(7)   [NOx*]
% y(8)   [HNOx]
% y(9)   [MNOx]
% y(10)  [RNOx]
% y(11)  [R*]
% y(12)  [P]
% y(13)  [D]
% Moment Equations
% y(14)  lambda0
% y(15)  lambda1
% y(16)  lambda2
% y(17)  delta0
% y(18)  delta1
% y(19)  delta2
% y(20)  mu0
% y(21)  mu1
% y(22)  mu2

global kd f0 fc0 kdim kia kp0 ktc ktd kfM kfD ka2 kd2 kda ka kdecomp kh3;

dy = zeros(22,1);
% balances
dy(1) = - kd*y(1);
dy(2) = - 2*kdim*y(2)^2 - kia*y(2)*y(13) - kp0*y(2)*(y(6)+y(4)+y(5)) -
kp0*y(2)*y(11) - kfM*y(2)*y(11) + kdecomp*y(9);
dy(3) = - ka2*y(3) + fc0*kd2*y(7)*y(5);
dy(4) = kia*y(2)*y(13) - kp0*y(2)*y(4) - fc0*kda*y(7)*y(4) + ka*y(9) +
kfM*y(2)*y(11);
dy(5) = 2*f0*kd*y(1) - kp0*y(2)*y(5) + ka2*y(3) - fc0*kd2*y(7)*y(5);
dy(6) = kia*y(2)*y(13) - kp0*y(2)*y(6) + kh3*y(7)*y(13) + kfD*y(13)*y(11);
```

164

```
dy(7) = - kh3*y(13)*y(7) - fc0*kda*y(7)*y(11) + ka*y(10) - fc0*kda*y(7)*y(4)
+ ka*y(9) -fc0*kd2*y(7)*y(5) + ka2*y(3);
dy(8) = kh3*y(7)*y(13) + kdecomp*y(9);
dy(9) = fc0*kda*y(7)*y(4) - ka*y(9) - kdecomp*y(9);
dy(10) = fc0*kda*y(7)*y(11) - ka*y(10);
dy(11) = kp0*y(2)*(y(6)+y(4)+y(5)) - (ktc+ktd)*y(11)^2 - fc0*kda*y(7)*y(11) +
ka*y(10) - kfM*y(11)*y(2) - kfD*y(11)*y(13);
dy(12) = kfM*y(11)*y(2) + kfD*y(11)*y(13) + (ktc+ktd)*y(11)^2;
dy(13) = kdim*(y(2)^2) - kia*y(2)*y(13) - kh3*y(7)*y(13) - kfD*y(13)*y(11);

%MW method of moments
dy(14) = kp0*y(2)*(y(5)+ y(4)+y(6)) - (ktc+ktd)*y(14)^2 - kfM*y(14)*y(2) -
kfD*y(13)*y(14) - fc0*kda*y(7)*y(14) + ka*y(17);%lambda0
dy(15) = kp0*y(2)*(y(5)+y(4)+y(6)+y(14)) - (ktc+ktd)*y(14)*y(15) -
kfM*y(15)*y(2) - kfD*y(13)*y(15) - fc0*kda*(y(7)*y(15)) + ka*y(18); %lambda1
dy(16) = -fc0*kda*(y(7)*y(16)) + ka*y(19) - (ktc+ktd)*y(14)*y(16) +
kp0*y(2)*(y(5)+y(4)+y(6)+y(14)+2*y(15)) - kfM*y(16)*y(2) - kfD*y(13)*y(16);
%lambda2
dy(17) = kda*fc0*y(7)*y(14) - ka*y(17); %delta0
dy(18) = kda*fc0*y(7)*y(15) - ka*y(18); %delta1
dy(19) = kda*fc0*y(7)*y(16) - ka*y(19); %delta2
dy(20) = 0.5*ktc*(y(14)^2) + ktd*(y(14)^2) + kfM*y(14)*y(2) +
kfD*y(14)*y(13); %mu0
dy(21) = ktc*(y(14)*y(15)) + ktd*(y(14)*y(15)) + kfM*y(15)*y(2) +
kfD*y(15)*y(13); %mu1
dy(22) = ktc*(y(14)*y(16)+ y(15)^2) +ktd*y(14)*y(16) + kfM*y(16)*y(2) +
kfD*y(16)*y(13); %mu2
end
```

Solution of FMM:

```
%Definition of Parameters
global R T kd f0 fc0 kdim kia kp0 kt0 ktc ktd kfM kfD ka2 kd2 kda ka kdecomp
kh3 MWm Keq Mn Mw M0 I0 TEMPORatio NOE0 TEMPO0 unibiresponse plotsresponse
conv;
R = 1.9859; %gas constant in cal/mol/k
T = 120.00 + 273.15; %temperature in K, can be changed
kd = 1.7e15*exp(-30000/R/T); %1/s
f0 = 0.54; %from AN thesis, 0.54 to 0.55
fc0 = 1; %<=1, controller efficiency
kdim = 188.97*exp(-16185.1/R/T); %L/mol/s
kia = 6.359e12*exp(-36598.55/R/T); %L/mol/s
kp0 = 4.266e7*exp(-7769.17/R/T); %L/mol/s
kt0 = 2.002e10*exp(-3081.84/R/T); %L/mol/s
ktd = 0; %L/mol/s or rather am told that ktd/kt0 = 0.0
ktc = kt0-ktd; %L/mol/s
kfM = 9.376e6*exp(-13372/R/T); %0 or 9.376e6*exp(-13372/R/T); %L/mol/s
kfD = 50; %0 or 50 L/mol/s
kda = 5.03e9*exp(-3722/R/T); %L/mol/s
ka = 2.0e13*exp(-29683/R/T); %1/s
kdecomp = 5.7e14*exp(-36639.6/R/T); %1/s
kh3 = 0.1*0.001; %L/mol/s
MWm = 104.12; %g/mol
Keq = ka/kda;
M0 = 8.7; %mol/L
conv = 0;
```

```matlab
TEMPORatio = 1.1;


%Ask if is the unimolecular or bimolecular process, default = bimolecular
unibiresponse = input('Unimolecular or bimolecular process? u/b [b]: ', 's');
if isempty(unibiresponse)
    unibiresponse = 'b';
end


if strcmp('b', unibiresponse) == true
    ka2 = 0; %if unimolecular 2.0*10^13*exp(-29683/R/T);, bi: 0; %%%1/s
    kd2 = 0; %if unimolecular 5.03*10^9*exp(-3722/R/T);, bi: 0 %%%L/mol.s
    I0 = 0.036;
    NOE0 = 0;
elseif strcmp('u', unibiresponse) == true
    ka2 = 2.0e13*exp(-29683/R/T);
    kd2 = 5.03e9*exp(-3722/R/T);
    I0 = 0;
    NOE0 = 0.050;
else
    error('Invalid input for unimolecular/bimolecular process');
end


TEMPO0 = fc0*TEMPORatio*I0;


%Make a vector of the initial conditions for the system of DE's

y = [I0 M0 NOE0 0 0 0 TEMPO0 0 0 0 0 0 0 1e-7 1e-5 1e-3 1e-7 1e-5 1e-3 1e-7
1e-5 1e-3];


time_interval = [0 300000]; % time interval
options = odeset('RelTol',1e-9,'AbsTol',[1e-9 1e-9 1e-9 1e-9 1e-9 1e-9 1e-9
1e-9 1e-9 1e-9 1e-9 1e-9 1e-9 1e-9 1e-9 1e-9 1e-9 1e-9 1e-9 1e-9 1e-9 1e-
9],'InitialStep',1,'BDF','on'); %ode solver options

% run an ode solver, in this case set up to use Gear's method (for stiff
ODEs), to solve the set of ODEs provided in FUNps
[t,y] = ode15s('FUNps', time_interval, y, options);

Mn = MWm.*((y(:,15)+y(:,18)+y(:,21))./(y(:,14)+y(:,17)+y(:,20)));
Mw = MWm.*((y(:,16)+y(:,19)+y(:,22))./(y(:,15)+y(:,18)+y(:,21)));
PDI = Mw./Mn;
lnm0m = log(M0./y(:,2));
conversion = (M0-y(:,2))./M0;
```

Optimal design, calculation of $\underline{X}$ matrix using RMM: (pseudo-code)

```
choose the high and low levels for each of the (i = 18) parameters
for (each set of experiments to evaluate (i.e., potential row of X), j)
     for (each parameter, i)
     Solve RMM for high and low levels, store results
     % Use finite difference method to use these high and low values to
     populate the X matrix
     X(j, i) = [(f(high, i)-f(low, i))/(theta(high, i)- theta(low, i))];
     end
end
```

Determination of optimal sets of experiments: (pseudo-code)

```
for (each combination of possibly evaluated sets
      construct  the  relevant  X  matrix  %  (i.e.,  row  exchange  using  the
      corresponding rows of x)
      compute the derivative |X'X|
      record the value
end
compare recorded values
select maximum value
the set of experiments corresponding to this maximum is the optimal choice
```